9-5-2013

# ANTIMICROBIAL ACTIVITY AND MECHANISTIC STUDY FOR THE POLY(PHENYLENE ETHYNYLENE) (PPE)-BASED CATIONIC CONJUGATED POLYELECTROLYTES AND OLIGO-PHENYLENE ETHYNYLENES

Ying Wang

Ying Wang
*Candidate*

Chemistry and Chemical Biology
*Department*

This dissertation is approved, and it is acceptable in quality and form for publication:

*Approved by the Dissertation Committee:*

David J. Keller , Chairperson

Stephen E. Cabaniss

John K. Grey

Eva Y. Chi

David G. Whitten

# ANTIMICROBIAL ACTIVITY AND MECHANISTIC STUDY FOR THE POLY(PHENYLENE ETHYNYLENE) (PPE)-BASED CATIONIC CONJUGATED POLYELECTROLYTES AND OLIGO-PHENYLENE ETHYNYLENES

**by**

**YING WANG**

B.S., Chemical Engineering, Jilin University, China, 2005
M.S., Physical Chemistry, Jilin University, China, 2008

DISSERTATION

Submitted in Partial Fullfillment of the
Requirtments for the Degree of

**Doctor of Philosophy**
**Chemistry**

The University of New Mexico
Albuquerque, New Mexico

**July, 2013**

## ACKNOWLEDGMENTS

So far, I have studied in Prof. Whitten's group for about four and a half years, it is the most wonderful experience I have during my 24-year formal schooling. In my opinion, Prof. Whitten is not just my research advisor, he is a well-known scientist, a respectable elder and a thoughtful grandpa! The pleasant moments, such as hiking, watching backetball games, having meals together and discussing history and my career, are so unforgettable. Although I will leave Prof. Whitten's group soon, he is my lifetime mentor!

I would also like to express my sincere appreciation to Prof. Chi, my co-advisor, who not only provides guidelines to my research, but also cares about me and my family. I feel so lucky to work together with Prof. Whitten and prof. Chi in the Center for Biomedical Engineering.

I am very grateful to my committee: Prof. Keller, Prof. Cabaniss and Prof. Grey. Thank you so much for serving as my committee members.

I would like to acknowledge the following individuals for their valuable helps and contributions to my dissertation research: Prof. Steve W. Graves, Dr. Yangli Tang, Dr. Zhijun Zhou, Dr. Liping Ding, Dr. Tom Cobitt, Eric Hill, Harry Pappas, Dr. Stephen Jett, Prof. David G. Bear and Prof. Andrew P. Shreve.

I would like to thank Prof. Schanze and his synthesis team at the University of Florida for providing some of the biocidal polymers. I also appreciate the helps from Karen McElveny, Isela Roeder, Stephanie Sanchez and Anne Trabaudo.

I would like to thank my wife, my parents and my parents-in-law for their love and support.

**ANTIMICROBIAL ACTIVITY AND MECHANISTIC STUDY FOR THE POLY(PHENYLENE ETHYNYLENE) (PPE)-BASED CATIONIC CONJUGATED POLYELECTROLYTES AND OLIGO-PHENYLENE ETHYNYLENES**

**by**

**YING WANG**

**B.S., Chemical Engineering, Jilin University, China, 2005**
**M.S., Physical Chemistry, Jilin University, China, 2008**
**Ph.D., Chemistry, The University of New Mexico, USA, 2013**

## ABSTRACT

My dissertation work focuses on recent progress made in elucidating the intermolecular interactions between a novel class of synthetic phenylene ethynylene (PPE)-based conjugated polyelectrolyte polymers (CPEs) and oligomers (OPEs) and multiscale cellular targets that give rise to their remarkable broad spectrum biocidal activity. We studied the interactions and self-assembly behaviors of the CPEs and OPEs with a set of vital biomolecules, including lipids, proteins and nucleic acids, that reveal the potential pathways by which the synthetic biocidal agents could exert toxicity. Then, we explored the antimicrobial effects and mechanisms of the CPEs and OPEs on multiple clinically relevant pathogens, with an emphasis on the morphological damages induced by the biocidal compounds towards the pathogens. The discussion about the cytotoxicity of these materials against mammalian cells and human tissues to can help us to explore the potential applications of the CPEs and OPEs as antiseptics. We also pose some unanswered questions about their antimicrobial mechanisms, which provide directions for the future study.

# Table of Contents

# Chapter 1. Introduction

## 1.1 Antimicrobial materials and mechanisms

The outbreak of global infectious diseases presents a major threat to public health. A recent example is the appearance and the subsequent rapid spread of haemolytic uraemic syndrome caused by enterohemorrhagic *E. coli* in Germany that has killed and sickened over 500 people (May 2011). The development of novel and effective antimicrobial agents is thus a critical worldwide healthcare need, especially for hospital environments where antibiotic resistance is prevalent.[1] One specific challenge is infections associated with medical implants and devices. As such, the development of antimicrobials that can be easily processed to form antiseptic surfaces is also critically needed.[2-3]

In the past two decades, a number of antimicrobial materials have been discovered and developed to combat pathogenic agents, including antibiotics, naturally occurring antimicrobial peptides (AMPs), and synthetic quaternary ammonium compounds.[4-5] However, antibiotics need to be used with caution because of the possibility of pathogens developing resistance.[6] AMPs are believed to act by non-specific mechanisms thus reducing the likelihood of induced resistance.[7] However, the development of AMPs as viable therapeutics has proven difficult due to the high cost of manufacturing, and to chemical, proteolytic, and physical instabilities of peptide-based materials,[8-9] toxicity, limited efficacy, and poor tissue distribution.[10-11] Synthetic mimics that capture the essential features and functions of AMPs while eliminating their disadvantages are thus particularly appealing antimicrobial agents. One such class of compounds is phenylene ethynylene (PPE)-based conjugated polyelectrolyte polymers (CPEs) and oligomers (OPEs) that exhibit broad-spectrum antimicrobial properties.[12] A briefly review about

some well-known chemical biocidal agents and their biocidal mechanisms against bacteria[13-14] will be discussed and then followed by an introduction to the physical and biocidal properties of the CPEs and OPEs in the next section. The mechanisms of action for some typical antiseptics and disinfectants are listed in Table 1.1.

**Table 1.1**. Summary of mechanisms of selected antiseptics and disinfectants.

| Target | Antiseptic or disinfectant | Mechanism of action |
|---|---|---|
| Cell envelope (cell wall, outer membrane) | Glutaraldehyde | Cross-linking of proteins |
| | EDTA, other permeabilizers | Gram-negative bacteria: removal of $Mg^{2+}$, release of some LPS |
| Cytoplasmic (inner) membrane | QACs | Generalized membrane damage involving phospholipid bilayers |
| | Chlorhexidine | Low concentrations affect membrane integrity, high concentrations cause congealing of cytoplasm |
| | Diamines | Induction of leakage of amino acids |
| | PHMB, alexidine | Phase separation and domain formation of membrane lipids |
| | Phenols | Leakage; some cause uncoupling |
| Cross-linking of macromolecules | Formaldehyde | Cross-linking of proteins, RNA, and DNA |
| | Glutaraldehyde | Cross-linking of proteins in cell envelope and elsewhere in the cell |
| DNA intercalation | Acridines | Intercalation of an acridine molecule between two layers of base pairs in DNA |
| Interaction with thiol groups | Silver compounds | Membrane-bound enzymes (interaction with thiol groups) |
| Effects on DNA | Halogens | Inhibition of DNA synthesis |
| | Hydrogen peroxide, silver ions | DNA strand breakage |
| Oxidizing agents | Halogens | Oxidation of thiol groups to disulfides, sulfoxides, or disulfoxides |
| | Peroxygens | Hydrogen peroxide: activity due to from formation of free hydroxy radicals (•OH), which oxidize thiol groups in enzymes and proteins; PAA: disruption of thiol groups in proteins and enzymes |

Reprinted with permission from ref. 13.

### 1.1.1 Antimicrobial agents that affect bacterial cell wall

Peptidoglycans are the main component of most bacterial cell walls, which protects the cell from the outside environment. Living active cells can constantly synthesize peptidoglycan for growth and propagation. In addition, the surface of Gram-negative bacteria is a layer of negatively charged lipopolysaccharides (LPS), which is stabilized by cationic divalent ions. Agents such as penicillin and EDTA can inhibit the synthesis of peptidoglycan and/or destabilize the cell wall. Penicillin can react with the peptidoglycan synthesis enzymes and create weak points on the cell wall and make the cell wall osmotically fragile.[14] EDTA can strongly chelate with the cationic divalent ions on the

outer membrane of the Gram-negative bacteria, then cause the release of LPS and change the permeability of the outer membrane.[15]

### 1.1.2 Antimicrobial agents that affect nucleic acid synthesis

The synthesis of DNA and RNA is a multistep enzyme-catalyzed reaction, which is subject to attacks at many points.[14] Antimicrobial agents, such as chloroquine, pyrimidines and halogens can cross the cell wall and membrane and interfere with nucleic acid synthesis. For example, chloroquine can bind and cross-link the DNA double helix. Hypochlorous acid (HOCl) has also been reported to be cable to completely inhibit the growth of *E. coli* cells by terminating DNA synthesis.[16]

### 1.1.3 Antimicrobial agents that block protein synthesis and denature protein

As with nucleic acid synthesis, protein synthesis in a living cell is also a long series of reactions. Aminoglycosides can insert into bacterial ribosome and mislead the mRNA to synthesize abnormal proteins.[16] Proteins are also fairly reactive with other chemical agents, such as aldehydes and oxidants, largely due to the reactive functional groups on the side chains of the protein. Glutaraldehyde, an important sterilizing agent, can strongly react with free amine groups on the protein and cross-link the proteins on the cell surface and elsewhere in the cell.

### 1.1.4 Antimicrobial agents that disrupt cell membrane function

The cell membrane carries out many vital functions, including serving as a sealed barrier. A damaged membrane can easily cause the death of the cell because of the disruption of metabolism and/or release of the cell contents.[14] Antimicrobial drug

polymyxins have been demonstrated to insert into the cell membrane and cause the release of proteins and nitrogen bases. Recently, a large class of antimicrobial macromolecules has been designed and developed.[17-18] The amine groups on these synthetic polymers, especially the quaternary amine, give these materials high antimicrobial activity. Most of these polymers have been referred to as membrane active agents, which implies a membrane-disrupting mechanism for their antimicrobial actions.

Since most of the current antimicrobial agents are either not efficient (especially after the appearance of multi-drug resistant superbugs) or too toxic to treat patients, there is still a great need for creation of new non-toxic broad-spectrum antimicrobial agents.[17]

## 1.2 Conjugated polyphenylene ethynylenes (CPEs) and oligo phenylene ethynylenes (OPEs)

### 1.2.1 Synthesis of the CPEs and OPEs

The CPEs and OPEs are a class of π-conjugated polymers and oligomers containing ionic side functional groups.[19-20] Depending on the charge of the functional groups, the CPEs and OPEs can be classified into these categories: cationic, anionic and polyampholytes having both anionic and cationic groups. The most common cationic side groups include quaternary ammonium and pyridinium. While the anionic groups generally are carboxylate, phosphonate, and sulfonate.

In the past two decades, a significant amount of the conjugated electrolytes with various structures have been synthesized, mostly through the carbon–carbon bond-forming reactions. The most widely used polymerization methods have been summarized by Liu and are shown in Scheme 1.1, which include $FeCl_3$-catalyzed or electrochemical

oxidization; the Yamamoto and Suzuki coupling reactions for poly(arylene)s; the Wittig, Gilch, Wessling, and Heck reactions for poly(arylene vinylene)s; and the Sonogashira coupling reactions for poly(arylene ethynylene)s."[19] The ring-opening metathesis polymerization of cyclooctatetraenes has also been widely used to prepare polyvinylene and its derivatives. Using these well-established methods, the conjugated polyelectrolytes, as well as the oligoelectrolytes, can be synthesized with various precursors. The CPEs and OPEs used in our study are entirely made by the palladium-catalyzed coupling methods (Sonogashira reactions). One example for the synthesis of a typical CPE is shown in Scheme 1.2.[21]

**Scheme 1.1**. Examples of most widely used polymerization methods; Ar, Ar1, and Ar2 represent aromatic structures.

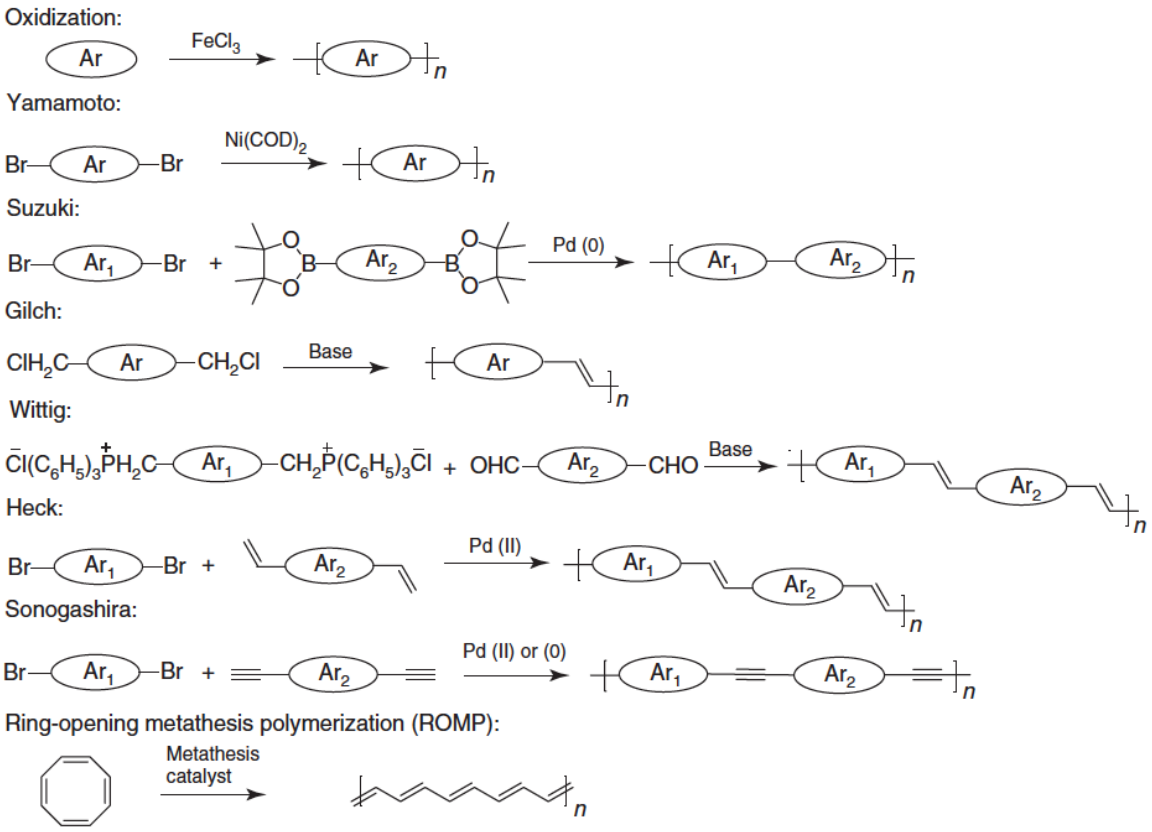


Reprinted with permission from ref 19.

**Scheme 1.2**. Synthesis of a typical cationic poly(phenylene ethynylene)

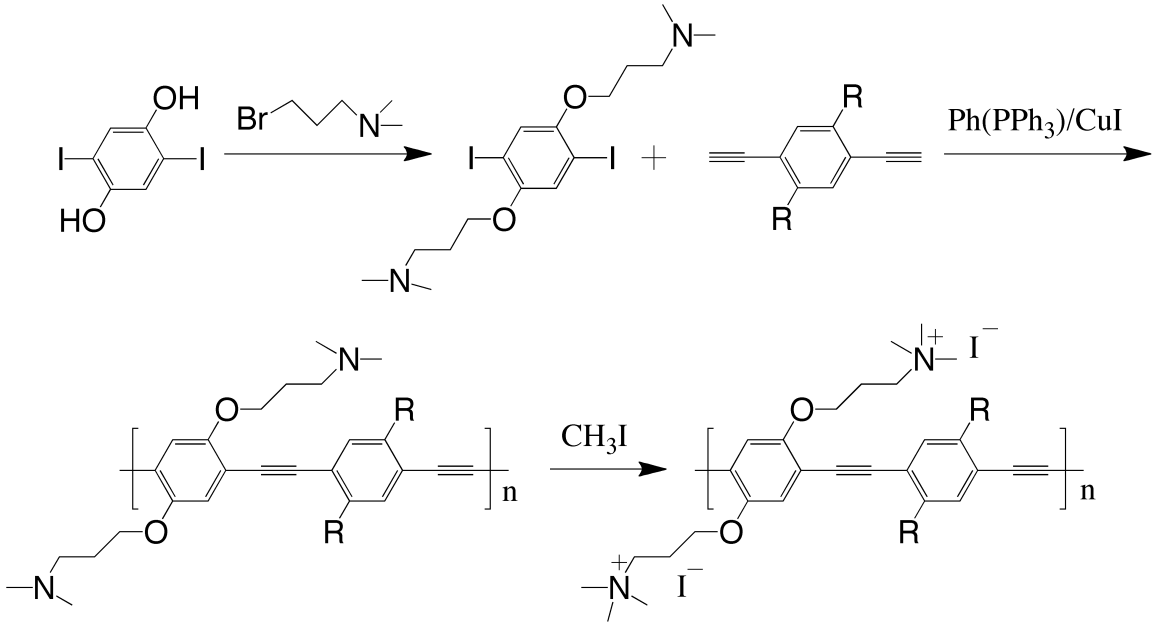

**Scheme 1.3**. Structures of the antimicrobial oligomers and polymers discussed in this dissertation.*

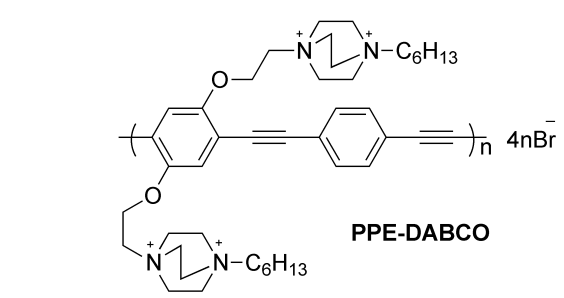


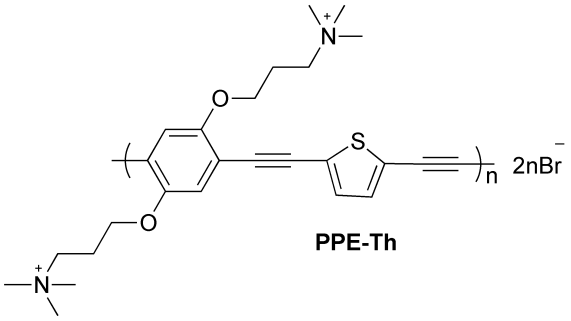


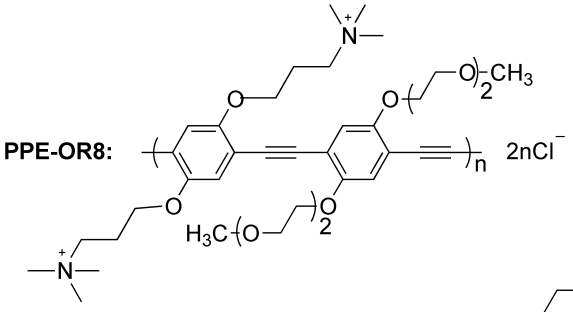


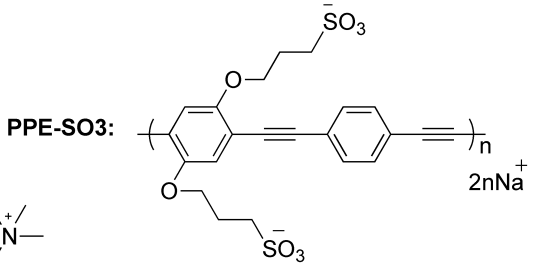


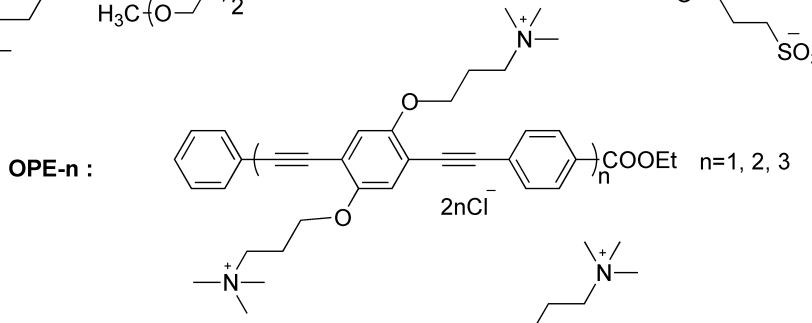


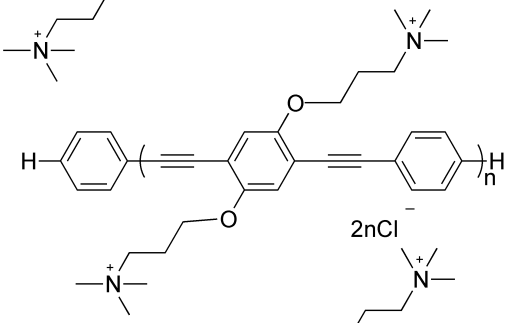


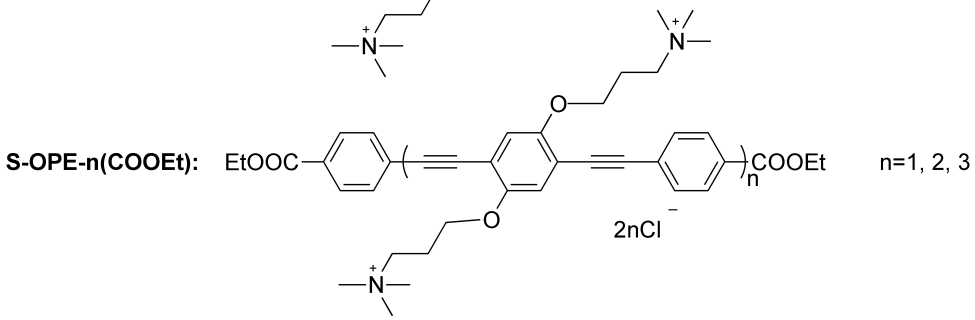


**PPE-NMe$_3$-n-COOEt:**

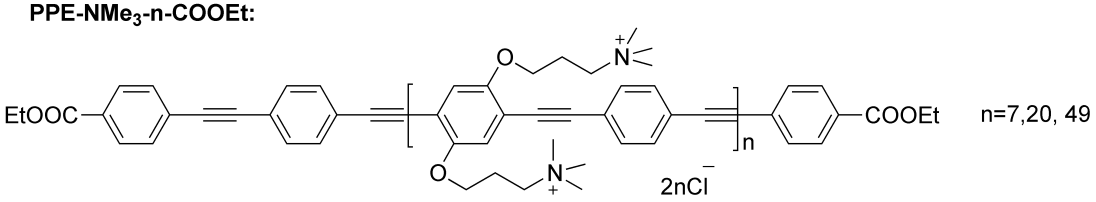

**EO-OPE-1(C3):** 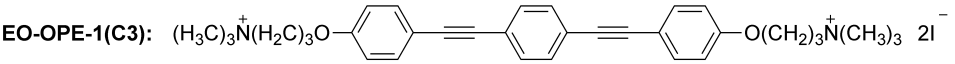

**EO-OPE-1(Th):** 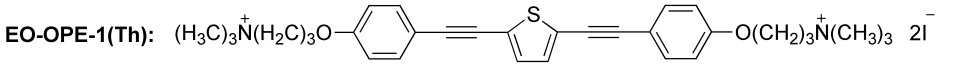

**EO-OPE-1(C2):** 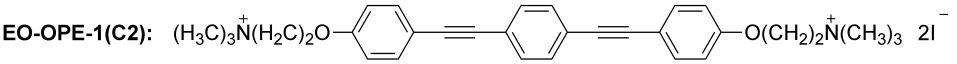

**EO-OPE-1(Th, C2):** 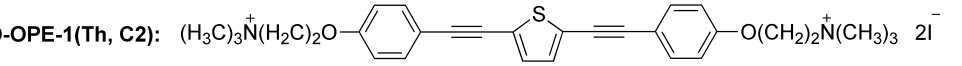

**EO-OPE-1(DABCO):**

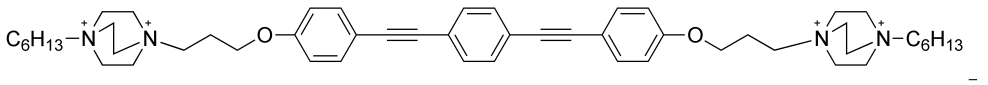

**EO-OPE-1(Th, DABCO):**

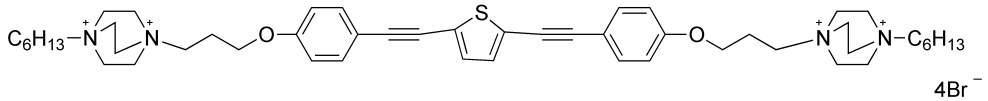

**Melittin:** Gly-Ile-Gly-Ala-Val-Leu-Lys-Val-Leu-Thr-Thr-Gly-Leu-Pro-Ala-Leu-Ile-Ser-Trp-Ile-Lys-Arg-Lys-Arg-Gln-Gln-NH2

**Amphotericin B:**

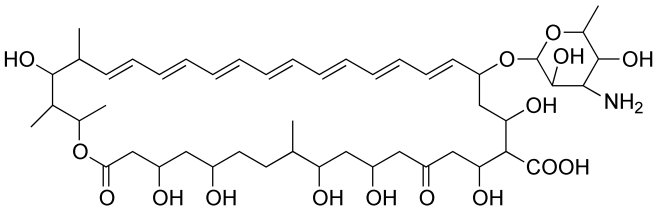

*n denotes the number of repeat units.

### 1.2.2 Physical properties of the CPEs and OPEs

The synthetic CPE and OPE materials (Scheme 1.3) are water-soluble and amphiphilic due to the combination of cationic side and end functional groups and the hydrophobic PPE backbone.[21-23] Many CPEs and OPEs are strongly fluorescent in the UV/visible region, and the fluorescence can be efficiently quenched by an oppositely charged quencher through an electron- or energy-transfer process. The efficient light-harvesting properties of these materials can result in low-lying singlet and triplet states that are capable of sensitizing singlet oxygen and generating reactive oxygen species (ROS) under UV/visible light irradiation, one example for the a representative CPE serving as an efficient singlet oxygen sensitizer is shown in Figure 1.1.[12] In particular, the presence of

the charged groups in the CPEs and OPEs allows them to interact strongly with oppositely charged ions in aqueous solutions and with charged planar or colloid surfaces/scaffolds, such as carboxymethylcellulose (CMC), carboxymethylamylose (CMA), DNA, and bovine serum albumin (BSA).[22, 24] Binding of the CPEs and OPEs towards these scaffolds results in pronounced changes in photophysical properties of these materials.

Nucleic acids, including DNA and RNA, are negatively charged at physiological pH. The cationic CPEs and OPEs are expected to interact with nucleic acids and possibly induce structural and/or chemical damage. The oligomeric OPE-2 has been demonstrated to bind, in a sequence-specific fashion, to the minor groove of the double-stranded DNA, making it a potentially useful compound for DNA sensing and detection.[25] Changes in DNA sequence, as small as a single nucleotide mismatch, can be detected via the changes in absorption, fluorescence and the induced CD signal of the oligomer that results from conformational and/or aggregation state change (possible formation of a J-dimer) the oligomer undergoes upon associating with DNA. The oligomeric OPE-n, S-OPE-n(H), and S-OPE-n(COOEt) are also found to readily bind to and self-assemble on anionic cellulose material such as CMC and CMA. Due to their opposite charges, OPE-cellulose association is likely controlled by electrostatic interactions. Additionally, electrophilic, nucleophilic and hydrophobic interactions are also expected to contribute to OPE-cellulose binding. Changes in the absorption and fluorescence spectra of the OPEs upon complexing with celluloses reveal that the smallest oligomers with just three phenyl rings could form a J-dimer on these anionic scaffolds. However, the observed spectral changes of larger oligomers upon associating with CMC and CMA can also be explained by the

planarization of the segment chromophores and the extension of the effective conjugation length within the molecular backbone of these larger oligomers rather than the formation of aggregates.

Due to the high molecular weight and relatively amphiphilic properties of the CPEs, they readily self-assemble into nano-scale aggregates in aqueous environments through intra- and/or inter-chain hydrophobic interactions. In contrast, the smaller OPEs in aqueous solutions are believed to be monomeric in the micromolar range. A computational study of a set of oligomers (S-OPE-n(H), n=1, 2 and 3, Scheme 1.3) found that the backbone of the smallest S-OPE-1(H) is planar and fully conjugated. However, the larger oligomers (S-OPE-2(H) and S-OPE3(H)) adopt non-planar conformations and the frontier orbitals of these larger oligomers are confined to near-planar regions, which are called "segment chromophores" (Figure 1.2).[22] These segment chromophores extend only to about 3 to 4 phenyl rings in length. Although the maximum absorption wavelengths of the CPEs and OPEs red-shift as the number of repeat unit first increases, there is little change when comparing the spectrum of S-OPE-3(H) to that of a CPE with 49 repeat units,[26] due to the existence of the segment chromophores within the molecular backbone of these PPE-based conjugated materials.

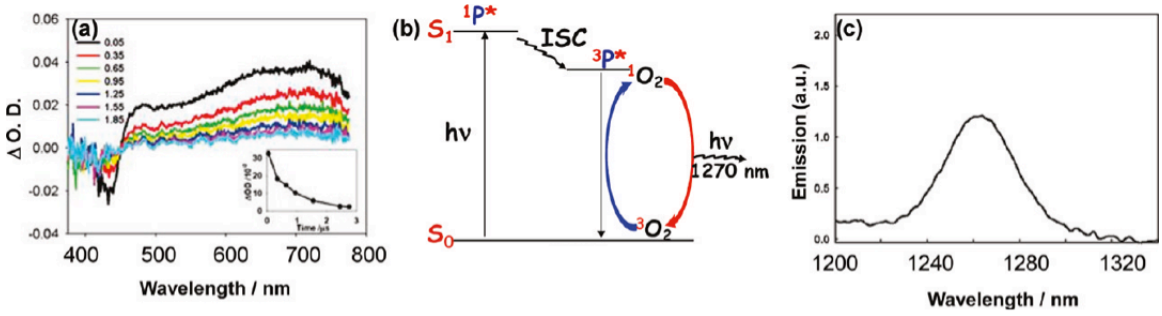


**Figure 1.1**. (a) Transient absorption difference spectra of PPE-DABCO in methanol, (b) schematic representation for the formation of singlet oxygen sensitized by the CPE, and

(c) singlet oxygen emission at λ≈1260 nm sensitized by PPE-DABCO in $CD_3OD$.

Note to figure 1.1: This work has been done in Dr. Kirk S. Schanze's lab at University of Florida. Transient absorption spectroscopy has been used extensively to study the triplet states of cationic CPEs and OPEs. Direct excitation of these PPE-based conjugated materials first produces a singlet excited state that undergoes intersystem crossing with moderate efficiency ($\phi_{isc}$ = 0.05-0.20) to produce a triplet state (triplet exciton). The triplet state is readily detected by transient absorption spectroscopy, in which a long-lived (τ = 5-20 μ s) absorption is observed throughout the visible and into the near infrared region (Figure 1.1a). The triplet of the PPE polymers is sufficiently energetic ($E_T \approx$ 2.0- 2.2 eV) such that it is able to undergo energy transfer to ground state triplet dioxygen leading to efficient production of $^1O_2$ (Figure 1.1b). Evidence that $^1O_2$ is produced is provided by near-infrared photoluminescence spectroscopy carried out with the cationic CPEs or OPEs in air-saturated $CD_3OD$ solution. Here the emission of the $^1O_2$ that is sensitized by the CPE is readily detected by its characteristic emission at 1260 nm (Figure 1.1c). Quantum yield experiments indicate that typical cationic CPEs produce $^1O_2$ with yields in the range from 0.01-0.1 in $CD_3$ OD solution. Modified with permission from ref 12.

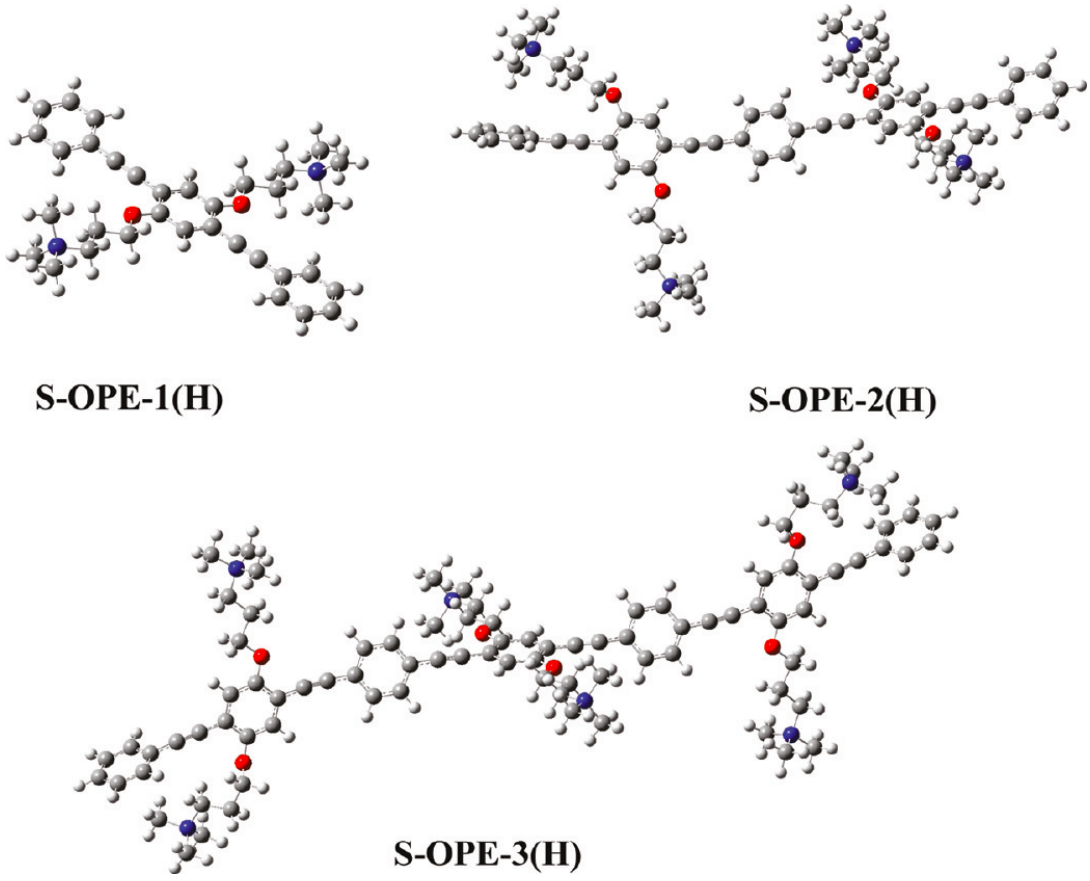


**Figure 1.2**. Computationally optimized structures for the S-OPE-n(H) series. Reprinted with permission from ref 22. Copyright 2011 ACS Publications.

### 1.2.3 Biocidal actives of the CPEs and OPEs

These cationic CPEs and OPEs exhibit significant light-enhanced biocidal activity and

efficient killing efficacy in the dark against a broad spectrum of clinically relevant pathogens, including bacteria, viruses, fungi and spores.[27] Furthermore, most of these materials are convenient to synthesize and amenable to be processed onto different substrates, including layer-by-layer coatings, covalent attachment or non-covalent incorporation into fibers, and capsules, which could greatly expand their applications as antiseptic materials and surfaces for controlling the spread of pathogens.[28-29]

The biocidal activity of a PPE-based conjugated polyelectrolyte was first reported by Lu and co-workers in 2005.[30] PPE-OR8 (Scheme 1.3) functionalized with quaternary ammonium groups has been demonstrated to efficiently bind to the cell envelopes of vegetative Gram-negative bacteria (*Escherichia coli*) and Gram-positive bacterial spores (*Bacillus anthracis, Sterne, B. anthracis*). Upon irradiation with white light, the viabilities of the attached bacteria and spores were significantly reduced.[13] Subsequently, the dark and light-enhanced biocidal activities of a series of CPEs have been investigated and reported.[31-32] It is important to note that light-irradiation alone has very limited toxicity against the model pathogens under our experimental conditions. Since the polymer chain length of the CPEs can not be precisely controlled and these macromolecules often have a broad range of molecular weights, oligomeric OPEs with controlled structures have been synthesized to study the structure-function relationship in their photophysical and biocidal properties.

The antimicrobial activities of the CPE and OPE materials arise from their interactions with the microbial targets, specifically the envelope or capsid of the targets, which are mainly biological assemblies of individual components, such as polysaccharides, proteins and lipids. Disruption of the structures, and thereby functions, of the biological

assemblies is one of the main causes of the inactivation of the microbial targets. In addition, some biomolecules are particularly susceptible to oxidative damages that lead to the loss-of-function. My dissertation work mainly focuses on the antimicrobial activities and mechanisms of cationic CPEs and OPEs with an emphasis on their interactions with the biological molecules and assemblies.

The bactericidal activities of the CPEs and OPEs have been investigated by my colleagues and collaborators.[33] For example, in the dark, most of the tested CPEs and OPEs at 10 μg/mL can significantly reduce the viability of the bacteria, in the presence of UV-irradiation, 0.5-1 μg/mL of the tested materials can almost completely kill the bacteria. The antimicrobial activities and mechanisms against bacteria as well as other model pathogens for the PPE-based materials will be discussed in the following chapters.

Considering the application of these materials, it is important to study their cytotoxicity towards humans and activity against biofilms, which are the most common living form of bacteria in the hospital environment. Our collaborators have tested the cytotoxicity of two OPEs (S-OPE-2(H) and S-OPE-3(H)) with human endothelial and epithelial cell monolayers and human skin tissues.[33] These studies show that, in the dark, S-OPE-2(H) is cytotoxic at 10-50 μg/ml and S-OPE-3(H) is cytotoxic at 50-100 μg/ml against the cell monolayers. In the presence of UV-light, both of the oligomers are toxic at 5-10 μg/ml. The skin irritation tests results further revealed that neither S-OPE-2(H) or S-OPE-3(H) is irritating against human skin under the specific experimental conditions employed in these standardized tests. These studies imply that the CPE and OPE materials show limited toxicity against mammalian cells and tissues at concentrations where they can efficiently kill microbial pathogens. (Note: In the cell monolayer test, the

cytotoxicity for a given test condition is defined as the concentration at which the cell relative viability is less than 70%. Skin irritation is defined as reversible damage to the skin after chemical exposure. If the relative viability of the cell in the shin tissue for a given test condition is greater than 50%, the chemical is considered a non-irritant.)

In most natural and hospital environments, microorganisms exist mainly in the form of biofilms rather than planktonic cells in solution.[34] In biofilms, the microbes are held together by a self-secreted matrix containing polysaccharides, proteins and DNA, which provides structural stability and protection for the microbes in the biofilm. In addition, the metabolic activity in biofilm is not uniform, in that the microbes on the biofilm surface have a high level of metabolic activity and cells in the center have a slow or no growth, and the slow growth rate is one reason for the high resistance of the biofilm microbes against antibiotics.

Recently, the efficacies of a set of oligomeric OPEs in exerting toxicity towards in vitro *E. coli* biofilms have been evaluated by my colleagues.[35] In the dark, all of the tested compounds exhibited better or similar killing abilities against the biofilm compared to the standard antibiotic kanamycin. The minimum biofilm eradication concentration (MBEC) of some of the tested "End-Only" oligomers (EO-OPE-1(DABCO), EO-OPE-1(DABCO Th) and EO-OPE-1(C2)) is in the range of 150-200 μg/ml for 24 h of dark treatment, while the MBEC value for kanamycin is over 1000 μg/ml under the same conditions (Table 1.2). With 1 h of UV-irradiation, the EO-OPEs exhibited significantly enhanced killing efficiency against the biofilm, with the MBEC values decreasing 3- to 4-fold compared to the values of 24 h dark treatment.

It is important to note that the high quantum yield for singlet oxygen generation of EO-

OPE-1 (C2 Th) does not translate to a high killing efficiency against the biofilm, which could be explained by its nonlinear conformation, which may make it difficult for the oligomer to penetrate through the biofilm, and the single positive charge of its quaternary ammonium side groups toward the biofilm as compared to other oligomers bearing the DABCO side groups with two positive charges. (Note: The MBEC is the lowest concentration at which bacteria from a biofilm cannot regrow.)

**Table 1.2**. MBEC values (μg/mL) of the tested oligomers against *E. coli* biofilm.*

| | EO-OPE-1 (DABCO) | EO-OPE-1 (Th, DABCO) | EO-OPE-1 (C2) | EO-OPE-1 (Th, C2) | Kanamycin |
|---|---|---|---|---|---|
| MBEC (dark) | 200 | 150 | 200 | >1000 | >1000 |
| MBEC (light) | 60 | 60 | 70 | 200 | |

*Modified with permission from ref 35. Copyright 2012 ACS Publications.

### 1.3 References


1. Page, K.; Wilson, M.; Parkin, I. P., Antimicrobial surfaces and their potential in reducing the role of the inanimate environment in the incidence of hospital-acquired infections. *J. Mater. Chem.* **2009,** *19* (23), 3819-3831.

2. Hetrick, E. M.; Schoenfisch, M. H., Reducing implant-related infections: active release strategies. *Chem. Soc. Rev.* **2006,** *35* (9), 780-789.

3. Malmsten, M., Antimicrobial and antiviral hydrogels. *Soft Matter* **2011,** *7* (19), 8725-8736.

4. Zasloff, M., Antimicrobial peptides of multicellular organisms. *Nature* **2002,** *415* (6870), 389-395.

5. Laopaiboon, L.; Hall, S. J.; Smith, R. N., The effect of a quaternary ammonium

biocide on the performance and characteristics of laboratory-scale rotating biological contactors. *J. Appl. Microbiol.* **2002,** *93* (6), 1051-1058.

6. Bonomo, R. A., Multiple antibiotic-resistant bacteria in long-term-care facilities: An emerging problem in the practice of infectious diseases. *Clin. Infect. Dis.* **2000,** *31* (6), 1414-1422.

7. Shai, Y., Mode of action of membrane active antimicrobial peptides. *Biopolymers* **2002,** *66* (4), 236-248.

8. Chi, E. Y.; Krishnan, S.; Randolph, T. W.; Carpenter, J. F., Physical stability of proteins in aqueous solution: Mechanism and driving forces in nonnative protein aggregation. *Pharmaceut. Res.* **2003,** *20* (9), 1325-1336.

9. Cleland, J. L.; Powell, M. F.; Shire, S. J., The Development of Stable Protein Formulations - a Close Look at Protein Aggregation, Deamidation, and Oxidation. *Crit. Rev. Ther. Drug* **1993,** *10* (4), 307-377.

10. Wimley, W. C.; Hristova, K., Antimicrobial Peptides: Successes, Challenges and Unanswered Questions. *J. Membrane Biol.* **2011,** *239* (1-2), 27-34.

11. Zaiou, M., Multifunctional antimicrobial peptides: therapeutic targets in several human diseases. *J. Mol. Med.* **2007,** *85* (4), 317-329.

12. Ji, E.; Corbitt, T. S.; Parthasarathy, A.; Schanzes, K. S.; Whitten, D. G., Light and Dark-Activated Biocidal Activity of Conjugated Polyelectrolytes. *ACS Appl. Mater. Interfaces* **2011,** *3* (8), 2820-2829.

13. McDonnell, G.; Russell, A. D., Antiseptics and disinfectants: activity, action, and resistance. *Clin. Microbiol. Rev.* **1999,** *12* (1), 147-79.

14. Cowan, M. K.; Talaro, K. P., *Microbiology: A Systems Approach*. 2 ed.; McGraw-

Hill Science: New York, **2008**.

15. Amro, N. A.; Kotra, L. P.; Wadu-Mesthrige, K.; Bulychev, A.; Mobashery, S.; Liu, G. Y., High-Resolution Atomic Force Microscopy Studies of the Escherichia coli Outer Membrane: Structural Basis for Permeability. *Langmuir* **2000,** *16* (6), 2789-2796.

16. Mckenna, S. M.; Davies, K. J. A., The Inhibition of Bacterial-Growth by Hypochlorous Acid - Possible Role in the Bactericidal Activity of Phagocytes. *Biochem. J.* **1988,** *254* (3), 685-692.

17. Timofeeva, L.; Kleshcheva, N., Antimicrobial polymers: mechanism of action, factors of activity, and applications. *Appl. Microbiol. Biotechnol.* **2011,** *89* (3), 475-92.

18. Kenawy, E. R.; Worley, S. D.; Broughton, R., The chemistry and applications of antimicrobial polymers: A state-of-the-art review. *Biomacromolecules* **2007,** *8* (5), 1359-1384.

19. Pu, K.-Y.; Wang, G.; Liu, B., Design and Synthesis of Conjugated Polyelectrolytes. In *Conjugated Polyelectrolytes*, Wiley-VCH Verlag GmbH & Co. KGaA: **2012**; pp 1-64.

20. Bunz, U. H. F., Poly(aryleneethynylene)s: Syntheses, properties, structures, and applications. *Chem. Rev.* **2000,** *100* (4), 1605-1644.

21. Zhao, X. Y.; Pinto, M. R.; Hardison, L. M.; Mwaura, J.; Muller, J.; Jiang, H.; Witker, D.; Kleiman, V. D.; Reynolds, J. R.; Schanze, K. S., Variable band gap poly(arylene ethynylene) conjugated polyelectrolytes. *Macromolecules* **2006,** *39* (19), 6355-6366.

22. Tang, Y. L.; Hill, E. H.; Zhou, Z. J.; Evans, D. G.; Schanze, K. S.; Whitten, D. G., Synthesis, Self-Assembly, and Photophysical Properties of Cationic Oligo(p-

phenyleneethynylene)s. *Langmuir* **2011,** *27* (8), 4945-4955.

23. Zhou, Z. J.; Corbitt, T. S.; Parthasarathy, A.; Tang, Y. L.; Ista, L. F.; Schanze, K. S.; Whitten, D. G., "End-Only" Functionalized Oligo(phenylene ethynylene)s: Synthesis, Photophysical and Biocidal Activity. *J. Phys. Chem. Lett.* **2010,** *1* (21), 3207-3212.

24. Wang, Y.; Zhou, Z. J.; Zhu, J. S.; Tang, Y.; Canady, T. D.; Chi, E. Y.; Schanze, K. S.; Whitten, D. G., Dark Antimicrobial Mechanisms of Cationic Phenylene Ethynylene Polymers and Oligomers against Escherichia coli. *Polymers* **2011,** *3*, 1199-1214.

25. Tang, Y. L.; Achyuthan, K. E.; Whitten, D. G., Label-free and Real-Time Sequence Specific DNA Detection Based on Supramolecular Self-assembly. *Langmuir* **2010,** *26* (9), 6832-6837.

26. Wang, Y.; Jones, E. M.; Tang, Y. L.; Ji, E. K.; Lopez, G. P.; Chi, E. Y.; Schanze, K. S.; Whitten, D. G., Effect of Polymer Chain Length on Membrane Perturbation Activity of Cationic Phenylene Ethynylene Oligomers and Polymers. *Langmuir* **2011,** *27* (17), 10770-10775.

27. Wang, Y.; Schanze, K. S.; Chi, E. Y.; Whitten, D. G., When Worlds Collide: Interactions at the Interface between Biological Systems and Synthetic Cationic Conjugated Polyelectrolytes and Oligomers. *Langmuir* **2013**, web ASAP.

28. Ista, L. K.; Dascier, D.; Ji, E.; Parthasarathy, A.; Corbitt, T. S.; Schanze, K. S.; WhittenII-, D. G., Conjugated-Polyelectrolyte-Grafted Cotton Fibers Act as "Micro Flypaper" for the Removal and Destruction of Bacteria. *ACS Appl. Mater. Interfaces* **2011,** *3* (8), 2932-2937.

29. Corbitt, T. S.; Sommer, J. R.; Chemburu, S.; Ogawa, K.; Ista, L. K.; Lopez, G. P.; Whitten, D. G.; Schanze, K. S., Conjugated Polyelectrolyte Capsules: Light-Activated

Antimicrobial Micro "Roach Motels". *ACS Appl. Mater. Interfaces* **2009,** *1* (1), 48-52.

30. Lu, L.; Rininsland, F. H.; Wittenburg, S. K.; Achyuthan, K. E.; McBranch, D. W.; Whitten, D. G., Biocidal activity of a light-absorbing fluorescent conjugated polyelectrolyte. *Langmuir* **2005,** *21* (22), 10154-9.

31. Chemburu, S.; Corbitt, T. S.; Ista, L. K.; Ji, E.; Fulghum, J.; Lopez, G. P.; Ogawa, K.; Schanze, K. S.; Whitten, D. G., Light-induced biocidal action of conjugated polyelectrolytes supported on colloids. *Langmuir* **2008,** *24* (19), 11053-11062.

32. Corbitt, T. S.; Ding, L. P.; Ji, E. Y.; Ista, L. K.; Ogawa, K.; Lopez, G. P.; Schanze, K. S.; Whitten, D. G., Light and dark biocidal activity of cationic poly(arylene ethynylene) conjugated polyelectrolytes. *Photochem. Photobiol. Sci.* **2009,** *8* (7), 998-1005.

33. Corbitt, T. S.; Ji, E.; Wang, Y.; Parthasarathy, A.; Wilde, K. N.; Hill, E. H.; Dascier, D.; Canavan, H. E.; Chi, E. Y.; Schanze, K. S.; Whitten, D. G., Conjugated Polyelectrolyte-Based Biocide Applications. In *Conjugated Polyelectrolytes*, Wiley-VCH Verlag GmbH & Co. KGaA: **2012**; pp 263-294.

34. Bryers, J. D., Medical Biofilms. *Biotechnol. Bioeng.* **2008,** *100* (1), 1-18.

35. Dascier, D.; Ji, E.; Parthasarathy, A.; Schanze, K. S.; Whitten, D. G., Efficacy of End-Only-Functionalized Oligo(arylene-ethynylene)s in Killing Bacterial Biofilms. *Langmuir* **2012,** *28* (31), 11286-11290.

# Chapter 2 Materials and Methods

## 2.1 Materials

The antimicrobial molecules (Scheme 1.3) used in this dissertation were synthesized as reported.[1-4] The concentrations of CPEs used in this study are based on repeat units and the concentrations of OPEs used in this study are molar concentrations. 1,2-dioleoyl-*sn*-glycero-3-phospho-(1'-*rac*-glycerol) (sodium salt) (DOPG) (Scheme 2.1), 1,2-dioleoyl-*sn*-glycero-3-phosphocholine (DOPC), 1,2-dioleoyl-*sn*-glycero-3-phosphoethanolamine (DOPE), 1,2-dipalmitoyl-*sn*-glycero-3-phospho-(1'-*rac*-glycerol) (sodium salt) (DPPG), 1,2-dihexadecanoyl-sn-glycero-3-phosphoethanolamine (DPPE), *E. coli* total lipid, cholesterol and lipid vesicle extrusion supplies were purchased from Avanti Polar Lipids (Alabaster, AL) and used as received. 5(6)-carboxyfluorescein (hereafter referred to as fluorescein) was purchased from Sigma-Aldrich (St. Louis, MO). Superfine Sephadex G-25 was obtained from GE Healthcare Bio-Science (Piscataway, NJ). Luria broth (LB) and agar were purchased from BD Biosciences (Franklin Lakes, NJ). Bacteriophages MS2 and T4 were obtained from the American Type Culture Collection (ATCC, Manassas, VA) along with their host bacteria, *E. coli* ATCC 15597 and *E. coli* ATCC 11303. *E. coli* strain ATCC 11303 and ATCC 29425, *Staphylococcus epidermidis* (*S. epi*) ATCC 14990, *Saccharomyces cerevisiae* (*S. cerevisiae*) strains ATCC 9763 and 204722 were also obtained from American Type Culture Collection (ATCC, Manassas, VA). The *P. aeruginosa* strain PAO1 was a generous gift from Dr. Tim Tolker-Nielsen. All other chemicals were purchased from Sigma-Aldrich or Alfa Aesar. Ultrapure water was used throughout the study (Milli-Q, 18.2 MΩ $cm^{-1}$ resistivity).

## 2.2 Multi-scale membrane tests

### 2.2.1 Preparation of fluorescein-loaded vesicles and vesicle leakage assays

Fluorescein-loaded large unilamellar vesicles (LUV) were prepared by extrusion.[5] Briefly, a phospholipid stock solution was dried under a flow of nitrogen and then placed under vacuum overnight. The dried lipid film was then hydrated to 2-4 mM with 100 mM fluorescein in water (adjusted to pH 7 with NaOH) with strong shaking for 1 hr at a temperature above the phase transition temperature of the lipid. The resulting suspension was subjected to 4 freeze-thaw cycles. Finally, LUVs were formed by extruding the lipid solution 19 times through a 100 nm pore size polycarbonate membrane using a mini-extruder (Avanti Polar Lipids). Free fluorescein was removed from the dye-loaded vesicles by column filtration (Sephadex G-25 superfine). The mobile phase used was 200 mM NaCl containing 10 mM HEPES at pH 7 (Buffer A). After separation, the phospholipid concentration of the dye-loaded vesicles was determined by the modified microprocedure of Barlett.[6] The hydrodynamic radii ($R_h$) of vesicles were determined by dynamic light scattering (DLS, DAWN HELEOS II, Wyatt Technology Corporation).[5]

**Scheme 2.1** Structures and phase transition temperatures ($T_m$) of lipids.[7]

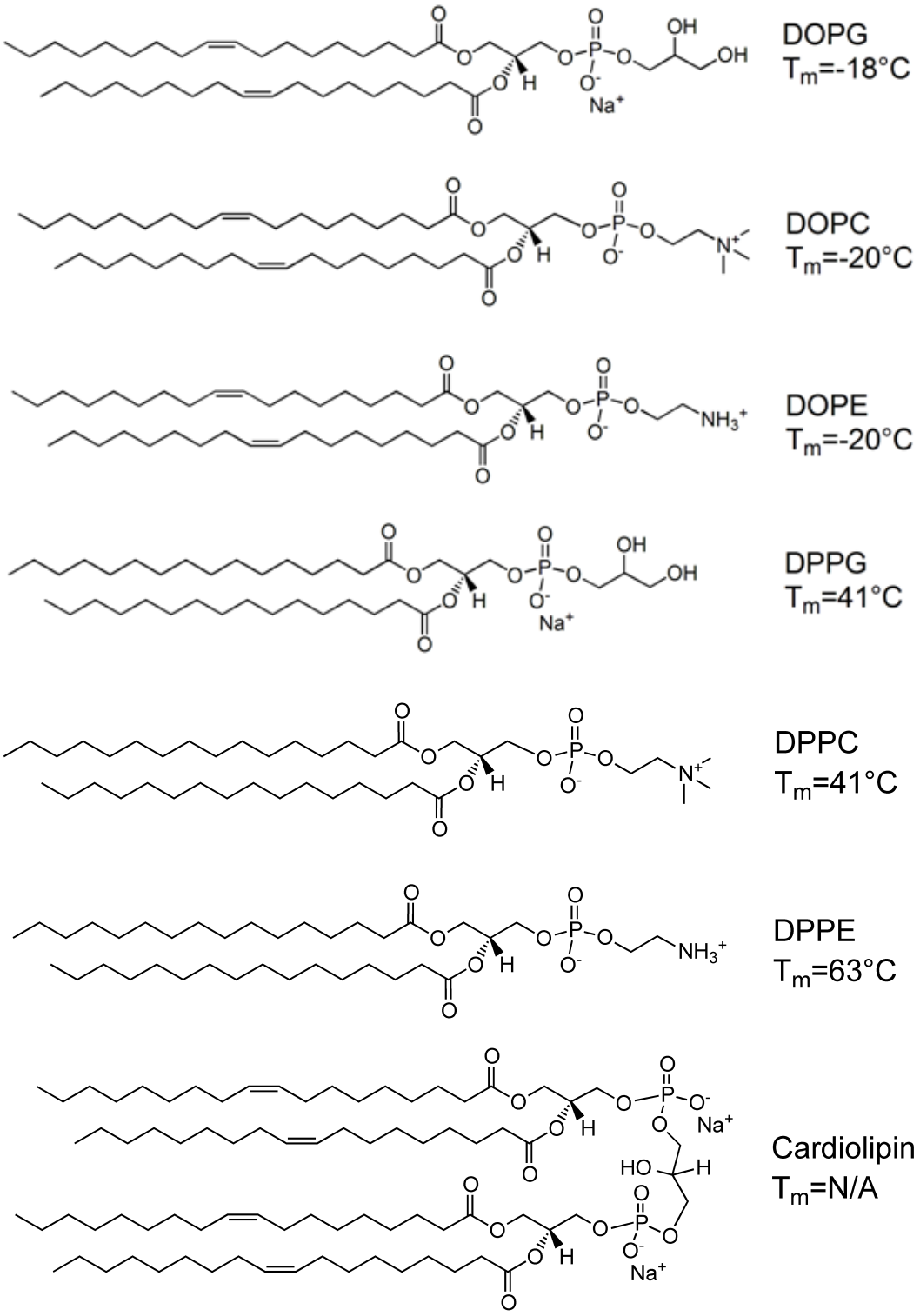


*E. coli* total lipid extract component (wt/wt%):
PE 57.5%, PG 15.1%, Cardiolipin 9.8%, Unknown 17.6%, $T_m$ N/A

Vesicle membrane stability in the presence of CPE/OPE was evaluated by a dye-release assay.[5] CPE or OPE was added to the dye-loaded vesicles at a (CPE/OPE):lipid molar ratio of 1:50 with a final lipid concentration between 0.2-0.3 mM. As the vesicle membrane is perturbed by the CPE or OPE, dye is released and the fluorescence intensity of the released dye was recorded at 520 nm (excitation at 485 nm) (SpectroMax M-5 microplate reader, Molecular Devices).[5] The CPE/OPE are not excited at this wavelength. Fluorescein leakage was calculated using equation (1):

$$Fluorescein\ Leakage = \frac{F - F_0}{F_{\max} - F_0} \quad (1)$$

where $F_0$ is the fluorescence intensity of the vesicles before the addition of CPE/OPE, $F$ is the fluorescence intensity of the sample after the addition of CPE/OPE, and $F_{max}$ is the maximum fluorescence intensity of the sample, achieved by the addition of 1 μL 0.5 M Triton-X100 solution to 100 μL of vesicles that caused complete lysis of the vesicles. Fluorescein leakage is taken as a measure of the extent of vesicle membrane disruption and all experiments were carried out at room temperature.

### 2.2.2 Photophysical measurements of the CPE/OPE-lipid complexes

The large unilamellar vesicles (LUVs) were made in pure water by an extrusion procedure as described previously.[5] The vesicle and CPE/OPE mixtures were prepared in pure water and kept at a lipid to CPE/OPE molar ratio of 50:1. The final lipid concentration was 0.2 mM. To assess changes in the compounds' conjugation lengths, absorbance spectra were measured using a microplate reader (SpectroMax M-5 microplate reader, Molecular Devices, Sunnyvale, CA). To assess changes in the

hydrophobicity of the compounds' microenvironments, emission spectra were recorded by a spectrofluorometer (QuantaMaster™ 50 spectrofluorometer, Photon Technology International, Birmingham, NJ).

### 2.2.3 Lipid monolayer insertion assays

Insertion of a CPE or an OPE into lipid monolayers held at a constant surface pressure were measured using a Teflon Langmuir trough equipped with a Wilhelmy plate and two identical mobile Delrin barriers (MicroMini Trough System, KSV Instruments Ltd., Finland).[8] The water subphase volume was 50 mL and the maximal working surface area was 100 $cm^2$. Phospholipids dissolved in a 7:3 chloroform:methanol mixture were first spread at the air-water interface. The deposited lipids were left undisturbed for 15 minutes to allow the complete evaporation of the organic solvent. The lipids were then compressed to a target surface pressure ($\pi$) of 30 mN/m, a bilayer equivalent pressure,[9] and the surface pressure was kept constant via a feedback loop. An aliquot of CPE or OPE was then injected into the water subphase using a micro-syringe without disturbing the monolayer. The final concentration of CPE or OPE in the subphase was 0.1 μM. All experiments were carried out at room temperature. Favorable interactions between the CPE or OPE that led to the insertion of the compound into the lipid monolayer caused an expansion of the lipid monolayer surface area at constant pressure. Percentage of surface area increase was calculated using the following equation:

$$Percentage\ of\ Area\ Increase = \frac{A - A_\circ}{A_\circ} \times 100\% \quad (2)$$

where $A_0$ is the trough area before the injection of CPE/OPE, $A$ is the trough area at time t after the addition of the CPE or OPE.

### 2.2.4 Formation and observation of giant vesicles

Giant vesicles were prepared and observed by a method modified from the literature.[10-11] Lipid mixtures (***E. coli* Total Lipids extract**, 1,2-dimyristoyl-sn-glycero-3-phosphoethanolamine-N-(lissamine rhodamine B sulfonyl) (ammonium salt) (**DMPE-Rh**) and 1,2-distearoyl-sn-glycero-3-phosphoethanolamine-N-(biotinyl(polyethylene glycol)-2000) (ammonium salt) (**Biotin-PEG-DSPE**) at molar ratio 97:0.5:2.5 respectively) or DOPE and DOPG at molar ration 80:20 were dissolved in chloroform, dried, and rehydrated with 10 mM 2-[4-(2-hydroxyethyl)-1-piperazinyl]ethanesulfonic acid (HEPES, pH 7.4) to a final concentration of 0.33 mg/ml at 37°C for 2 hours. The observation microchambers (internal volume ~100 μL) were made by microscope slides and cover slips, and sealed with double-side tape. The microchamber was incubated with neutravidin solution (0.1 mg/ml in 10 mM HEPES) for 15 min. After rinsing with the HEPES buffer, the microchamber was incubated with giant vesicle solution for 5 min and then rinsed again to remove unattached vesicles. A 2 μL aliquot of CPEs or OPEs (50 μg/mL for the OPEs and 10 μg/mL for the CPEs in 10 mM HEPES) were added to the chamber. The immobilized vesicle was then imaged by a fluorescence microscope (Zeiss Imager A2, Excitation filter BP 545/25 nm, Emission filter BP 605/70 nm, Thornwood, NY).

### 2.2.5 Small angle X-Ray scattering (SAXS)

SAXS experiments were carried out at the Stanford Synchrotron Radiation Laboratory (Palo Alto, CA) (BL4–2) as described in literature.[12] Briefly, *E. coli* total lipid extract or mixed 8:2 (molar ratio) DOPE:DOPG lipids were dissolved in chloroform, dried, and

rehydrated with Millipore water to a final concentration of 25 mg/ml at room temperature. The vesicle solutions were sonicated for an hour in ice-water bath and extruded through a 100 nm polycarbonate membrane (Avanti) to make small unilamellar vesicles (SUV). CPEs and OPEs were prepared in water (EO-OPEs was prepared in 10% DMSO in water) and mixed with the SUVs at various CPE/OPE-to-lipid molar ratios. SAXS data were collected using 11-keV x-rays.

### 2.2.6 NMR spectroscopy

$^{31}$P solid-state NMR spectra were recorded on a Bruker Avance III Widebore 300 NMR spectrometer as described in the literature.[13] The reported Hahn echo pulse sequence was used in the current study. The NMR samples were prepared by hydrating a 25 mg dry phospholipid film with 100 μL water or EO-OPE-1(C3) solution at appropriate concentrations by vigorous vortexing. In order to thoroughly hydrate the lipid sample and mix the test compounds with lipid membrane, the samples were subjected to 10 freeze-thaw-vortex cycles. 7 mm CPMASS probe was used in the NMR spectroscopy.

### 2.2.7 Cryo-TEM

Cryo-TEM imaging was performed by a modified method from the literature[14] at the Scripps Research Institute. Large unilamellar vesicles (LUV) composed of DOPE:DOPG (8:2, molar ratio) were made by an sonication-extrusion method to a final concentration of 10 mg/ml in water at room temperature and mixed with the CPEs or OPEs at various molar ratios. A 3 μL aliquot of each sample was applied to the grid (Protochips, Raleigh, NC, CF-2/0.5-4C) and then vitrified in liquid ethane using a Vitrobot (FEI Company, Hillsboro, Oregon). Cryo-TEM imaging was carried out on an FEI TF20 microscope

operating at a low lose, 200 kV condition using a Gatan cryo-transfer holder and the Leginon data collection software.[15]

### 2.3 Pathogen culture and biocidal tests

#### 2.3.1 Bacterial growth conditions

All bacterial cells were grown in Luria broth (LB) and *E. coli* BL21(DE3)pLysS was grown in Luria broth with carbenicillin and chloramphenicol at concentrations of 50 and 34 μg/ml, respectively. A fresh bacterial culture was inoculated from an overnight culture followed by approximately three hours of incubation at 37℃ to the exponential growth phase ($O.D._{600}$~0.5-0.8). At this growth phase, the bacterial cells were collected by centrifugation and washed twice with 10 mM PBS (138 mM NaCl and 2.7 mM KCl at pH 7.4). The cell pellet was resuspended with PBS buffer to $O.D._{600}$~0.5.

The *P. aeruginosa* cells were prepared in a chemostat.[16] Prior to inoculation into a chemostat, a single colony from a nutrient agar slant was inoculated into fresh of nutrient broth (NB) and grown overnight. A chemostat culture was established by inoculating the overnight culture into citrate minimal medium. The chemostat was maintained at a flow rate of 1.0 mL $min^{-1}$ with constant stirring. The concentration of the chemostat culture was maintained at $10^7$ /mL cells.

#### 2.3.2 Yeast strains and culture conditions

*S. cerevisiae* (ATCC 9763) vegetative cells were grown in YPD medium (1% Yeast extract, 2% Peptone and 2% Glucose). A fresh yeast culture was inoculated from an overnight culture and incubated for varying periods at 30°C to obtain different growth phases. Yeast cells were collected by centrifugation and washed twice with PBS buffer

(10 mM sodium phosphate, 138 mM NaCl, and 2.7 mM KCl at pH 7.4). The cell pellet was resuspended with PBS buffer to $O.D._{600}$ ~ 1.0. A highly sporulated yeast strain (ATCC 204722) was used to prepare ascospores/asci. The yeast cells were first grown in the YPAD medium (1% Yeast extract, 2% Peptone, 0.04% Adenine sulfate and 2% Glucose) overnight at room temperature. The recovered cells at exponential phase were pelleted, washed with PBS and then prepared for sporulation on an acetate agar (0.1% glucose, 0.18% KCl, 0.25% yeast extract, 0.82% sodium acetate · $3H_2O$ and 1.5% agar) for one week. The harvested asci were washed, briefly sonicated and resuspended in PBS to $O.D._{600}$ ~ 1.2. The germinated asci or spores were prepared via incubating with the germination solution (2% glucose and 0.37% $NH_4Cl$) for 20 hours at room temperature.

### 2.3.3 Antifungal activity

A sample consisting of 10 μg/ml of the CPEs, OPEs, or Amphotericin B (AmB) were used for the antifungal test against *S. cerevisiae* vegetative cells (ATCC 9763). The yeast cell solutions were incubated with the biocidal agents at 30°C in the dark with continuous shaking for 60 min. The UV-light irradiation experiments were carried out in a photoreactor (4 UV-lamps, LZC-ORG, Luzchem Research Inc., Ottawa, Canada) at room temperature for 30 min (Figure 2.1A). Two irradiation sources were employed based on the different light-absorbing properties of the CPEs and OPEs. LZC-420 (centered at ~420 nm) and UVA (centered at ~350 nm) were used to irradiate CPEs and OPEs, respectively. The sporicidal activity of the CPEs and OPEs (30 μg/ml) were evaluated against the asci (ATCC 204722) with or without germination in the dark or under UV-irradiation (10 lamps in the photoreactor) for 60 min (Figure 2.1B). The ability of a CPE or an OPE to inactivate vegetative cells and spores was determined by the plate

counting method and was calculated as log ($N_o$/N), where N is the number of colony forming units (CFU) of the yeast solution after exposure to a CPE or an OPE and $N_o$ is the CFU of a control (without biocidal material or UV-irradiation). The Log CFU reductions caused by the biocidal treatments relative to the control are reported. The reported values and errors were averages and standard deviations of duplicate measurements, respectively.

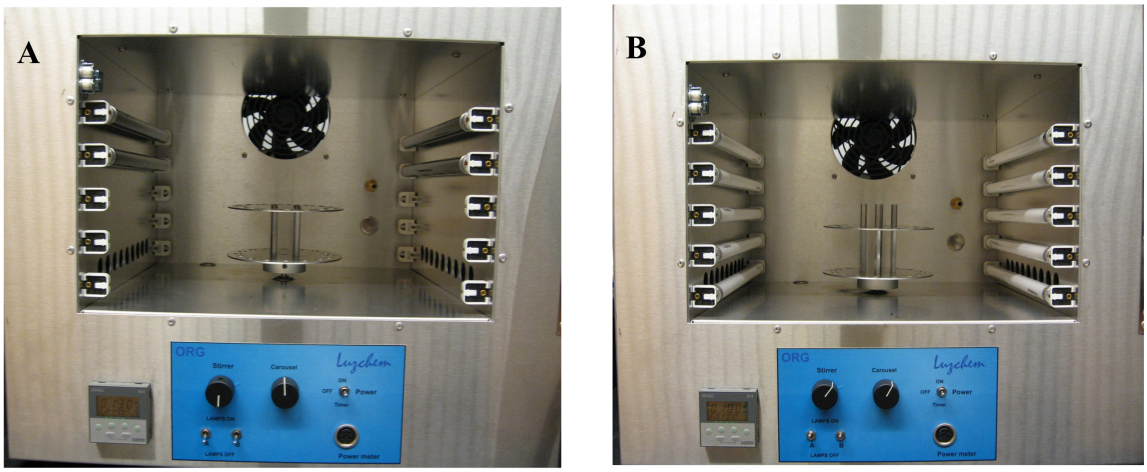


**Figure 2.1**. Typical photoreactor setups with 4 lamps (A) and 10 lamps (B).

### 2.3.4 Bacteriophage preparation and titer

*E. coli* host cells were grown in LB. The fresh *E. coli* culture was inoculated from an overnight culture followed by approximately three hours of incubation at 37℃ to the exponential growth phase ($O.D._{600}$~0.5). *E. coli* cells were then collected by centrifugation and washed twice with *E. coli* minimal medium (glucose 28 mM, $Na_2HPO_4$ 42 mM, $KH_2PO_4$ 22 mM, $NH_4Cl$ 18.7 mM, NaCl 8.5 mM, $MgSO_4$ 1 mM, and $CaCl_2$ 0.09 mM at pH 7.2) . The cell pellet was then resuspended in the minimal medium. An aliquot of phage stock solution was added to the corresponding bacterial host suspension and the phage-bacteria mixture was incubated for 15 min at 37 °C. The

mixture was then transferred into fresh *E. coli* minimal medium and incubated overnight for viral replication and cell lysis. The phage solution was then centrifuged at 3500 rpm for 30 min, and the supernatant was filtered using 0.22-μm filters to remove unlysed bacteria and bacterial debris. The phage titer was determined by plaque forming units (PFU). Briefly, *E. coli* cells in the exponential growth phase (ATCC 15597 and 11303 for MS2 and T4 bacteriophage, respectively) were incubated with the various dilutions of the phage solution for 15 min at 37 °C and then transferred into molten soft LB agar with gentle mixing. The soft agar mixture was then poured onto pre-solidified LB plates. After incubation for 6-8 hrs, the numbers of PFU were counted and phage solutions were diluted to $10^6$ ~$10^7$ PFU/ml with the minimal medium for further use.

### 2.3.5 Phage inactivation

CPE and OPE solutions (10 μg/ml) were incubated with virus solutions in the dark or under UV-light for 1 hour. The UV-light irradiation experiments were carried out in a photoreactor (10-lamps, LZC-ORG, Luzchem Research Inc., Ottawa, Canada). Two illumination sources were employed due to the different light-absorbing properties of the CPEs and OPEs. The viral inactivation ability of a CPE or an OPE was determined by phage titer as described in the previous section and calculated as log ($N_o$/N), where N is the PFU of the phage solution after exposure to a CPE or an OPE and $N_o$ is the PFU of a control (without CPEs, OPEs, or UV-irradiation). Log ($N_o$/N) reduced by the different treatments compared to control are reported. The reported values were averages of duplicate measurements.

### 2.4 Biocidal mechanism investigation

#### 2.4.1 Destruction of bacterial cell walls and membranes

An aliquot of pathogen suspension (~$10^{6-8}$ colony forming units (CFU)/mL) was mixed with 10 μg/ml CPEs, OPEs or melittin followed by incubation at 37℃ for various periods in the dark or under UV-irradiation. The mixture of the pathogen cells and antimicrobial material was centrifuged at 3,000-10,000 rpm for 10 minutes to collect the samples.

The supernatant of the *E. coli* samples were decanted and its absorbance at 260 nm was measured (300 μL for the 96-well plate on the SpectroMax M2e microplate reader, Molecular Devices, Sunnyvale, CA). The UV-light irradiation experiments were carried out in a photoreactor (10 lamps, LZC-ORG, Luzchem Research Inc., Ottawa, Canada) at room temperature as described before.

The cell pellets were resuspended with 2% glutaraldehyde and incubated at 4 °C for three hours to preserve the interface between pathogen cells and antimicrobial compounds, followed by washing with PBS buffer. Then, the fixed cells were dehydrated by sequential treatment with increasing concentrations of ethanol for 15 minutes and dehydrated with absolute ethanol twice. The dehydrated samples were dried at room temperature and transferred onto a piece of clean silicon wafer. The dried samples were sputtercoated with 10 nm thick gold/palladium. Morphologies of the bacterial cells were observed by SEM (Quanta 3D, Dual beam FEGSEM/FIB, FEI, Hillsboro, OR). For TEM imaging, cell pellets were fixed with 2% glutaraldehyde for one day and then 1% osmium tetroxide for one hour at room temperature. The samples were dehydrated by sequential treatment with increasing concentrations of ethanol. Then, the cells were embedded in resin (Spurr's resin kit, Electron Microscopy Sciences, Hatfield, PA), sectioned and

imaged by TEM (Hitachi H7500, Tokyo, Japan).

*E. coli* (ATCC 29425) and PAO1 cells (~$10^8$/ml) were incubated with OPE-1 (42.5 μg/ml) for 60 min in 0.85% NaCl sterile solution and kept in the dark. Then, the samples were stained with SYTO 60/SYTOX Green[21] (Molecular Probes, Carlsbad, CA) and examined by Laser Scanning Confocal Microscope (Zeiss LSM 510 Meta, Thornwood, NY) as described previously.

### 2.4.2 Bacterial cytoplasmic membrane permeability assay

Cytoplasmic membrane permeabilization caused by the addition of CPE compounds and melittin was determined by a modified protocol from literature.[17] The *E. coli* cells are first diluted to $10^7$ CFU/ml with the HEPES buffer (5 mM HEPES and 5 mM glucose at pH 7.2) followed by the addition of the membrane potential-sensitive cyanine dye diSC3-5 to a final concentration of 0.4 μM. The mixture of E. coli cells and diSC3-5 was incubated in the dark for one hour. Then 100 mM KCl and various amounts of OPEs or melittin were added to the *E. coli* suspensions and incubated for another 30 minutes in the dark. Emission intensity of diSC3-5 was recorded by a spectrofluorometer at 674 nm (QuantaMaster 50 spectrofluorometer, Photon Technology International, Birmingham, NJ) with an excitation wavelength of 651 nm. A negative control sample was also prepared by incubating *E. coli* cells with the dye. The fluorescent intensity of this control was used as background. The membrane permeability assays were run in duplicates and the measurements were reproducible. Since the CPEs can strongly influence the fluorescence of diSC3-5, the effect of CPEs on membrane permeability was not determined.

### 2.4.3 Circular dichroism tests on model proteins

An aliquot of a CPE or OPE was added to 3 mL of 0.1 mg/mL model protein solution in 10 mM phosphate buffer (2 mM $NaH_2PO_4$ and 8 mM $Na_2HPO_4$ at pH 7.4) and incubated at 37℃ for one hour in the dark. The final concentration of CPE or OPE was 10 μg/mL. Circular dichroism spectra from 200 to 500 nm were recorded on an Aviv CD spectrometer (Model 420, Aviv Biomedical Inc.) in quartz cuvettes at room temperature.

### 2.4.4 Minimum inhibitory concentration (MIC) determination against bacteria

MIC values were determined by a modified method from literature.[18-19] The *E. coli* and PAO1 cells were diluted with the minimal medium (28 mM glucose, 42 mM $Na_2HPO_4$, 22 mM $KH_2PO_4$, 18.7 mM $NH_4Cl$, 8.5 mM NaCl, 1 mM $MgSO_4$, and 0.09 mM $CaCl_2$ at pH 7.2. 50 μg/ml carbenicillin and 34 μg/ml chloramphenicol were added to the medium for *E. coli* BL21(DE3)pLysS) to ~$10^5$ CFU/ml. The diluted cell solutions were then incubated with twofold serial dilutions of the antimicrobial compounds in a 96-well plate at 37℃ overnight. $O.D._{600}$ was obtained on a microplate reader (SpectroMax M2e, Molecular Devices, Sunnyvale, CA) to monitor cell growth. The MIC values ($MIC_{90}$) reported herein are the minimum concentrations needed to inhibit 90% of the cell growth. Positive controls without antimicrobial compounds and negative controls without bacteria were also measured. The reported values are the averages of duplicate measurements.

### 2.4.5 Hemolysis assay

The hemolytic activities of CPEs, OPEs and melittin were determined by the release of hemoglobin from human red blood cells (RBCs) when incubated with the antimicrobial

compounds.[19-20] Fresh human RBCs were obtained by centrifuging human whole blood at 2,000*g* for 5 min and washed with Tris buffer (10 mM Tris and 150 mM NaCl at pH 7.2). A RBC stock solution was made by a 200-fold dilution of the RBC suspension (0.5% red blood cell) with the Tris buffer. The RBC stock solutions along with various amounts of the antimicrobial compounds were incubated at 37℃ for 1 hour in microcentrifugation tubes. Then, the mixtures were centrifuged at 3500*g* for 10 minutes. 100 μL aliquots of the supernatant were transferred to a 96-well plate and mixed with 100 μL of Tris buffer. The hemolytic concentrations ($HC_{50}$, concentrations of antimicrobial compounds that caused 50% cell hemolysis) were determined by measuring the absorbance of hemoglobins at 540 nm using a microplate reader (SpectroMax M5, Molecular Devices, Sunnyvale, CA). A positive control of cells incubated with 1% Triton-X100 was also prepared. A negative control of the RBC solution without antimicrobial compounds was also prepared. The reported values were the averages of duplicate measurements.

**2.4.6 Protein SDS-PAGE and DNA electrophoresis**

SDS-PAGE and DNA electrophoretic methods were used to characterize protein and DNA damage in *E. coli* cells. Fresh *E. coli* cells in exponential growth phase ($4\times10^8$ CFU/mL) were incubated with 25 μg/ml EO-OPE-1(C3) in PBS in the dark or under UV irradiation for 1 hour. A 12 μL aliquot of each *E. coli* sample was mixed with 6 μL of 3X standard SDS-PAGE sample loading buffer and heated in boiling water for 10 min followed by centrifugation. The supernate of denatured cell samples was loaded directly onto the 12% precast polyacrylamide-gel (BIO-RAD, 456-1043S). Electrophoresis was performed at 200 V for approximately 30 min, after which the gel was stained with Coomassie brilliant blue R. For DNA electrophoresis, fresh bacterial cells (*E. coli*

BL21(DE3), $1\times10^8$ CFU/mL) were incubated with 1 μg/mL EO-OPE-1(C3) in PBS in the dark or under UV irradiation for 1 hour. The plasmid DNA was extracted from each bacterial sample using a Miniprep Kit (QIAGEN Inc., Valencia, CA) according to the manufacturer's manual. A 10 μL aliquot of each plasmid sample was mixed with 2 μL of 6X loading buffer and loaded onto a 1% agarose-gel. Electrophoresis was carried out at 100 V for approximately 40 min.

### 2.4.7 Yeast cell SEM imaging

Samples for ultrastructural examination were prepared as described above. For SEM imaging, cell pellets were resuspended in 2.5% glutaraldehyde and incubated at room temperature overnight to preserve the interface between the cells and antimicrobial agents, followed by washing with PBS buffer. Fixed cells were dehydrated by sequential treatment with increasing concentrations of ethanol for 30 minutes. The dehydrated samples were dried at room temperature and sputtercoated with ~12 nm thick gold/palladium. Samples were observed by SEM (Quanta 3D, Dual beam FEGSEM/FIB, FEI, Hillsboro, OR).

### 2.4.8 Phage TEM imaging

High concentrations of the viruses (~$10^{11}$ PFU/ml for T4 and ~$10^{12}$ PFU/ml for MS2) and CPE or OPE (50 μg/ml) were used for TEM imaging (Hitachi H7500, Tokyo, Japan). The same phage inactivation protocol was used as described in the previous section. Samples (5 μL) were applied to freshly cleaned carbon-coated copper grids, washed with pure water, and negatively stained with 2% uranyl acetate for 2 min. The grids were then dried in air and imaged at 70-100K fold magnification with 200μm condenser aperture

and 20μm objective aperture.

### 2.4.9 Phage SDS-PAGE

SDS-PAGE method was used to characterize MS2 phage capsid protein cleavage.[21] One liter MS2 phage was prepared as described above and purified according to a modified protocol.[22-23] Briefly, the purification of MS2 phage particle was performed by separating unlysed *E. coli* cells and cell debris by centrifugation followed by poly(ethylene glycol)-8000 (PEG-8000)/NaCl selective precipitation. After an overnight incubation at 4°C, the fine precipitates were collected by centrifugation at 18,000 rcf for 1 hr at 4 °C. The pellet was collected and resuspended in TNM buffer (10 mM Tris, 100 mM NaCl and 0.1 mM $MgCl_2$ at pH 7.4). The phage suspension was passed through a 0.22-μm filter, and the filtrate was concentrated by an Amicon centrifuge filter with a molecular weight cut-off of 30000 (Millipore, Billerica, MA). Further purification of the phage particles was accomplished by Sepharose CL-4B (Sigma) column to remove residual PEG-8000, DNA, and RNA from the host cells. Then, the purified phage solution was incubated with EO-OPE-1(Th) under UV light or in the dark for 1 hour. 20 μl of the inactivated phage sample was mixed with 10 μl of 3X standard SDS-PAGE sample loading buffer and heated in boiling water for 2 min. The denatured virus samples were loaded directly onto the gels. Electrophoresis was performed at 30 mA for approximately 1 hour, after which the gel was stained with either silver (Silver Stain Plus Kit, Bio-Rad) or Coomassie brilliant blue R.

## 2.5 References

1. Zhao, X. Y.; Pinto, M. R.; Hardison, L. M.; Mwaura, J.; Muller, J.; Jiang, H.;

Witker, D.; Kleiman, V. D.; Reynolds, J. R.; Schanze, K. S., Variable band gap poly(arylene ethynylene) conjugated polyelectrolytes. *Macromolecules* **2006,** *39* (19), 6355-6366.

2. Tang, Y. L.; Hill, E. H.; Zhou, Z. J.; Evans, D. G.; Schanze, K. S.; Whitten, D. G., Synthesis, Self-Assembly, and Photophysical Properties of Cationic Oligo(p-phenyleneethynylene)s. *Langmuir* **2011,** *27* (8), 4945-4955.

3. Zhou, Z. J.; Corbitt, T. S.; Parthasarathy, A.; Tang, Y. L.; Ista, L. F.; Schanze, K. S.; Whitten, D. G., "End-Only" Functionalized Oligo(phenylene ethynylene)s: Synthesis, Photophysical and Biocidal Activity. *J. Phys. Chem. Lett.* **2010,** *1* (21), 3207-3212.

4. Ji, E. K.; Parthasarathy, A.; Corbitt, T. S.; Schanze, K. S.; Whitten, D. G., Antibacterial Activity of Conjugated Polyelectrolytes with Variable Chain Lengths. *Langmuir* **2011,** *27* (17), 10763-10769.

5. Wang, Y.; Tang, Y. L.; Zhou, Z. J.; Ji, E.; Lopez, G. P.; Chi, E. Y.; Schanze, K. S.; Whitten, D. G., Membrane Perturbation Activity of Cationic Phenylene Ethynylene Oligomers and Polymers: Selectivity against Model Bacterial and Mammalian Membranes. *Langmuir* **2010,** *26* (15), 12509-12514.

6. Bartlett, G. R., Phosphorus Assay in Column Chromatography. *J. Biol. Chem.* **1959,** *234* (3), 466-468.

7. Wang, Y.; Chi, E. Y.; Schanze, K. S.; Whitten, D. G., Membrane activity of antimicrobial phenylene ethynylene based polymers and oligomers. *Soft Matter* **2012,** *8*, 8547–8558..

8. Ding, L. P.; Chi, E. Y.; Chemburu, S.; Ji, E.; Schanze, K. S.; Lopez, G. P.; Whitten, D. G., Insight into the Mechanism of Antimicrobial Poly(phenylene ethynylene)

Polyelectrolytes: Interactions with Phosphatidylglycerol Lipid Membranes. *Langmuir* **2009,** *25* (24), 13742-13751.

9. Seelig, A., Local-Anesthetics and Pressure - a Comparison of Dibucaine Binding to Lipid Monolayers and Bilayers. *Bio. Chem. Hoppe-Seyler* **1987,** *368* (10), 1272-1272.

10. Yamaguchi, Y.; Tanaka, T.; Kobayashi, S.; Wakamiya, T.; Matsubara, Y.; Yoshida, Z., Light-emitting efficiency tuning of rod-shaped pi conjugated systems by donor and acceptor groups. *J. Am. Chem. Soc.* **2005,** *127* (26), 9332-9333.

11. Bolinger, P. Y.; Stamou, D.; Vogel, H., Integrated nanoreactor systems: Triggering the release and mixing of compounds inside single vesicles. *J. Am. Chem. Soc.* **2004,** *126* (28), 8594-8595.

12. Mishra, A.; Gordon, V. D.; Yang, L. H.; Coridan, R.; Wong, G. C. L., HIV TAT forms pores in membranes by inducing saddle-splay curvature: Potential role of bidentate hydrogen bonding. *Angew. Chem. Int. Ed.* **2008,** *47* (16), 2986-2989.

13. Bechinger, B., Detergent-like properties of magainin antibiotic peptides: a 31P solid-state NMR spectroscopy study. *Biochim. Biophys. Acta* **2005,** *1712* (1), 101-8.

14. Wu, G.; Khant, H. A.; Chiu, W.; Lee, K. Y. C., Effects of bilayer phases on phospholipid-poloxamer interactions. *Soft Matter* **2009,** *5*, 1496–1503.

15. Suloway, C.; Pulokas, J.; Fellmann, D.; Cheng, A.; Guerra, F.; Quispe, J.; Stagg, S.; Potter, C. S.; Carragher, B., Automated molecular microscopy: the new Leginon system. *J. Struct. Biol.* **2005,** *151* (1), 41-60.

16. Corbitt, T. S.; Ding, L. P.; Ji, E. Y.; Ista, L. K.; Ogawa, K.; Lopez, G. P.; Schanze, K. S.; Whitten, D. G., Light and dark biocidal activity of cationic poly(arylene ethynylene) conjugated polyelectrolytes. *Photochem. Photobiol. Sci.* **2009,** *8* (7), 998-

1005.

17. Wu, M. H.; Maier, E.; Benz, R.; Hancock, R. E. W., Mechanism of interaction of different classes of cationic antimicrobial peptides with planar bilayers and with the cytoplasmic membrane of Escherichia coli. *Biochemistry* **1999,** *38* (22), 7235-7242.

18. Rennie, J.; Arnt, L.; Tang, H. Z.; Nusslein, K.; Tew, G. N., Simple oligomers as antimicrobial peptide mimics. *J. Ind. Microbiol. Biot.* **2005,** *32* (7), 296-300.

19. Zhou, C.; Qi, X.; Li, P.; Chen, W. N.; Mouad, L.; Chang, M. W.; Leong, S. S.; Chan-Park, M. B., High potency and broad-spectrum antimicrobial peptides synthesized via ring-opening polymerization of alpha-aminoacid-N-carboxyanhydrides. *Biomacromolecules* **2010,** *11* (1), 60-7.

20. Yang, L. H.; Gordon, V. D.; Mishra, A.; Sorn, A.; Purdy, K. R.; Davis, M. A.; Tew, G. N.; Wong, G. C. L., Synthetic antimicrobial, oligomers induce a composition-dependent topological transition in membranes. *J. Am. Chem. Soc.* **2007,** *129* (40), 12141-12147.

21. Hotze, E. M.; Badireddy, A. R.; Chellam, S.; Wiesner, M. R., Mechanisms of Bacteriophage Inactivation via Singlet Oxygen Generation in UV Illuminated Fullerol Suspensions. *Environ. Sci. Technol.* **2009,** *43* (17), 6639-6645.

22. Kuzmanovic, D. A.; Elashvili, I.; Wick, C.; O'Connell, C.; Krueger, S., Bacteriophage MS2: Molecular weight and spatial distribution of the protein and RNA components by small-angle neutron scattering and virus counting. *Structure* **2003,** *11* (11), 1339-1348.

23. Hooker, J. M.; Kovacs, E. W.; Francis, M. B., Interior surface modification of bacteriophage MS2. *J. Am. Chem. Soc.* **2004,** *126* (12), 3718-3719.

# Chapter 3. Interaction of the CPEs and OPEs with Model Lipid Membranes

## 3.1 Introduction

### 3.1.1 Introduction to the membrane perturbation test

Recent investigations have shown that the naturally occurring antimicrobial peptides and their synthetic mimics mainly target the lipid bilayer of the bacterial membrane and that the membrane perturbation ability of these molecules is highly dependent on the lipid composition of the membrane.[1-5] Both the light-activated and dark biocidal activities of CPEs and OPEs are also linked to their interactions with bacterial cell membranes.[6] Thus, it is important to understand the structure-function relationship of our CPEs and OPEs with lipid membranes. Moreover, because of the significant differences in the lipid composition between prokaryotic and eukaryotic cell membranes,[7] understanding the interaction of CPEs and OPEs with different lipid membranes is of primary importance.

Although the CPEs and OPEs are structurally diverse, they are generally amphiphilic due to the hydrophilic, charged side chains positioned along the rod-like hydrophobic PPE backbone. In order for cell lysis to occur, the permeability barrier, which includes the cytoplasmic membrane, of the *E. coli* cells needs to be compromised. Since this membrane is located underneath the cell surface, it is difficult to visualize its disruption. So, in our study, we examined their interactions with unilamellar vesicles with lipid compositions mimicking those of mammalian or bacterial membranes. The behavior of the anionic CPE, PPE-$SO3^{2-}$ (Scheme 1.3), was also studied. We employed fluorescent dye release assays to study the interaction of CPEs and OPEs with model membranes.[6] As part of our investigation of the structure-function relationship of the CPEs and OPEs, a series of CPEs and OPEs with the same backbones but a range of different numbers of

repeat units (**n**) with **n** varying from 1 to 49, or chain lengths, were also synthesized.[8] We used model phospholipid membranes composed of DOPG/DOPE or *E. coli* lipid extracts as alternatives in this study, both of which are routinely used as models of the *E. coli* plasma membrane.[9] We have investigated membrane binding and perturbation activities of the CPE and OPE compounds in the dark. Morphological changes induced by CPE and OPE compounds were characterized by fluorescence imaging of single giant vesicles and cryo-TEM imaging of large unilamellar vesicles (LUVs). Molecular level changes to bilayer lipid membrane structure were determined by small angle X-ray scattering (SAXS) and solid-state NMR (SS-NMR) experiments.

### 3.1.2 Introduction to the models for membrane disruption by AMPs

The design of the synthetic antimicrobial agents was partly inspired by the naturally occurring antimicrobial peptides (AMPs) that function as a part of innate immunity in virtually all-living organisms.[10-11] Although the size, sequence, and conformation of AMPs vary substantially, most of these peptides are cationic and amphiphilic.[3] AMPs have been extensively studied during the past 30 years by a wide range of techniques to examine the mechanisms of AMP's antimicrobial activity. It is now generally accepted that the bacterial cytoplasm membrane is one of the AMP's main targets. The ability of AMPs to disrupt lipid membranes has been well-documented and remains an active research area.[1, 5] The common cationic and amphiphilic properties shared by both AMPs and the CPEs/OPEs are expected to give rise to the same chemical and physical driving forces for lipid membrane binding and disruption. It is thus useful to consider CPE/OPE – membrane interactions in the context of known membrane disruption models of AMPs (Figure 3.1).[12] We briefly review the membrane action models of AMPs here as these

models have been discussed in more detail elsewhere.

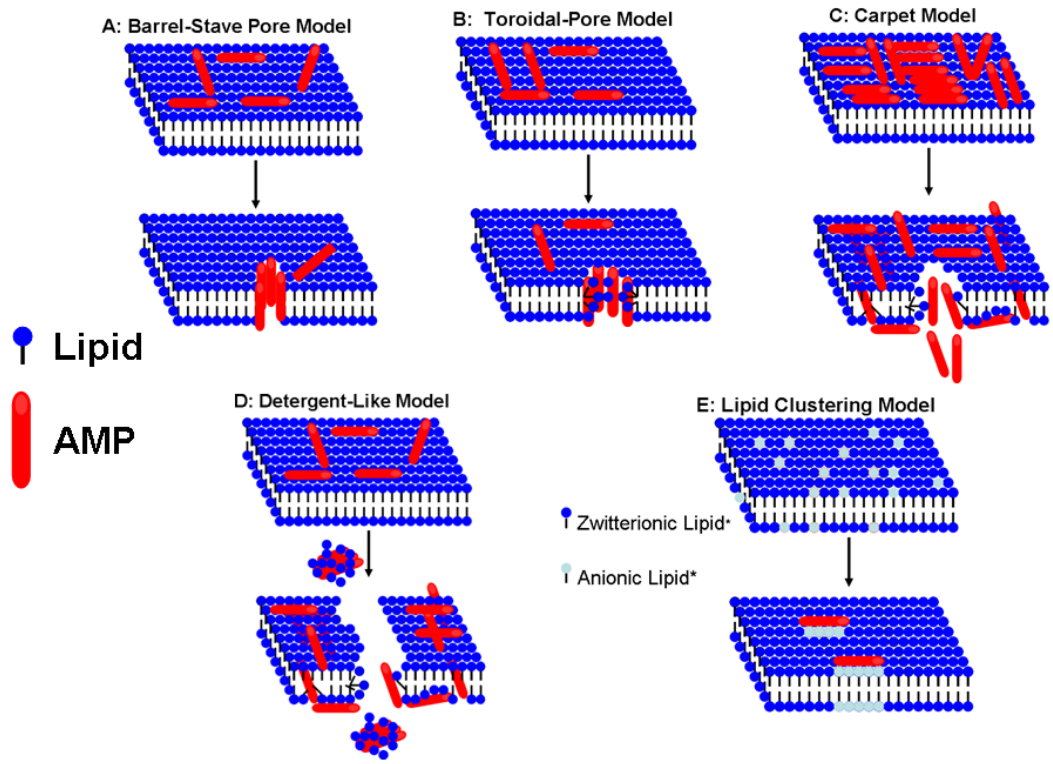


**Figure 3.1**. Prevailing models of AMP-membrane interactions.
*The differently colored lipid headgroups represent different charges in Figure 3.1E.

### 3.1.2.1 Barrel-Stave pore model

In this model, the AMPs first attach to the lipid membrane surface with their long axis parallel to the membrane surface (Figure 3.1A). As the local concentration of the peptide increases, the peptides adopt a more ordered conformation and cooperatively insert into the membrane. As a result, permanent transmembrane pores are formed by the alignment of the hydrophobic region of the peptides with the hydrophobic core of the lipid bilayer, where the hydrophilic region of the peptide forms the interior of the transmembrane pore.[2, 4] Thus, the formation of barrel-stave pores requires precise alignment of facial amphipathicity and hydrophobic matching of the AMPs with the bilayer. Additionally cooperative and specific peptide-peptide interactions are required. It has been shown that

transmembrane pores induced by the AMP alamethicin are consistent with the barrel-stave model.[13-14]

#### 3.1.2.2 Toroidal-Pore model

In this model, the membrane bound AMPs insert into the lipid bilayer and force the outer leaflet to bend continuously to fuse with the inner leaflet (Figure 3.1B). As a result, somewhat reversible transmembrane pores are formed by both the hydrophilic peptide regions and lipid head groups.[3] In this case, the peptide does not need to span the entire bilayer – smaller peptides can also induce and stabilize toroidal-pores. The AMP Melittin has been found to induce toroidal-pores in model lipid membranes.[15]

#### 3.1.2.3 Carpet and detergent-like models

In addition to the above two pore-forming models, AMPs can also permeabilize lipid membranes through non-pore mechanisms. In the carpet model, the peptides accumulate extensively on the outer leaflet of the lipid bilayer, inducing the expansion of the outer leaflet and causing a strain between the two leaflets of the membrane (Figure 3.1C). At local peptide concentrations above a threshold level, the strain caused by the peptides will be released through the collapse of the lipid membrane.[16] Some peptides may self-aggregate into micelles in aqueous solutions.[17] According to the detergent-like model, the peptide micelles may interact with the lipid bilayer and remove lipid molecules, which result in the catastrophic collapse of the membrane (Figure 3.1D). The peptide micelles could also insert into the lipid bilayer, increasing the transient membrane permeability. Short peptides which cannot span the lipid bilayer can still permeabilize the membrane through the non-pore models. Cecropin P1 and Warnericin RK are believed to disintegrate lipid membranes through these non-pore models.[18-19]

### 3.1.2.4 Lipid clustering model

Many bacterial cytoplasm membranes are composed of both zwitterionic and anionic lipids and the lipids are not distributed uniformly. Fishov and coworkers have shown that some lipid domains are enriched in a specific type of lipid in *E. coli* cell membranes.[20] Therefore, the cationic AMPs attached to membranes may cluster anionic lipids and induce lipid phase separation in the bacterial membrane (Figure 3.1E). This AMP-lipid interaction may change lipid lateral packing and increase membrane permeability where leakage of cell content could occur at phase boundary defects.[21]

### 3.1.2.5 Interfacial activity model

Based on an extensive study of vesicle perturbation assay results, Wimley proposed the interfacial activity model to explain the membrane activity of AMPs.[4] It is frequently observed for many AMPs that upon adding the peptides to a homogeneous dye-loaded vesicle suspension, dye release occurs instantly and then plateaus within several minutes to levels lower than anticipated for complete dye release. This puzzling phenomenon is commonly explained as the "all-or-none" mechanism, where a fraction of vesicles releases all of the dye and the rest releases none. Numerical simulations show that if the AMPs are truly pore-forming molecules, complete dye release should occur within a very short time period (less than 1 second). Taking these experimental and computational results together, Wimley concluded that most AMPs may not induce true permanent pores in the lipid membrane and that the observed partial dye release may result from AMP induced transient membrane permeability changes, vesicle fusion, or vesicle aggregation. This model emphasizes the "imperfect" amphiphilic properties of AMPs, which provides them with the ability to interact with and reorganize the lipid packing of

the interfacial region of the bilayer. The peptides may also translocate across the membrane and in the process disrupt lipid organization and cause toxicity by inducing the release of cell content.

Since the interactions of AMPs with lipid membranes are very complex and different AMPs may interact with the membranes through different mechanisms, none of the above models adequately explains all of the observed phenomena. But the models provide a good basis for interpreting the membrane activity of AMPs as well as other membrane active agents. It is important to note that aside from the properties of AMPs described above, a number of other parameters can significantly influence AMP's membrane perturbation mechanisms, including membrane composition, peptide to lipid molar ratio, temperature and solvent conditions.[4, 13]

### 3.2 Results and Discussion

#### 3.2.1 Interaction of the CPEs and OPEs with large unilamellar vesicles (LUV)

It is widely accepted that the AMPs and their synthetic mimics mainly target the lipid bilayer of the cell membrane.[3] The phospholipid compositions of bacterial cell membranes and mammalian cell membranes are very different.[22-23] The principal phospholipid components in mammalian cell membranes are phosphatidylcholine (PC), phosphatidylethanolamine (PE), cholesterol, and sphingomyelin.[7] Human erythrocyte cells contain mostly PC and 5-10% of negatively charged phosphatidylserine (PS) lipids. Because of the asymmetric distribution of erythrocyte membrane lipids, more than 95% of PS lipids reside on the inner leaflet of the membrane. Thus, the outer leaflet of the mammalian membrane is near neutral.[24] On the other hand, the dominant lipids in the bacterial cytoplasmic membrane are phosphatidylglycerol (PG), PE, and

diphosphatidylglycerol. Most Gram-negative bacterial membranes, including *E. coli*, contain 60-70% PE and 20-30% PG. As a result, the bacterial membrane is highly negatively charged. Based on the differences in lipid composition between mammalian and bacterial membranes, three vesicle compositions were studied (Table 3.1). The membrane perturbation activities of the CPE/OPE used in this report were evaluated by fluorescein release assays (Figures 3.2, 3.3 and 3.4).

**Table 3.1**. Vesicle abbreviations and corresponding compositions and sizes.

| vesicles | lipid composition | hydrodynamic radius (nm) | net surface charge |
|---|---|---|---|
| V-1 | DOPC/cholesterol 67/33 | 56±5 | neutral |
| V-2 | DOPG/DOPE 20/80 | 58±4 | negative |
| V-3 | *E. coli* Total Lipid | 61±2 | negative |

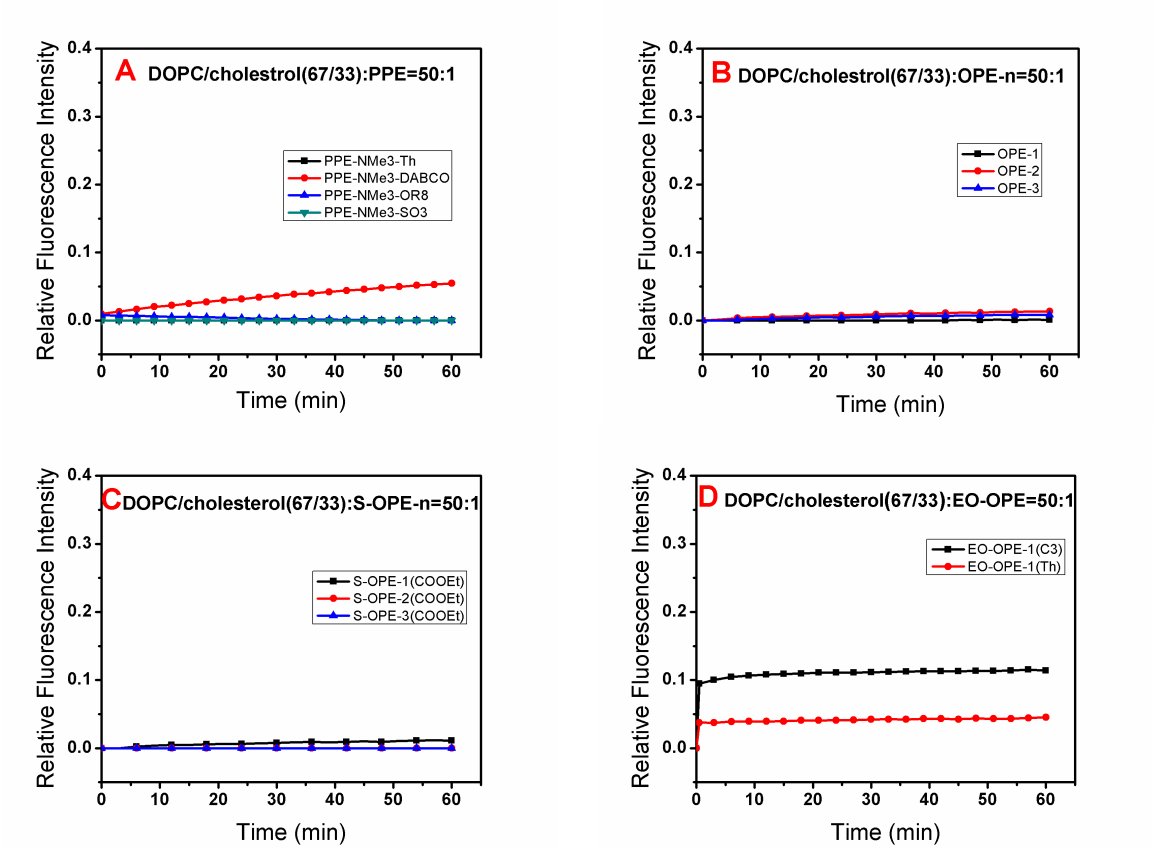


**Figure 3.2**. Fluorescein leakage profiles from DOPC/cholesterol (67/33) vesicles with the

addition of a CPE or OPE in buffer A, at room temperature. (Excitation wavelength: 485 nm) Fluorescence from vesicles incubated alone was subtracted.

### 3.2.1.1 Interaction with mammalian membrane mimic

V-1, composed of PC lipids and cholesterol, is used as a model for mammalian cell membranes. Only PPE-DABCO, EO-OPE-1(C3) and EO-OPE-1(Th) caused measurable membrane disruption against V-1 (Figure 3.2). All other CPE and OPE are inactive. (Note: "inactive" and "no release" refer to no dye release in excess to that of vesicles incubated alone through the entire incubation period).

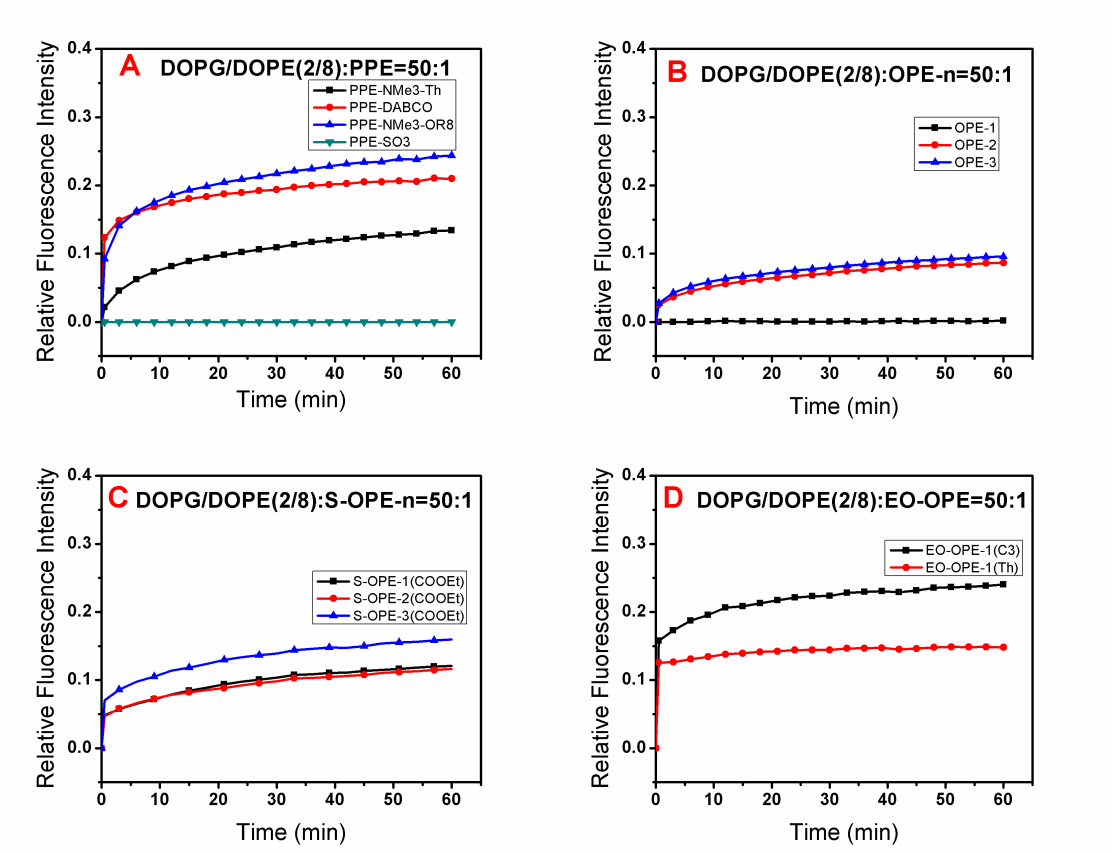


**Figure 3.3**. Fluorescein leakge profiles from DOPG/DOPE (20/80) mixed vesicles with the addition of a CPE or OPE in buffer A, at room temperature. (Excitation wavelength: 485 nm) Fluorescence from vesicles incubated alone was subtracted.

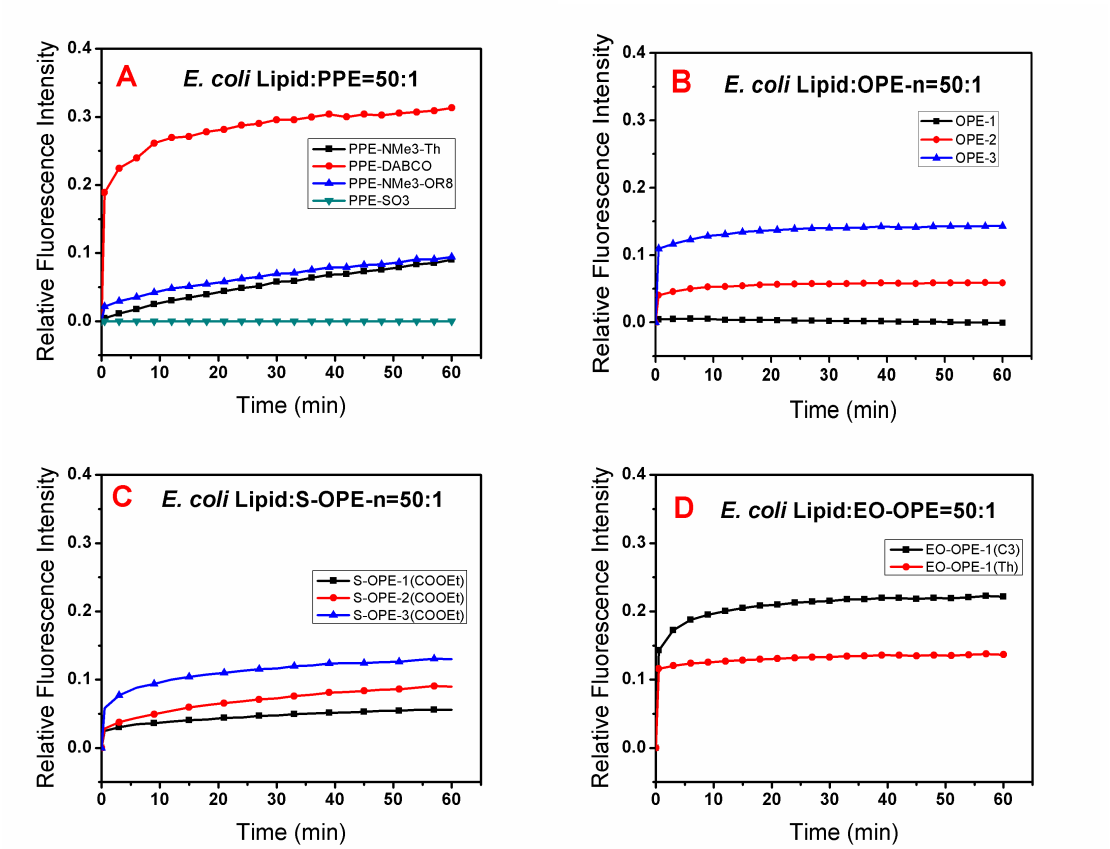


**Figure 3.4**. Fluorescein leakage profiles from *E. coli* total lipid vesicles with the addition of CPE or OPE in buffer A, at room temperature. (Excitation wavelength: 485 nm) Fluorescence from vesicles incubated alone was subtracted.

### 3.2.1.2 Interaction with bacteria membrane mimics

V-2, composed of DOPG and DOPE, is used as a model for bacterial membranes. Most of the cationic CPE/OPE show good activity against V-2 (Figure 3.3). Specifically, PPE-$NMe_3$-OR8, PPE-DABCO and EO-OPE-1(C3) induce approximately 20% dye release. PPE-$NMe_3$-Th, OPE-2 and 3 and the three S-OPE-n oligomers cause ~ 10% release. In contrast, the anionic PPE-$SO_3^{2-}$ and OPE-1, the shortest molecule tested (based on the distance along the long molecular axis), are inactive. V-3, made from *E. coli* total lipid extract, was used as a better mimic of the bacterial membrane. Dye release of the V-3 vesicles induced by CPE/OPE are comparable to the leakage induced in V-2 vesicles (Figure 3.4). PPE-DABCO and OPE-3 were slightly more effective in inducing

leakage in V-3 vesicles compared to V-2, and EO-OPE-1(C3) and EO-OPE-1(Th) caused a similar amount of dye leakage in V-2 and V-3. However, S-OPE-n caused a somewhat lower dye leakage in V-3 vesicles compared to V-2. Notably, OPE-1 and PPE-$SO_3^{2-}$ are still inactive against V-3 vesicles. It is worth noting that the active CPE/OPE exhibit concentration-dependent membrane disruption against V-3; at higher CPE/OPE:lipid ratios, higher levels of dye release were observed (data not shown).

#### 3.2.1.3 Summary of CPE/OPE interaction with model membranes

The cationic CPE and OPE used in this study possess significant structural diversity, but most of them show similar membrane selectivity and, sometimes, even similar membrane perturbation ability. Generally, most of the CPE/OPE are inactive against the mammalian cell membrane model V-1 and can induce significant dye leakage from bacterial membrane models V-2 and V-3. PPE-DABCO, EO-OPE-1(C3) and EO-OPE-1(Th) interact with V-1 in a different way from other CPE/OPE. They can perturb V-1 and induce the release of the entrapped dye. One possible reason for PPE-DABCO's poor membrane selectivity could be the high positive charge density on its side chains, which endows PPE-DABCO with the ability to disrupt vesicles composed of zwitterionic lipids. In addition, the hydrophobic alkyl portion of PPE-DABCO's side chains can facilitate their hydrophobic interactions with lipid acyl tails in a similar way to the interaction of detergents with lipids.[25] Our previous work demonstrated that PPE-DABCO does not incorporate in the lipid bilayer rapidly or efficiently.[26] Therefore, it is reasonable to attribute PPE-DABCO's high membrane perturbation activity to the unique properties of its side chains. Meanwhile, the most important structural feature of EO-OPE-1(C3) and EO-OPE-1(Th) is their linear conformation (no side-chains on the backbones), which

should permit them to easily penetrate into the lipid bilayer. The estimated molecular lengths of EO-OPE-1(C3) and EO-OPE-1(Th) (the distance between the two nitrogen atoms within the terminal quaternary amine groups) are comparable with the lipid bilayer thickness.[27] It is expected that these two molecules can easily coordinate electrostatic and hydrophobic interactions with the lipid bilayer and therefore can disrupt V-1 more easily than OPE-n or S-OPE-n. It is worth noting that EO-OPE-1(C3), should have a more linear conformation than its thiophene-substituted counterpart, EO-OPE-1(Th), which may account for its higher membrane disrupting activity against all the vesicles tested. On the other hand, only PPE-$SO_3^{2-}$ and OPE-1 are inactive against bacterial membrane mimics V-2 and V-3. The inactivity of PPE-$SO_3^{2-}$ vs. V-1 and V-3 is attributed to the anionic polymer's inability to associate with the negatively charged membrane due to electrostatic repulsion. Therefore no leakage was observed. Several models, for example "barrel-stave", "toroidal pore" and "carpet" (figure 3.1), have been proposed to explain the antimicrobial mechanism of antimicrobial peptides.[3] Furthermore, it has been assumed that only peptides long enough to span the membrane are able to form stable pores.[28] Of the CPE and OPE compounds studied here, only OPE-1 is shorter than the hydrophobic thickness of the lipid bilayer,[27] which may be a cause of its inactivity.

The OPE-n and S-OPE-n show size-dependent membrane perturbation against V-2 and V-3. The longer oligomers exhibit stronger activity than the smaller counterparts and this trend correlates with their biocidal activities in the dark. Tew and co-workers observed that PE lipids facilitate dye leakage due to their negative curvature, which renders transmembrane pore formation energetically more favorable.[9] A similar phenomenon was observed in this study. When DOPE in V-2 was replaced with DOPC, most of the

CPE/OPE, except OPE-1 and PPE-$SO_3^{2-}$, exhibited much lower membrane disruption activity compared to V-2, one representative example is OPE-3 could induce 10% release of the entrapped fluorescein from V-2 (Figure 3.3B), however, it was almost inactive against the vesicle made by DOPG/DOPC (20/80) under the same condition. Photophysical studies of the interaction of CPE with different vesicles have been previously reported.[26, 29] It is noteworthy that when mixing OPE-n or S-OPE-n with different vesicles, the fluorescence intensities of these oligomers increase remarkably. Figure 3.5 shows a representative set of fluorescence data. The most pronounced change in these spectra is the large enhancement of fluorescence intensity, which suggests that the microenvironment of the oligomers has substantially changed from an aqueous to a hydrophobic environment after the addition of vesicles.[30-31] Moreover, fluorescence increase occurred immediately after mixing the oligomers with vesicles (data not shown). In addition, DLS data show that mixing V-1 and V-3 vesicles with OPE-n results in 2-3 nm increase in the vesicle diameters (data not shown). Taken together, it is reasonable to assume that the active CPE/OPE are first absorbed onto the negatively charged vesicle surface and then spontaneously reorient to create membrane defects or transmembrane pores.

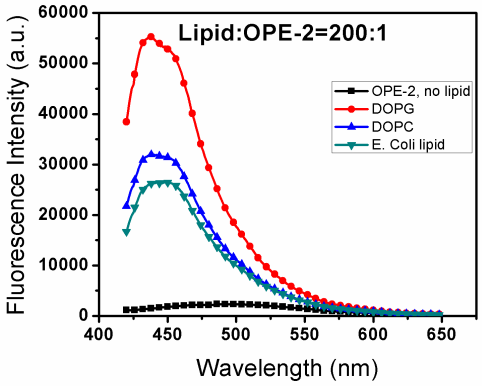

**Figure 3.5**. Fluorescence emission spectra of OPE-2 and its mixtures with different vesicles in buffer A, at room temperature. (Excitation wavelength: 375 nm)

As shown in Figures 3.2, 3.3 and 3.4, the partial release of the entrapped dye from different vesicles upon mixing with CPE/OPE is a fast process. Like antimicrobial peptides, it is reasonable to postulate that these CPE/OPE can create a stress on the membrane and induce pore formation either by increasing membrane tension and/or reducing membrane line tension.[32-33] The entrapped dye molecules are expelled through the pore due to the membrane tension and chemical potential difference of the dye inside and outside the vesicles. In addition, most of the dye release profiles level off within 10 minutes of mixing and the extent of dye release is much less than 100%. This leveling off is a common phenomenon that has been reported for most antimicrobial agents and we hypothesize that this could be attributed to two possible causes. First, the fast release of the entrapped dye molecules relieves the membrane tension, and at the same time, line tension at the pore's edge drives the closure of the pores, resulting in the self-healing of the vesicles.[34-35] Another possible cause is that the leakage process follows an "all-or-none" mechanism[36] caused by the non-uniform distribution of CPE/OPE with vesicles, where only when the amount of the attached CPE/OPE to a vesicle is higher than a threshold level, pores form and the fast and complete release of the entrapped dye occurs. However, below the threshold, the attached CPE/OPE can not cooperate efficiently to create membrane defects or pores for dye release.

### 3.2.1.4 Conclusion

Results from our dye release experiments show that most CPE and OPE materials used in this study selectively interact with specific types of membrane lipids. For the polymer series, the functional groups on the side chains dominate their membrane perturbation

activity. Specifically, the high charge density and hydrophobic alkyl chains of PPE-DABCO's side chains give rise to the polymer's high perturbation activity against all the vesicles used. Not surprisingly, PPE-DABCO also has poor membrane selectivity. For the three oligomers studied, molecular length greatly influences their interactions with lipid bilayers. OPE-n and S-OPE-n exhibit size-dependent activity against bacterial membrane mimics, where longer oligomers exhibit higher activity than their smaller counterparts. EO-OPE, the oligomers without side chains, exhibit high membrane perturbation activity and poor selectivity. These results give us insights into the relationship between molecular structure and membrane perturbation ability of biocidal CPE and OPE. The observation that specific oligomers and polymers have high selectivity towards model bacterial membranes and little activity towards model mammalian membranes indicates these materials may be efficient and yet non toxic antimicrobials.

### 3.2.2 Chain length effect of the CPEs and OPEs on their membrane perturbation activities

Over the last decade, new synthetic amphiphilic antimicrobial agents with tunable structure have been reported.[24, 37] One of the most remarkable features of these synthetic compounds is their high toxicity to bacterial cells and low hemolytic activity against human red blood cells. In addition, the antimicrobial ability of these molecules is related to their insertion or perturbation ability against bacterial cell wall and membranes. Herein, photophysical investigation, dye release assays and monolayer insertion assays were used to explore the membrane perturbation ability of a series of CPEs and OPEs that differ in their number of repeat units.

### 3.2.2.1 Photophysical investigation

Since the photophysical properties of the CPEs and OPEs is highly dependent on their solution microenvironment,[1, 3] a set of photophysical measurements were obtained to elucidate the changes of the microenvironments of the CPEs and OPEs when they come into contact with lipid vesicles composed of either DOPC lipids (a mammalian cell membrane mimic) or *E. coli* total lipid extract (a bacterial cell membrane mimic). We have shown earlier that in aqueous solutions the OPEs are monomeric in the μM range.[38] In contrast, the CPEs readily aggregate in aqueous solutions via intra- or inter-chain stacking of the conjugated backbone and this type of aggregation drastically decreases the fluorescence emission intensity of the CPEs compared to OPEs.[1] Thus, fluorescence emission intensities of the compounds were measured to probe changes in the aggregation state of the compounds in the presence of different lipid vesicles. Absorbance measurements were made to probe changes in conjugation length, or segment chromophores,[39] of the compounds where red shifts indicate increases of the conjugation length in the molecular backbone.

All CPEs and OPEs exhibit similar spectral changes, including absorbance spectral shifts and increases in emission intensity, upon incubation with the two types vesicles; Figure 3.6 shows a set of representative absorbance and emission spectra for oligomeric S-OPE-3 and polymeric PPE-$NMe_3$-7-COOEt alone or incubated with the two different vesicles. As shown, absorbance maxima of both OPEs and CPEs undergo red-shifts at different extents, with the *E. coli* total lipids inducing the largest changes (Figures 3.6A and 3.6C). The emission intensity of the OPEs and CPEs significantly increased in the presence of lipid vesicles and the *E. coli* total lipids again induced the largest increases.

Parameters obtained from the photophysical characterizations of the CPE and OPE compounds are summarized in Table 3.2. Our data show that the maximum absorbance wavelengths of OPEs in water increased with chain length while the maximum absorbance wavelengths of the CPEs did not exhibit such a trend (Table 3.2). This is probably due to the ability of the long chains of the CPEs, which are longer than the average conjugation length of the segment chromophores[39] within the backbone, to form intra- and/or inter-chain aggregates.[40-42]

As shown in Table 3.2 and Figure 3.6, when CPEs and OPEs are mixed with different model membranes, their photophysical properties change drastically. Specifically, *E.coli* total lipid extract vesicles induced significant red-shifts in the absorbance maxima for all CPE and OPEs compounds, while DOPC vesicles induced little or no change. The red-shifts could be partly due to segment planarization of the CPEs or OPEs from their interactions with the *E. coli* lipid membrane, thus extending the conjugation length of the CPEs and OPEs along their backbones.[43-45] Moreover, the addition of lipid vesicles greatly increases the fluorescence emission intensity of both the CPEs and OPEs (Figure 3.6), suggesting that when exposed to lipid membranes, the microenvironment of CPEs and OPEs changed from an aqueous to a hydrophobic environment and consequently, nonradiative processes have been significantly reduced.[1, 3] Meanwhile, the lipid vesicles induced blue-shifts in the CPEs' emission spectra (Figure 3.6D and Table 3.2), implying that the conformation of the CPEs may have changed from an aggregated state to a more extended state and that this conformational change was facilitated by the lipid membranes.[46-49] Overall, changes in spectral characteristics induced by the *E. coli* lipid vesicles were significantly larger than those induced by the mammalian-mimicking

vesicles, indicating that the interactions of the CPE and OPE compounds with *E. coli* lipid vesicles were stronger and more extensive compared to the mammalian membrane mimic.

Our results indicate that the amphiphilic CPEs and OPEs bind to lipid vesicles readily and upon binding, properties such as conjugation length and aggregation state of the compounds change. The binding of the CPEs and OPEs to the lipid vesicles membranes was further confirmed by increases in $R_h$ values of the vesicles after the addition of a CPE or OPE to the vesicles, for example, $R_h$ of *E. coli* vesicles increased from $67 \pm 3$ nm to $75 \pm 2$ and $91 \pm 3$ nm upon the addition of S-OPE-2(COOEt) and PPE-$NME_3$-20-COOEt, respectively. The binding of the antimicrobial agents to vesicles have been shown to be in part driven by electrostatic interactions. Favorable entropy increases by the release of interfacial water through the binding of CPE or OPE to membranes may also contribute to their high affinity towards membranes.[43]

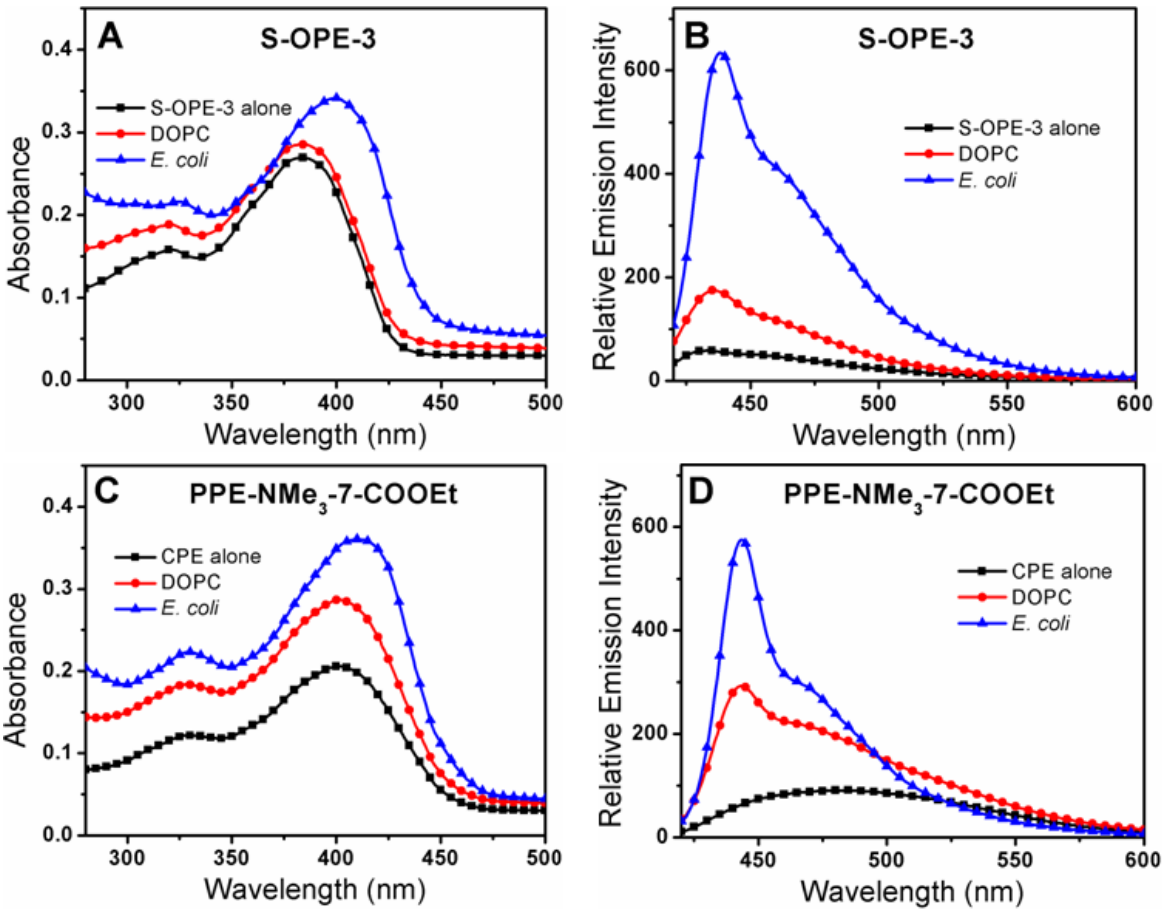


**Figure 3.6**. Absorbance (A, C) and fluorescence emission (B, D) spectra of oligomeric S-OPE-3(COOEt) and polymeric PPE-$NMe_3$-7-COOEt and their mixtures with different lipid vesicles in water at room temperature. The excitation wavelengths for S-OPE-3(COOEt) and PPE-$NMe_3$-7-COOEt are 383 nm and 401 nm respectively.

**Table 3.2.** Photophysical characterization of the CPEs and OPEs in different solutions at room temperature. The maximum absorbance wavelength of each compound in water was selected as the excitation wavelength for all the corresponding emission spectra. DOPC and *E. coli* total lipid concentrations were 0.2 mM and 0.2 mg/ml, respectively. Lipid to CPE or OPE ratio was 50:1.

| Antimicrobial Agent | Maximum Absorbance Wavelength (nm) | | | Maximum Emission Wavelength (nm) | | |
|---|---|---|---|---|---|---|
| | $H_2O$ | *E. coli* | DOPC | $H_2O$ | *E. coli* | DOPC |
| S-OPE-1(COOEt) | 359 | 370 | 360 | 433 | 436 | 434 |
| S-OPE-2(COOEt) | 377 | 395 | 379 | 437 | 436 | 434 |
| S-OPE-3(COOEt) | 383 | 399 | 383 | 431 | 436 | 436 |

| | | | | | | |
|---|---|---|---|---|---|---|
| PPE-$NMe_3$-7-COOEt | 401 | 409 | 401 | 484* | 443 | 443 |
| PPE-$NMe_3$-20-COOEt | 404 | 415 | 406 | 479* | 444 | 445 |
| PPE-$NMe_3$-49-COOEt | 404 | 415 | 406 | 486* | 443 | 443 |

*The emission spectra of the CPEs in water were broad and flat.

### 3.2.2.2 Disruption of mammalian and bacterial membrane mimicking vesicles

Vesicles of two different lipid compositions were prepared to mimic mammalian and bacterial cell membranes[40] (Table 3.3). V-1, composed of PC lipids and cholesterol, is used as a model for mammalian cell membranes. Figure 3.7 shows the fluorescein leakage profiles from V-1 vesicles incubated with the different CPEs and OPEs. In all cases, no dye release in excess to that of vesicles incubated alone is observed during the incubation period. Clearly, the antimicrobial molecules in the concentration range tested are inactive at disrupting the mammalian membrane mimic.

**Table 3.3.** Vesicle abbreviations and their corresponding compositions, sizes, and overall charges.

| Vesicles | Lipid Composition | Hydrodynamic Radius (nm) | Net Surface Charge |
|---|---|---|---|
| V-1 | 67:33 DOPC:cholesterol | 56±5 | Neutral |
| V-2 | *E. coli* Total Lipid | 61±2 | Negative |

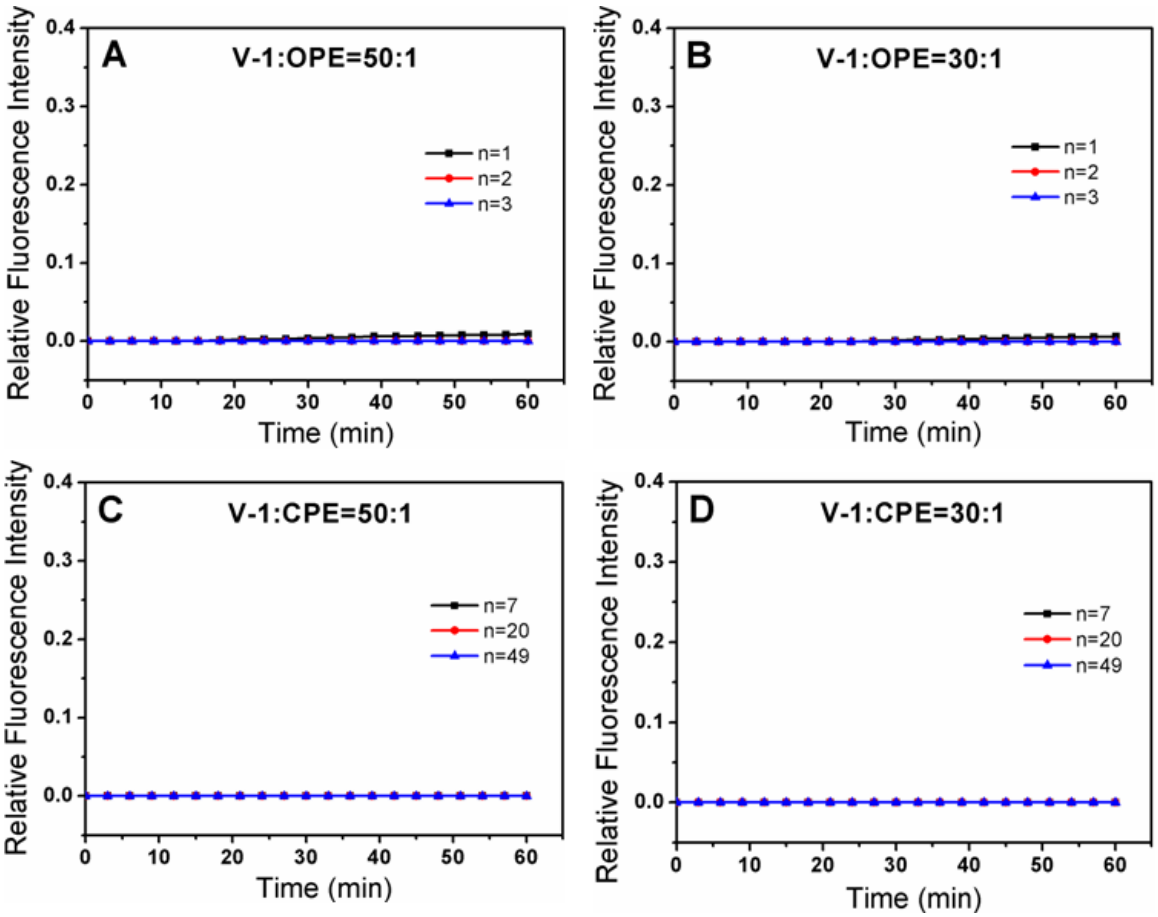


**Figure 3.7**. Fluorescein leakage profiles from DOPC:cholesterol (67:33) vesicles (V-1) with the addition of a CPE or an OPE in buffer A at room temperature (Excitation/Emission wavelength: 485/520 nm). Fluorescence from vesicles incubated alone was subtracted.

Vesicles V-2, made from *E. coli* total lipid extract, were used as a model for the bacterial membrane. As shown in Figure 3.8, all CPEs and OPEs tested induced dye release, indicative of membrane disruption against V-2 vesicles. Moreover, the extent of dye release was highly dependent on the molecular size and concentration of OPEs and CPEs (Figure 3.8). Increasing the chain length of the oligomers enhanced their membrane perturbation activity (Figure 3.8A and B). In contrast, the polymers showed the opposite trend -- increasing the number of repeat units decreased the polymer's membrane perturbation ability (Figure 3.8C and D).

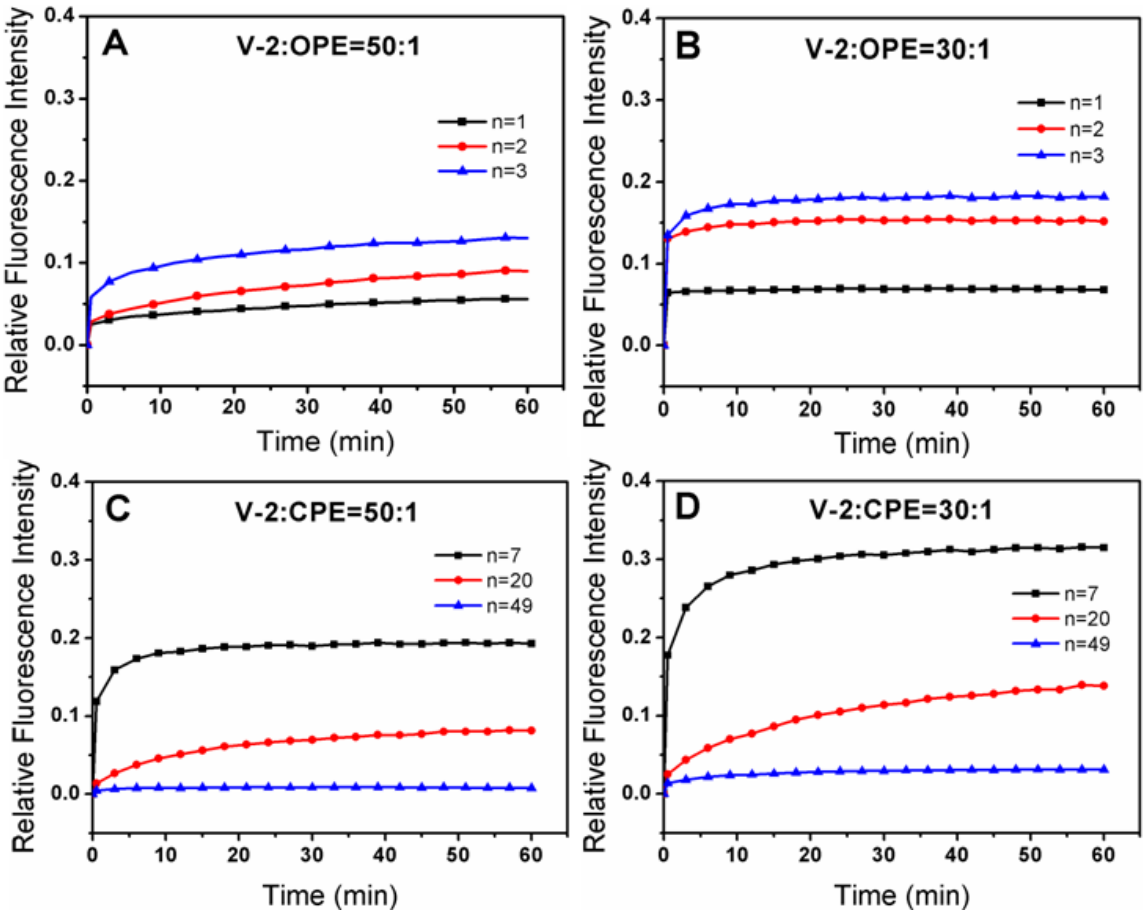


**Figure 3.8**. Fluorescein leakage profiles from *E. coli* total lipid vesicles (V-2) with the addition of CPE or OPE in buffer A, at room temperature (Excitation/Emission wavelength: 485/520 nm). Fluorescence from vesicles incubated alone was subtracted.

The results from dye leakage assays show that the CPEs and OPEs selectively perturb the bacterial membranes and that the membrane disruption ability is highly dependent on chain length. For the oligomers tested, increasing the chain length enhanced their ability to incorporate or perturb lipid membranes that led to the leakage of dye molecules from inside the vesicles to the bulk phase. In contrast, increasing the chain length of polymers reduced their membrane perturbation ability probably by enhancing their tendency to form aggregates via intra- and/or interchain stacking. As a result, the effective concentration of the polymers that could interact with the lipid vesicles is reduced. Additionally, formation of aggregates can also reduce the polymer's cooperativity in

inducing membrane surface defects, which may proceed by a highly synergistic mechansim.[36]

### 3.2.2.3 Lipid monolayer insertion assays

Monolayer insertion assays are often used to evaluate the interaction and the membrane insertion ability of naturally occurring antimicrobial peptides and synthetic biocidal agents.[50] In the current study, insertion assays of CPEs and OPEs into lipid monolayers at the air/water interface composed of DPPG and DPPE were carried out at constant surface pressure to evaluate the effect of chain length on their membrane insertion ability. DPPE is zwitterionic and was used instead of DOPC lipids for insertion assays because DPPE forms a more stable monolayer. Moreover, since DPPE and DPPG monolayers are both in the lipid-condensed phase under the experimental conditions, where as DOPC would be in a liquid-expanded phase, the effect of membrane fluidity or lipid packing will have minimal influence on insertion results.

Figure 3.9 shows insertion isotherms of the CPEs and OPEs into DPPG monolayers held at 30 mN/m on water at room temperature. Note that CPEs and OPEs alone did not give rise to any surface pressure at the air-water interface (data not shown). Insertion results shown in Figure 3.9 are thus due to favorable interactions between DPPG monolayer and the CPEs or OPEs. Consistent with results obtained from dye leakage assays, the CPEs and OPEs show repeat unit dependent monolayer insertion ability. Specifically, increasing chain length increased the extent of insertion of OPE oligomers, while the opposite trend is observed for CPEs. The longest CPE, PPE-$NMe_3$-49-COOEt, did not insert into the DPPG monolayer at 0.1 μM. However, increasing the concentration to 0.5 μM resulted in extensive insertion (data not shown). In contrast, none of the CPEs

or OPEs tested inserted into the lipid monolayers composed of the zwitterionic DPPE lipids (data not shown). Taken together, results obtained from lipid monolayer insertion assays provide additional evidence for the size-dependent membrane perturbation ability of CPEs and OPEs and their selectivity towards negatively charged membranes.

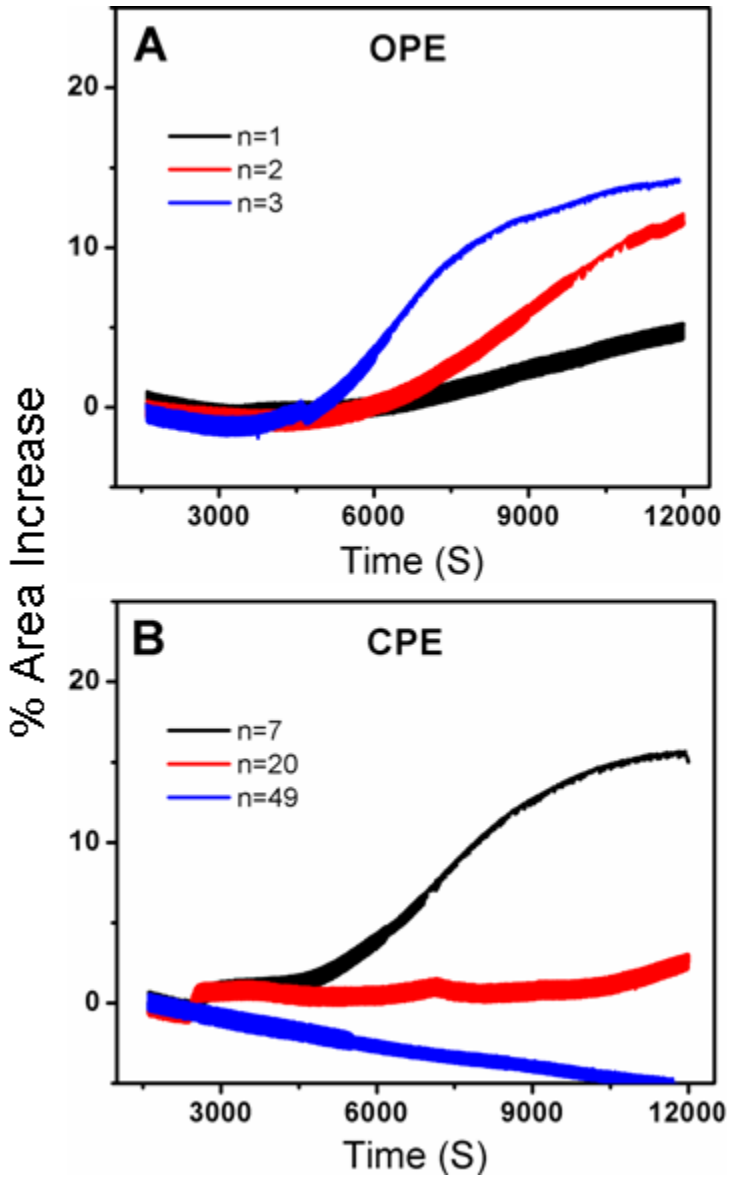


**Figure 3.9**. Insertion profiles of CPEs (0.1μM) or OPEs (0.1μM) into DPPG monolayers held at 30 mN/m on water at room temperature.

#### 3.2.2.4 Conclusions

Our study clearly demonstrates that cationic CPEs and OPEs exhibit affinity towards both mammalian and bacterial-mimicking lipid membranes and that they selectively perturb bacterial model membranes. The dye release assays reveal that all CPEs and OPEs are inactive against model mammalian membranes in the concentration ranges tested. However, they show significant membrane perturbation activity against model bacterial membranes and that they readily insert into negatively charged lipid monolayers at the air/water interface. Moreover, the materials exhibit chain-length dependent membrane perturbation ability where increasing chain length increased the ability of the oligomers to incorporate and perturb membranes and the reverse trend was observed for the polymers. Taken together, there might be an optimum chain-length for these PPE-based antimicrobial compounds that corresponds to the highest membrane perturbation efficiency. The results of current study will serve as a guide to design more efficient and nontoxic materials resistant to bacteria growth and biofilm formation.

### 3.2.3 Visualization of the membrane failure induced by the CPEs and OPEs and their membrane perturbation mechanisms

#### 3.2.3.1 Visualization of the interactions with giant vesicles

The membrane perturbation actions of OPE-1 and EO-OPE-1(C3) were visualized and compared by imaging single giant vesicles (Figure 3.10). Upon the addition of OPE-1 to giant vesicles composed of *E. coli* total lipids, the vesicle disintegrated and disappeared quickly. Thus, OPE-1 efficiently incorporated into lipid bilayer and may induce lipid phase separation followed by the lysis of the vesicle structure, which may undergo the carpet or detergent-like membrane destabilizing model.[12] EO-OPE-1(C3) can also

dramatically change the morphology of the lipid vesicle. However, the residual lipid-OPE structure was still observable and no further morphology changes or vesicle disintegration occurred even upon prolonged observation (image not shown). It is worth noting that as a control, the addition of 10 mM HEPES buffer alone did not cause any visible damage to the vesicle (data not shown). Quantitatively, EO-OPE-1(C3) possesses much higher membrane perturbation ability against both model bacterial and mammalian cell membranes than OPE-1.[6] Herein, the single giant vesicle assay is employed as a qualitative measurement to observe the membrane disruption actions for the OPEs used for the current study. The actual concentration of the OPEs interacting with the vesicle is difficult to determine, but is estimated to be much lower than 50 μg/ml (see Experimental Methods).

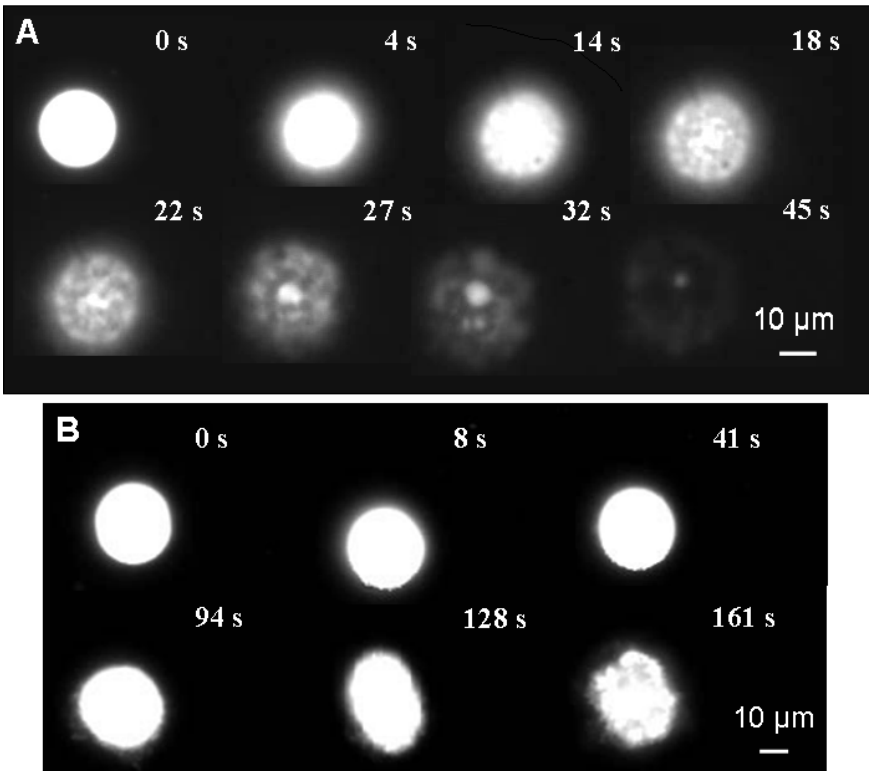


**Figure 3.10**. Time lapse fluorescence microscopy images showing the damage of giant vesicle caused by the addition of OPE-1 (A) and EO-OPE-1(C3) (B) at room temperature. The vesicle is composed by *E. coli* total lipid and labeled with DMPE-Rh and Biotin-

PEG-DSPE (0.5% and 2.5% molar percentage respectively). The elapsed time after the addition of antimicrobial agent is labeled for each image.

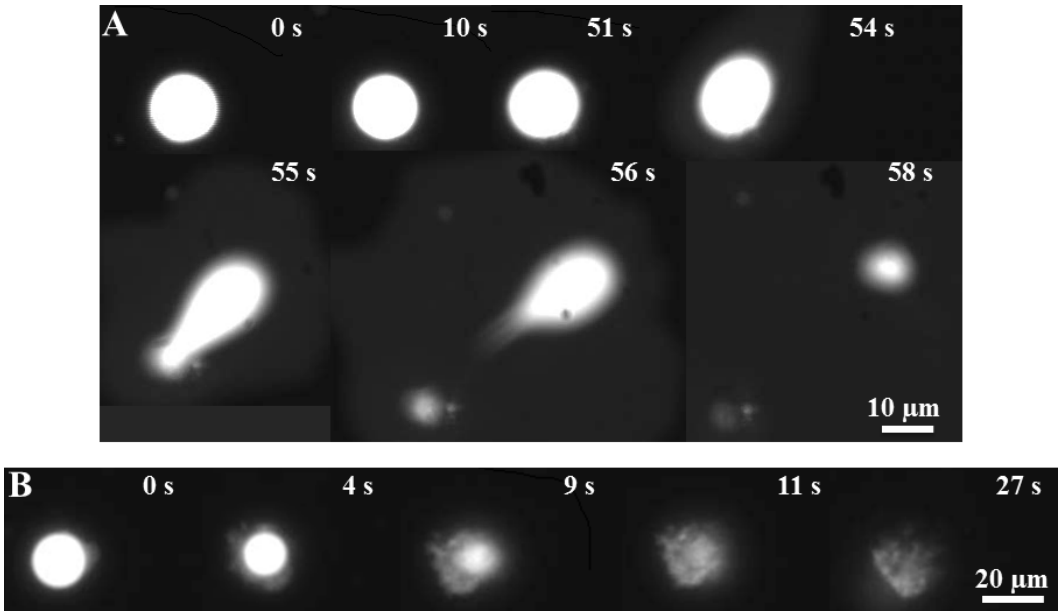


**Figure 3.11**. Time lapse fluorescence microscopy images showing the damage of a giant vesicle caused by the addition of PPE-DABCO (10 µg/mL) (A) and OPE-3 (50 µg/mL) (B) at room temperature. The vesicle is composed of *E. coli* total lipids and labeled with 0.5 mol% of DMPE-Rh for imaging and 2.5 mol% of Biotin-PEG-DSPE for localization to the slide surface.[23] The elapsed time after the addition of the antimicrobial agent is labeled in each image.

The same technique has also been used to image membrane morphological changes induced by polymeric PPE-DABCO and oligomeric OPE-3. As shown in Figure 3.11A, upon the addition of PPE-DABCO to a giant vesicle composed of *E. coli* total lipids, the vesicle appeared relatively intact until it suddenly ruptured 55 – 56 s after PPE-DABCO addition and then mostly disappeared at around 58 s. In contrast, after the addition of OPE-3, the giant vesicle immediately started to change, shrinking in size and becoming diffuse and eventually losing its structural integrity by 27 s (Figure 3.11B). During the process, the well-defined and bright lipid membrane became amorphous in shape and inhomogeneous in brightness, indicating that lipid-OPE-3 complexes may have been

formed (Figure 3.11B). These images show that both PPE-DABCO and OPE-3 exhibit strong disruptive activities against the model bacterial membrane and that the two compounds cause membrane disruptions *via* different mechanisms. However, this assay does not give further insights into the molecular scale structural transformations of the bilayer induced by the two biocidal compounds.

#### 3.2.3.2 Cryo-TEM imaging

To more closely examine membrane changes induced by the biocidal compounds, cryo-TEM was used to image LUVs before and after exposure to two different OPEs, OPE-2 and EO-OPE-1(C3). The cryo-TEM image of LUVs (Figure 3.12A) showed largely round vesicles with diameters of around 100 nm. The addition of OPE-2 appeared to induce vesicle fusion, resulting in the formation of many dumbbell-like bilayer structures (Figure 3.12B). The vesicle fusion process may proceed by the attachment of OPE-2 to vesicle surface, thereby changing its charge distribution and reducing vesicle-vesicle electrostatic repulsion, resulting in vesicle fusion. Similarly, the addition of EO-OPE-1(C3) to vesicles also caused vesicle fusion (Figure 3.12C). In addition, EO-OPE-1(C3) induced significant roughness to a number of vesicles (Figure 3.12C and D), which could be an early stage of membrane failure/collapse. Although cryo-TEM is a powerful technique in visualizing assemblies of soft biological materials with minimal disturbance to the sample, as compared to conventional TEM where samples are dried on a substrate, it does have the limitation that only a very thin section of the samples are visualized. Structures larger than sample thickness, for example, visible aggregates of OPE-membrane complexes formed during the experiment, were not imaged. As such, cryo-TEM imaging does not capture the full range of OPE and CPE-induced membrane

changes.

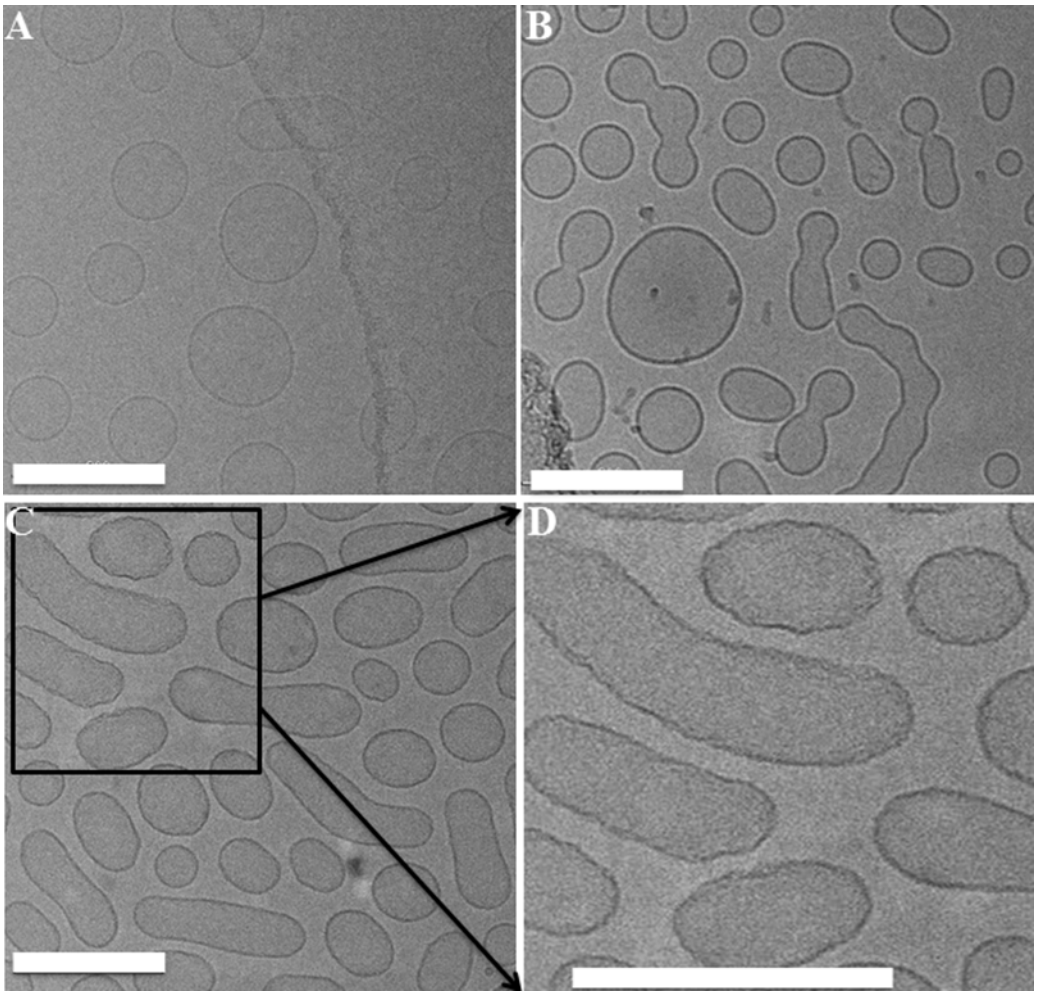


**Figure 3.12**. Cryo-TEM micrographs of DOPG/DOPE vesicles (10 mg/mL) alone (A), incubated with 2.16 mg/mL OPE-2 (B) 1.53 mg/mL EO-OPE-1(C3) (C) for 30 min in the dark. A closer view for the EO-OPE-1(C3) treated vesicles shown in D. The lipid to OPE molar ratio is 25:1. The scale bars represent 200 nm.

### 3.2.3.3 Small angle X-ray scattering

SAXS can resolve Å-scale structural details of ordered lipid phases in bilayer membranes and has been used to detect the presence of lipid ordered structures in a bulk background.[51] As described above, the potent antimicrobial activity of EO-OPE-1(C3) stems from its high membrane activity; it is of particular interest to further investigate its membrane perturbation mechanism by SAXS. In addition to vesicles composed of *E. coli*

total lipid extract, vesicles made of 20:80 DOPG:DOPE were also used for the SAXS assay (see Experimental Methods). For vesicles alone, only one broad peak with low scattering intensity is detected for each lipid composition (Figure 3.13, red lines), which suggests the existence of a lamellar phase for the SUVs.[52] After exposure to EO-OPE-1(C3), scattering profiles of the vesicles dramatically changed. Multiple, new and sharp scattering peaks are observed in both membrane systems. The peak at q = 0.3296 $Å^{-1}$ is due to EO-OPE-1(C3) (data not shown). The peak positions (q values) of the DOPG:DOPE model membrane exposed to EO-OPE-1 have the characteristic ratio of 1: $\sqrt{3} : 2 : \sqrt{7}$, indicative of an inverted hexagonal phase (Figure 3.13A).[53] A similar trend is observed for the vesicles composed of the more complex *E. coli* total lipids (Figure 3.13B), although the exact positions of the new peaks deviate from that of an inverted hexagonal phase and the nature of the new lipid phase at present is unclear. Tew and co-workers have systematically investigated the membrane perturbation activity of a series of antimicrobial meta-phenylene ethynylene oligomers via SAXS and other technologies.[9, 54] Similar to what we have observed for EO-OPE-1(C3), one of Tew's membrane active oligomers, AMO-2, was capable of forming a complex with *E. coli* lipid membranes/vesicles and induce a hexagonal structure. The deviation of the SAXS peak positions from the characteristic inverted hexagonal phase has been attributed to the complex lipid distribution from the bacterial membrane extracts. As described in the single giant vesicle imaging section, the EO-OPE-1(C3) and *E. coli* membrane complex was not soluble in the aqueous solvent, which also supports the assumption of the possible formation of hydrophobic inverted hexagonal complex. At the current stage, we can not rule out the possibility of the formation of other bicontinuous cubic phases for the

EO-OPE-1(C3) and *E. coli* membrane complex. However, these changes indicate that the oligomer is capable of inducing specific structural changes to the lamellar lipid phase. Wimley proposed the interfacial activity model to explain the membrane activity of antimicrobial peptides. Based on Wimley's theory and our previous dye release assays, OPE-1 and EO-OPE-1(C3) may not be able to induce the formation of permanent transmembrane pores in lipid vesicles such as barrel stave pores.

We also used SAXS to characterize the effects of oligomeric OPE-2 and polymeric PPE-Th on lipid membrane structure. After exposure to OPE-2 and PPE-Th, scattering profiles of the vesicles changed dramatically (Figures 3.13C and D). A number of new and sharp scattering peaks were observed. The peak positions ($q$ values) of the model membranes treated by OPE-2 and PPE-Th have the characteristic ratio of 1:2:3:4, indicative of a new multi-lamellar structure.[55] As a control, DMSO, which was used to increase the solubility of the OPEs, had negligible effect on the membrane structure (Figure 3.14). Therefore, the emergence of the new peaks due to the formation of multilamellar structures, were solely caused by the interactions between the CPE and OPE compounds with the model membrane. The SAXS experiments demonstrate that both polymeric and oligomeric biocidal compounds are capable of inducing structural reorganization of the lipid membrane on the molecular scale.

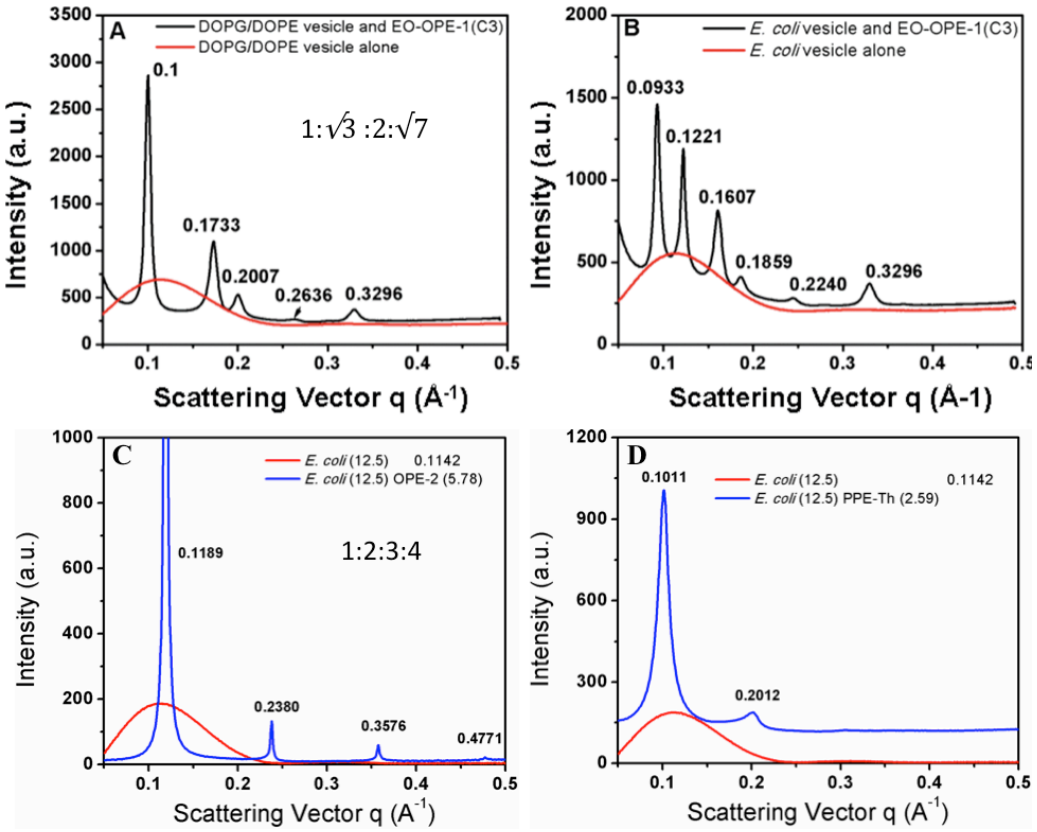


**Figure 3.13**. SAXS data for EO-OPE-1(C3) (3.8 mg/ml) complexed with 20:80 DOPG/DOPE (12.5 mg/ml) (A) and EO-OPE-1(C3) (3.8 mg/ml) (B), OPE-2 (5.78 mg/mL) (C) and PPE-Th (2.59 mg/mL) (D) complexed with *E. coli* total lipid (12.5 mg/mL) model membranes.

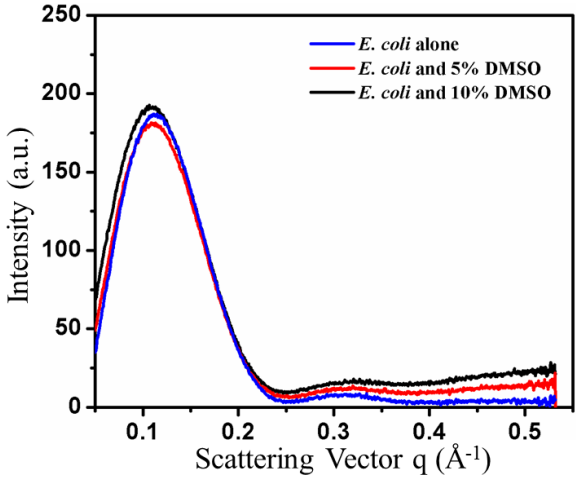


**Figure 3.14**. SAXS data for *E. coli* total lipid (12.5 mg/ml) model membranes alone and incubated with DMSO.

### 3.2.3.4 $^{31}$P solid state NMR

In addition to SAXS, $^{31}$P SS-NMR spectroscopy was also used to investigate the bulk phase behavior of model membranes in the presence of increasing amounts of EO-OPE-1(C3). In these experiments, the anisotropy (orientation of the phosphate head groups) of the lipid self-assemblies exhibit distinct NMR line shapes for different phases. The $^{31}$P NMR signal of the bacterial mimic DOPG/DOPE membrane is characteristic of a randomly dispersed lipid bilayer (bottom spectrum in Figure 3.15). The addition of 1.5 mg EO-OPE-1(C3) (to 25 mg of lipid) caused a significant decrease in the signal intensity in the high field and induced an additional peak at the isotropic chemical shift position, indicating the formation of isotropic non-bilayer phases, such as micelles, inverted micelles, or various cubic phases.[56] With increasing concentrations of EO-OPE-1(C3) (2.5-5 mg), the lipid sample showed a single sharp isotropic peak, indicating that EO-OPE-1(C3) did not induce the formation of new structures other than the isotropic phases in this concentration range. The addition of Triton X-100, a well-known non-ionic detergent that is widely used as a lipid membrane solubilizing agent, also gave rise to a weak isotropic peak, which implies that the two compounds induced similar bulk phase changes to the lipid membranes (Figure 3.15). SS-NMR data were also collected from vesicles composed of *E. coli* total lipid extract. The appearance of non-bilayer phases caused by the addition of EO-OPE-1(C3) to this model membrane was also observed (Figure 3.16). However, since the exact composition of the total lipid extract is unknown, the NMR spectra could not be further resolved.

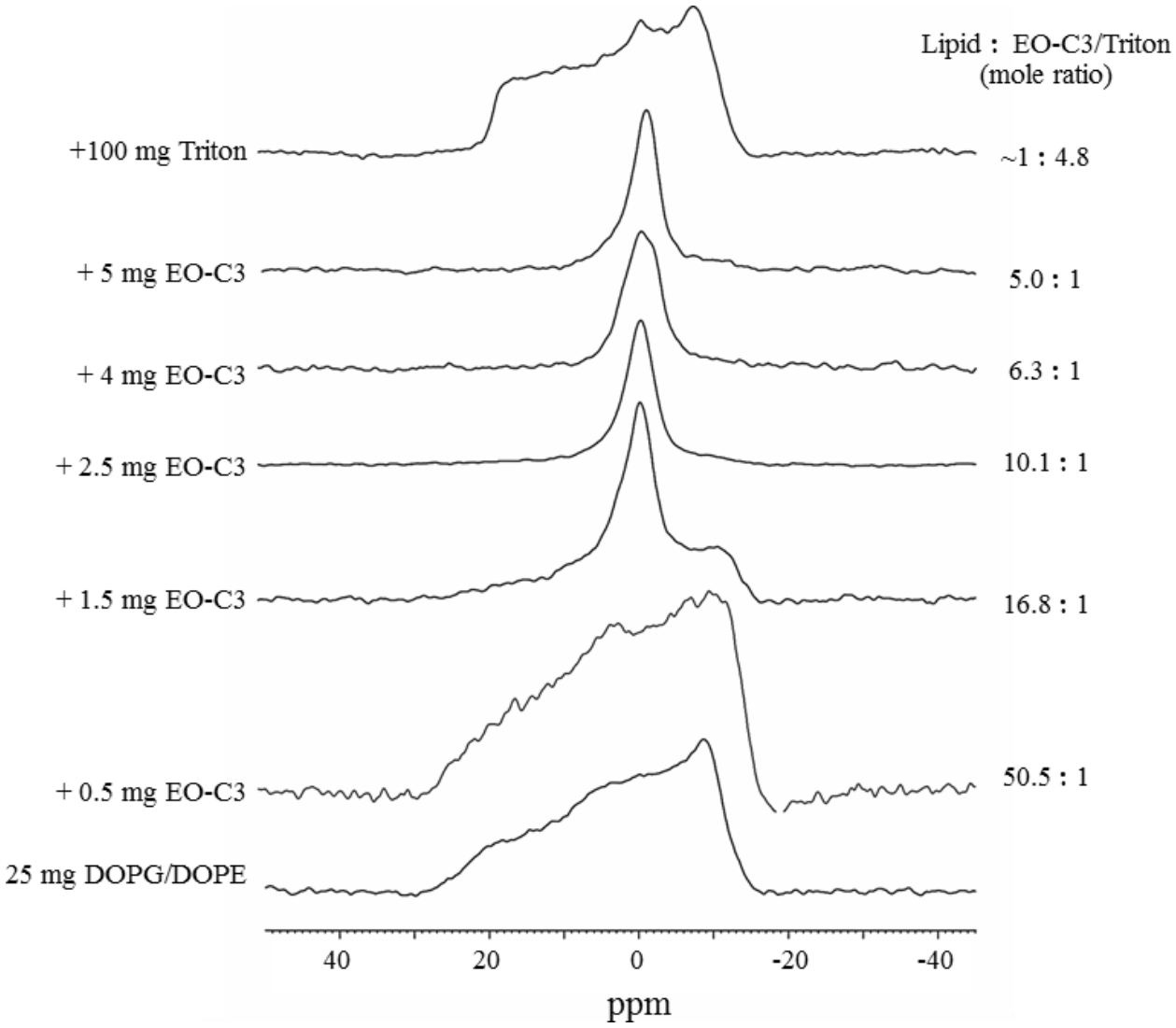


**Figure 3.15**. $^{31}$P SS-NMR spectra of 25 mg DOPG/DOPE (molar ration 2:8) model membranes mixed with various amounts of EO-OPE-1(C3) and 100 mg Triton.

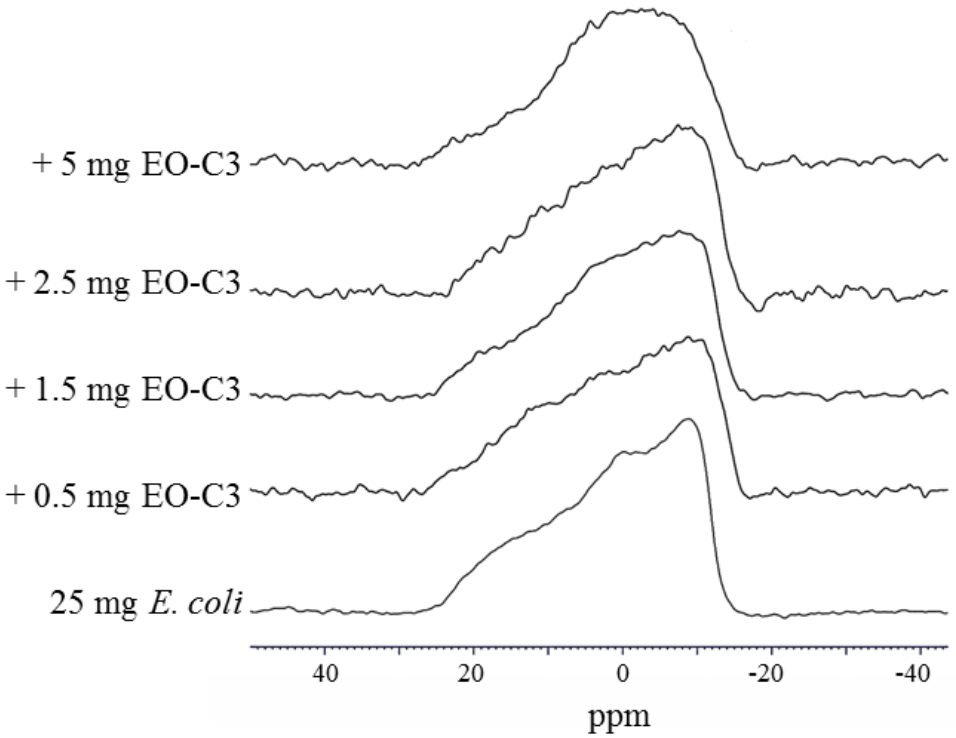


**Figure 3.16**. $^{31}$P SS-NMR spectra of 25 mg model membranes made by *E. coli* lipid extracts mixed with various amounts of EO-OPE-1(C3).

### 3.2.3.5 Conclusions

Results from the membrane perturbation study confirm that the CPE and OPE materials are membrane active and induce membrane changes from morphological to molecular scale. Giant vesicle imaging shows disintegration of vesicles while cryo-TEM imaging provided clear evidence of OPE and CPE-induced membrane fusion and roughening. Our results also provide a molecular scale structural basis for the observed membrane morphological and functional changes (i.e., membrane permeabilization from vesicle release studies). The CPE and OPE materials can disrupt the lamellar membrane structure and induce the formation of non-bilayer structures, such as hexagonal and cubic phases and micellar structures. It is important to note that, due to different sample requirements by the different analytical methods, such as concentration, sample thickness,

hydration state, and lamellarity, each method probes the interactions between the biocidal compounds and model membranes under a specific set of conditions that give insights to specific aspects of biocide-induced membrane perturbation.[146] Recent simulation studies show that OPE-3 with ionic side groups may strongly associate with the model bacterial membrane and disrupt the bilayer by the formation of water channels (Figure 3.17A).[57] However, EO-OPE-1(C3) with the ionic groups at the ends of the molecule is unlikely to form transmembrane, water-permeable pores in the same membrane (Figure 3.17B).[58] It has been suggested that these PPE-based materials most likely disrupt the lipid membrane via carpet or detergent-like mechanisms. Our multi-scale characterization of the dark membrane perturbation activity of the CPEs and OPEs using model *E. coli* plasma membranes so far support a carpet or detergent-like mechanism by which these antimicrobial compounds induce membrane collapse and phase transitions.

Most of the naturally occurring antimicrobial peptides (AMPs) are cationic and amphiphilic, and it is widely accepted that the bacterial cytoplasmic membrane is one of the primary targets of the AMPs. Several models have been proposed to explain the membrane perturbation mechanisms of the AMPs.[20] While the membrane disruption models are conceptually useful, many fundamental aspects about the membrane activity of AMPs remain unclear.[29] Considering the common cationic and amphiphilic nature shared by both CPEs/OPEs and AMPs, these materials may bind and disrupt the lipid membrane with similar chemical and physical driving forces. Although multiple biophysical and biochemical techniques have been used to study the structural and functional changes model lipid membranes undergo when exposed to CPEs and OPEs, a fundamental molecular-level mechanistic understanding of the membrane

permeabilization actions of the CPE and OPE materials is still lacking. “The Blindfolded Men and the Elephant” story has been used to describe the problems in understanding the antimicrobial mechanisms of the AMPs.[59] Just like the six blindfolded people “observing” the elephant, each technique used in our studies only reports one aspect of the membrane perturbation mechanism(s) of the PPE-based materials under a specific set of experimental conditions.

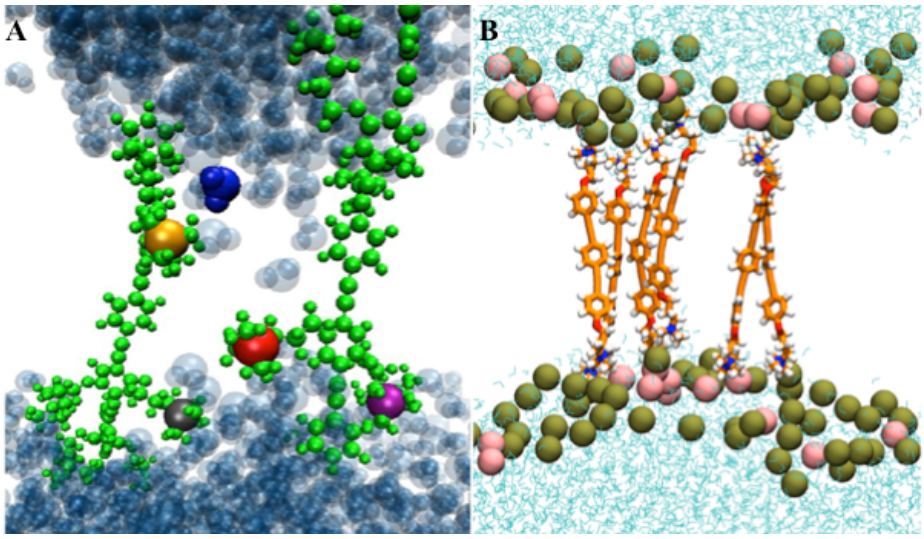


**Figure 3.17**. Two different representations of snapshots from simulation studies of the OPE-DOPG/DOPE membrane interactions (A) Nitrogen atoms in the cationic quaternary ammonium groups of OPE-3 are illustrated in gray, red, yellow, and purple. The backbones of the OPE molecules creating the pore are shown in green. Waters are shown as diffuse blue spheres. Reprinted with permission from ref 57. Copyright 2012 ACS Publications. (B) The backbones of EO-OPE-1(C3) are shown in orange. Nitrogen atoms in the cationic quaternary ammonium groups are illustrated in blue. The phosphorus atoms on the lipid hand groups are shown in tan and pink. Waters are shown in cyan. Reprinted from ref. 58 with kind permission from Springer Science+Business Media.

### 3.3 References

1. Zasloff, M., Antimicrobial peptides of multicellular organisms. *Nature* **2002,** *415* (6870), 389-395.

2. Bechinger, B.; Lohner, K., Detergent-like actions of linear amphipathic cationic

antimicrobial peptides. *Bba-Biomembranes* **2006,** *1758* (9), 1529-1539.

3. Brogden, K. A., Antimicrobial peptides: Pore formers or metabolic inhibitors in bacteria? *Nat. Rev. Microbiol.* **2005,** *3* (3), 238-250.

4. Wimley, W. C., Describing the Mechanism of Antimicrobial Peptide Action with the Interfacial Activity Model. *ACS Chem. Biol.* **2010,** *5* (10), 905-917.

5. La Rocca, P.; Biggin, P. C.; Tieleman, D. P.; Sansom, M. S. P., Simulation studies of the interaction of antimicrobial peptides and lipid bilayers. *Bba-Biomembranes* **1999,** *1462* (1-2), 185-200.

6. Wang, Y.; Tang, Y. L.; Zhou, Z. J.; Ji, E.; Lopez, G. P.; Chi, E. Y.; Schanze, K. S.; Whitten, D. G., Membrane Perturbation Activity of Cationic Phenylene Ethynylene Oligomers and Polymers: Selectivity against Model Bacterial and Mammalian Membranes. *Langmuir* **2010,** *26* (15), 12509-12514.

7. Graham, J. M.;Higgins, J. A. Membrane Analysis; Springer; New York, **1997**.

8. Wang, Y.; Jones, E. M.; Tang, Y. L.; Ji, E. K.; Lopez, G. P.; Chi, E. Y.; Schanze, K. S.; Whitten, D. G., Effect of Polymer Chain Length on Membrane Perturbation Activity of Cationic Phenylene Ethynylene Oligomers and Polymers. *Langmuir* **2011,** *27* (17), 10770-10775.

9. Yang, L. H.; Gordon, V. D.; Trinkle, D. R.; Schmidt, N. W.; Davis, M. A.; DeVries, C.; Som, A.; Cronan, J. E.; Tew, G. N.; Wong, G. C. L., Mechanism of a prototypical synthetic membrane-active antimicrobial: Efficient hole-punching via interaction with negative intrinsic curvature lipids. *Proc. Natl. Acad. Sci. USA* **2008,** *105* (52), 20595-20600.

10. Gabriel, G. J.; Som, A.; Madkour, A. E.; Eren, T.; Tew, G. N., Infectious disease:

Connecting innate immunity to biocidal polymers. *Mat. Sci. Eng. R* **2007,** *57* (1-6), 28-64.

11. Palermo, E. F.; Kuroda, K., Structural determinants of antimicrobial activity in polymers which mimic host defense peptides. *Appl. Microbiol. Biot.* **2010,** *87* (5), 1605-1615.

12. Wang, Y.; Chi, E. Y.; Schanze, K. S.; Whitten, D. G., Membrane activity of antimicrobial phenylene ethynylene based polymers and oligomers. *Soft Matter* **2012,** *8*, 8547–8558.

13. Huang, H. W., Molecular mechanism of antimicrobial peptides: The origin of cooperativity. *Bba-Biomembranes* **2006,** *1758* (9), 1292-1302.

14. Bechinger, B., The structure, dynamics and orientation of antimicrobial peptides in membranes by multidimensional solid-state NMR spectroscopy. *Bba-Biomembranes* **1999,** *1462* (1-2), 157-183.

15. Yang, L.; Harroun, T. A.; Weiss, T. M.; Ding, L.; Huang, H. W., Barrel-stave model or toroidal model? A case study on melittin pores. *Biophys. J.* **2001,** *81* (3), 1475-1485.

16. Shai, Y., Mode of action of membrane active antimicrobial peptides. *Biopolymers* **2002,** *66* (4), 236-248.

17. Stella, L.; Mazzuca, C.; Venanzi, M.; Palleschi, A.; Didone, M.; Formaggio, F.; Toniolo, C.; Pispisa, B., Aggregation and water-membrane partition as major determinants of the activity of the antibiotic peptide trichogin GA IV. *Biophys. J.* **2004,** *86* (2), 936-945.

18. Gazit, E.; Miller, I. R.; Biggin, P. C.; Sansom, M. S. P.; Shai, Y., Structure and orientation of the mammalian antibacterial peptide cecropin P1 within phospholipid

membranes. *J. Mol. Biol.* **1996,** *258* (5), 860-870.

19. Verdon, J.; Falge, M.; Maier, E.; Bruhn, H.; Steinert, M.; Faber, C.; Benz, R.; Hechard, Y., Detergent-Like Activity and alpha-Helical Structure of Warnericin RK, an Anti-Legionella Peptide. *Biophys. J.* **2009,** *97* (7), 1933-1940.

20. Vanounou, S.; Pines, D.; Pines, E.; Parola, A. H.; Fishov, I., Coexistence of domains with distinct order and polarity in fluid bacterial membranes. *Photochem. Photobiol.* **2002,** *76* (1), 1-11.

21. Epand, R. M.; Epand, R. F., Lipid domains in bacterial membranes and the action of antimicrobial agents. *Bba-Biomembranes* **2009,** *1788* (1), 289-294.

22. Cronan, J. E., Bacterial membrane lipids: Where do we stand? *Annu. Rev. Microbiol.* **2003,** *57*, 203-224.

23. Vance, D. E.; Vance, J. Biochemistry of Lipids, Lipoproteins and Membranes, 2nd ed.; Elsevier Science: Amsterdam, **1991**; Vol. 20.

24. Som, A.; Tew, G. N., Influence of lipid composition on membrane activity of antimicrobial phenylene ethynylene oligomers. *J. Phys. Chem. B* **2008,** *112* (11), 3495-3502.

25. Ahyayauch, H.; Bennouna, M.; Alonso, A.; Goni, F. M., Detergent effects on membranes at subsolubilizing concentrations: transmembrane lipid motion, bilayer permeabilization, and vesicle lysis/reassembly are independent phenomena. *Langmuir* **2010,** *26* (10), 7307-13.

26. Ding, L. P.; Chi, E. Y.; Chemburu, S.; Ji, E.; Schanze, K. S.; Lopez, G. P.; Whitten, D. G., Insight into the Mechanism of Antimicrobial Poly(phenylene ethynylene) Polyelectrolytes: Interactions with Phosphatidylglycerol Lipid Membranes. *Langmuir*

**2009,** *25* (24), 13742-13751.

27. Sperotto, M. M.; Mouritsen, O. G., Dependence of Lipid-Membrane Phase-Transition Temperature on the Mismatch of Protein and Lipid Hydrophobic Thickness. *Eur. Biophys. J. Biophy.* **1988,** *16* (1), 1-10.

28. Ambroggio, E. E.; Separovic, F.; Bowie, J. H.; Fidelio, G. D.; Bagatolli, L. A., Direct visualization of membrane leakage induced by the antibiotic peptides: Maculatin, citropin, and aurein. *Biophys. J.* **2005,** *89* (3), 1874-1881.

29. Ding, L. P.; Chi, E. Y.; Schanze, K. S.; Lopez, G. P.; Whitten, D. G., Insight into the Mechanism of Antimicrobial Conjugated Polyelectrolytes: Lipid Headgroup Charge and Membrane Fluidity Effects. *Langmuir* **2010,** *26* (8), 5544-5550.

30. Zhao, X. Y.; Pinto, M. R.; Hardison, L. M.; Mwaura, J.; Muller, J.; Jiang, H.; Witker, D.; Kleiman, V. D.; Reynolds, J. R.; Schanze, K. S., Variable band gap poly(arylene ethynylene) conjugated polyelectrolytes. *Macromolecules* **2006,** *39* (19), 6355-6366.

31. Tang, Y. L.; Zhou, Z. J.; Ogawa, K.; Lopez, G. P.; Schanze, K. S.; Whitten, D. G., Photophysics and self-assembly of symmetrical and unsymmetrical cationic oligophenylene ethynylenes. *J. Photochem. Photobiol.* **2009,** *207* (1), 4-6.

32. Huang, H. W.; Chen, F. Y.; Lee, M. T., Molecular mechanism of peptide-induced pores in membranes. *Phys. Rev. Lett.* **2004,** *92* (19), 1983041-1983044.

33. Rodriguez, N.; Cribier, S.; Pincet, F., Transition from long- to short-lived transient pores in giant vesicles in an aqueous medium. *Phys. Rev. E* **2006,** *74* (6), 619021-6190210.

34. Karatekin, E.; Sandre, O.; Guitouni, H.; Borghi, N.; Puech, P. H.; Brochard-Wyart,

F., Cascades of transient pores in giant vesicles: Line tension and transport. *Biophys. J.* **2003,** *84* (3), 1734-1749.

35. Srividya, N.; Muralidharan, S., Determination of the line tension of giant vesicles from pore-closing dynamics. *J. Phys. Chem. B* **2008,** *112* (24), 7147-7152.

36. Orioni, B.; Bocchinfuso, G.; Kim, J. Y.; Palleschi, A.; Grande, G.; Bobone, S.; Park, Y.; Kim, J. I.; Hahm, K. S.; Stella, L., Membrane perturbation by the antimicrobial peptide PMAP-23: A fluorescence and molecular dynamics study. *Bba-Biomembranes* **2009,** *1788* (7), 1523-1533.

37. Rennie, J.; Arnt, L.; Tang, H. Z.; Nusslein, K.; Tew, G. N., Simple oligomers as antimicrobial peptide mimics. *J. Ind. Microbiol. Biot.* **2005,** *32* (7), 296-300.

38. Ji, E. K.; Parthasarathy, A.; Corbitt, T. S.; Schanze, K. S.; Whitten, D. G., Antibacterial Activity of Conjugated Polyelectrolytes with Variable Chain Lengths. *Langmuir* **2011,** *27* (17), 10763-10769.

39. Tang, Y. L.; Hill, E. H.; Zhou, Z. J.; Evans, D. G.; Schanze, K. S.; Whitten, D. G., Synthesis, Self-Assembly, and Photophysical Properties of Cationic Oligo(p-phenyleneethynylene)s. *Langmuir* **2011,** *27* (8), 4945-4955.

40. Traiphol, R.; Potai, R.; Charoenthai, N.; Srikhirin, T.; Kerdcharoen, T.; Osotchan, T., Effects of Chain Conformation and Chain Length on Degree of Aggregation in Assembled Particles of Conjugated Polymer in Solvents-Nonsolvent: A Spectroscopic Study. *J. Polym. Sci. Pol. Phys.* **2010,** *48* (8), 894-904.

41. Arnrutha, S. R.; Jayakannan, M., Probing the pi-stacking induced molecular aggregation in pi-conjugated polymers, oligomers, and their blends of p-phenylenevinylenes. *J. Phys. Chem. B* **2008,** *112* (4), 1119-1129.

42. Okuyama, K.; Hasegawa, T.; Ito, M.; Mikami, N., Electronic-Spectra of Tolane in a Supersonic Free Jet - Large-Amplitude Torsional Motion. *J. Phys. Chem.* **1984,** *88* (9), 1711-1716.

43. Chen, L. H.; Xu, S.; McBranch, D.; Whitten, D., Tuning the properties of conjugated polyelectrolytes through surfactant complexation. *J. Am. Chem. Soc.* **2000,** *122* (38), 9302-9303.

44. Miteva, T.; Palmer, L.; Kloppenburg, L.; Neher, D.; Bunz, U. H. F., Interplay of thermochromicity and liquid crystalline behavior in poly(p-phenyleneethynylene)s: pi-pi interactions or planarization of the conjugated backbone? *Macromolecules* **2000,** *33* (3), 652-654.

45. James, P. V.; Sudeep, P. K.; Suresh, C. H.; Thomas, K. G., Photophysical and theoretical investigations of oligo(p-phenyleneethynylene)s: Effect of alkoxy substitution and alkyne-aryl bond rotations. *J. Phys. Chem. A* **2006,** *110* (13), 4329-4337.

46. Tan, C. Y.; Alas, E.; Muller, J. G.; Pinto, M. R.; Kleiman, V. D.; Schanze, K. S., Amplified quenching of a conjugated polyelectrolyte by cyanine dyes. *J. Am. Chem. Soc.* **2004,** *126* (42), 13685-13694.

47. Liu, Y.; Ogawa, K.; Schanze, K. S., Conjugated polyelectrolyte based real-time fluorescence assay for phospholipase C. *Anal. Chem.* **2008,** *80* (1), 150-158.

48. Kaur, P.; Yue, H. J.; Wu, M. Y.; Liu, M.; Treece, J.; Waldeck, D. H.; Xue, C. H.; Liu, H. Y., Solvation and aggregation of polyphenylethynylene based anionic polyelectrolytes in dilute solutions. *J. Phys. Chem. B* **2007,** *111* (29), 8589-8596.

49. Ngo, A. T.; Karam, P.; Fuller, E.; Burger, M.; Cosa, G., Liposome encapsulation of conjugated polyelectrolytes: Toward a liposome beacon. *J. Am. Chem. Soc.* **2008,** *130*

(2), 457-459.

50. Ege, C.; Lee, K. Y. C., Insertion of Alzheimer's A beta 40 peptide into lipid monolayers. *Biophys. J.* **2004,** *87* (3), 1732-1740.

51. Turner, D. C.; Gruner, S. M., X-ray diffraction reconstruction of the inverted hexagonal (HII) phase in lipid-water systems. *Biochemistry-Us* **1992,** *31* (5), 1340-55.

52. Mishra, A.; Gordon, V. D.; Yang, L. H.; Coridan, R.; Wong, G. C. L., HIV TAT forms pores in membranes by inducing saddle-splay curvature: Potential role of bidentate hydrogen bonding. *Angew. Chem. Int. Ed.* **2008,** *47* (16), 2986-2989.

53. Koltover, I.; Salditt, T.; Radler, J. O.; Safinya, C. R., An inverted hexagonal phase of cationic liposome-DNA complexes related to DNA release and delivery. *Science* **1998,** *281* (5373), 78-81.

54. Yang, L. H.; Gordon, V. D.; Mishra, A.; Sorn, A.; Purdy, K. R.; Davis, M. A.; Tew, G. N.; Wong, G. C. L., Synthetic antimicrobial, oligomers induce a composition-dependent topological transition in membranes. *J. Am. Chem. Soc.* **2007,** *129* (40), 12141-12147.

55. Alexandridis, P.; Olsson, U.; Lindman, B., A Record Nine Different Phases (Four Cubic, Two Hexagonal, and One Lamellar Lyotropic Liquid Crystalline and Two Micellar Solutions) in a Ternary Isothermal System of an Amphiphilic Block Copolymer and Selective Solvents (Water and Oil). *Langmuir* **1998,** *14* (10), 2627-2638.

56. Strandberg, E.; Ulrich, A. S., NMR methods for studying membrane-active antimicrobial peptides. *Concept Mag. Reson. A* **2004,** *23A* (2), 89–120.

57. Hill, E. H.; Stratton, K.; Whitten, D. G.; Evans, D. G., Molecular Dynamics Simulation Study of the Interaction of Cationic Biocides with Lipid Bilayers:

Aggregation Effects and Bilayer Damage. *Langmuir* **2012**, 28, 14849-14854.

58. Li, Y.; Guo, H., Atomistic simulations of an antimicrobial molecule interacting with a model bacterial membrane. *Theor. Chem. Acc.* **2012,** *132* (1), 1-8.

59. Wimley, W. C.; Hristova, K., Antimicrobial Peptides: Successes, Challenges and Unanswered Questions. *J. Membrane Biol.* **2011,** *239* (1-2), 27-34.

# Chapter 4. Interactions with Proteins and Nucleic Acids

## 4.1 Introduction

In addition to exhibiting biocidal activity against bacteria, the CPEs and OPEs can also efficiently inactivate the wildtype Sterne strain of *Bacillus anthracis* spore, yeast spore[1] and two model viruses (T4 and MS2 bacteriophages).[2] Unlike those of bacteria, the surfaces of these pathogens are comprised of a significant amount of proteins, implying that proteins and protein assemblies can also be targets of the CPE and OPE materials. Moreover, the CPEs and OPEs can create defects on the cell envelope[3] and viral capsid,[2] which may facilitate their entrance into the cell and viral interior. Once inside, the CPEs and OPEs can interact and potentially disrupt other (cellular) targets, such as DNA, RNA, and polysaccharides (cellulose). It is evident that the CPE and OPE materials can induce damage to multiple cellular targets. Proteins in the cytoplasm are believed to be another target, particularly for $^1O_2$ generated under UV-irradiation as amino acids are readily oxidized by $^1O_2$ with a rate constant in the range of $10^7$-$10^8$ $M^{-1}s^{-1}$.[4-5] Moreover, secondary ROS could react with a broader range of targets in the cell, including the DNA and RNA. The ROS sensitized by the CPE and OPE materials can directly or indirectly covalently modify biomolecules in the cytoplasm, thereby inducing toxicity. Furthermore, proteins and nucleic acids are believed the main targets of the singlet oxygen-mediated damage (Figure 4.1).[4]

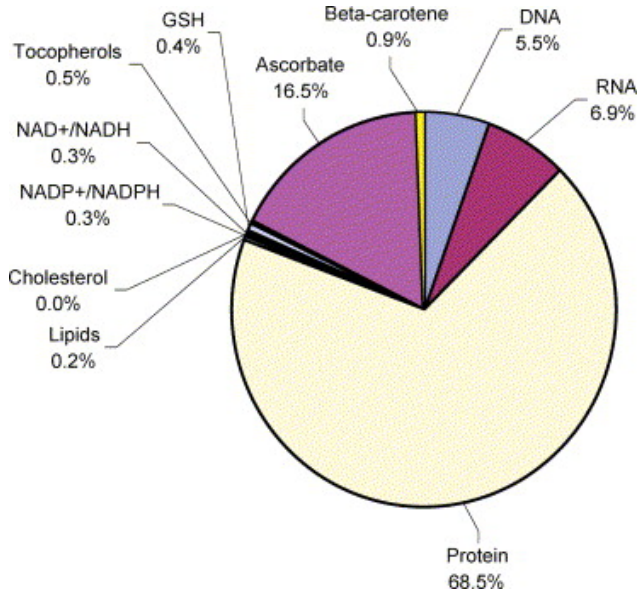


**Figure 4.1**. Predicted consumption of $^1O_2$ by intracellular targets calculated using the rate constant data given in and the average concentration of each component within a typical leukocyte cell. Reprinted with permission from ref 4.

## 4.2 Results and Discussion

### 4.2.1 Interactions with proteins

Since proteins are a key component of biological cells,[6] studying their interactions with CPEs and OPEs will provide further insight into CPEs and OPEs' toxicity mechanisms. In this study, the effects of CPEs and OPEs on the secondary structure of three model proteins, bovine serum albumin (BSA), lysozyme, and cytochrome C were evaluated. Lysozyme and cytochrome C are well-folded small globular proteins that have been extensively studied. BSA possesses a high degree of homology with human serum albumin (HSA).[7-8] Serum albumins are abundant in the mammalian circulatory system and carry out various important physiological functions.[9] More important, BSA is a more hydrophobic protein with high surface activity compared to the highly soluble and charged lysozyme and cytochrome C, and should serve as a better model for membrane

proteins. The physicochemical properties of these model proteins are summarized in Table 4.1.[10-12] The addition of CPEs and OPEs did not induce any changes in the CD spectra of lysozyme or cytochrome C (data not shown), suggesting that no conformational changes to the native protein structures were induced. This is probably due to the electrostatic repulsion between the cationic CPEs and OPEs with the two positively charged proteins (see Table 4.1) that prevented their association. In contrast, some degree of structural perturbation was observed for BSA incubated with CPEs and OPEs in the dark (Figures 4.2 and 4.3). In particular, the addition of PPE-Th caused the most significant loss to the protein's secondary structures (200-260 nm). Furthermore, the BSA/PPE-Th mixture is also uniquely CD active in 400-500 nm region, where PPE-Th absorbs (inset of Figure 4.2). By itself, the PPE-Th polymer is not CD active in this region (data not shown). PPE-Th is known to be highly lipophilic and this property may be responsible for its ability to denature the relatively hydrophobic BSA.[13] Furthermore, complexing PPE-Th with BSA render the polymer CD-active, indicating that distinct structures are formed. PPE-DABCO also induces conformational change in BSA, albeit to a lesser extent compared to PPE-Th. In contrast, only small conformational changes are observed when BSA is incubated with the oligomers (Figure 4.3). Although none of the model proteins used in this study is a bacterial membrane protein, the result can provide some insights of to the interaction between our antimicrobial compounds and proteins. When a bacterial cell becomes associated with PPE-Th, one mode of its toxic pathway may be the denaturation of membrane proteins.

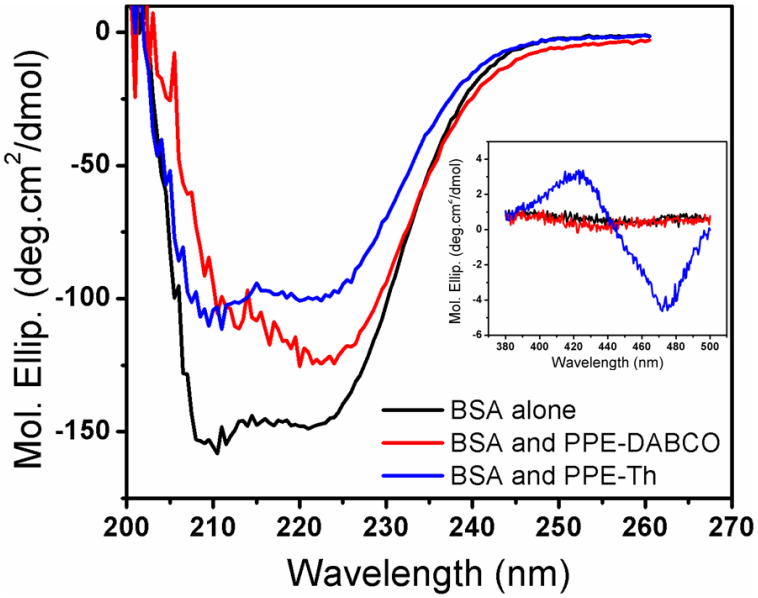


**Figure 4.2**. Circular dichroism spectra of BSA (0.1 mg/ml) and its complexes with CPEs (10 µg/ml) in phosphate buffer at room temperature. CPEs alone do not have any circular dichroism signal.

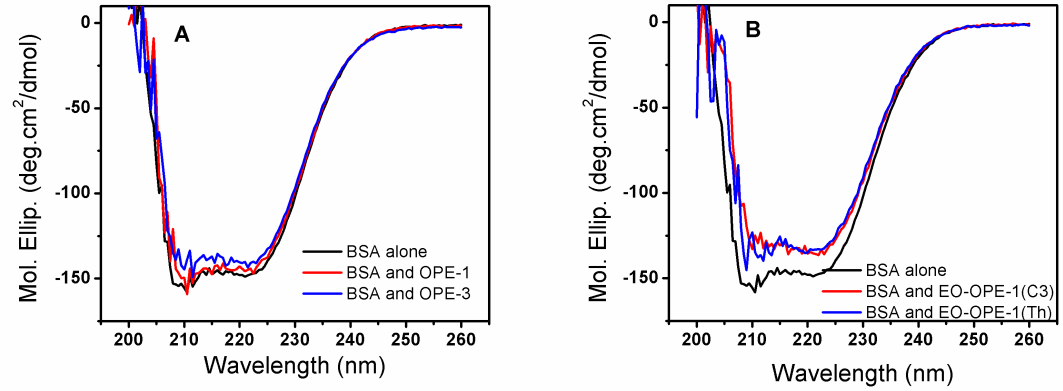


**Figure 4.3**. Circular dichroism spectra of BSA (0.1 mg/ml) along or in the presence of OPEs (10 µg/ml) in phosphate buffer (2 mM $NaH_2PO_4$, 8 mM $Na_2HPO_4$, pH 7.4) at room temperature. OPEs alone do not have any circular dichroism signal.

**Table 4.1**. Physicochemical properties of model proteins used in this study.

| Protein | BSA | Lysozyme | Cytochrome C |
|---|---|---|---|
| Isoelectric Point | 4.8 | 10.6 | 10~10.5 |
| Net charge* | - | + | + |
| Molecular Weight (KDa) | 66 | 14 | 12 |
| Main Secondary Structure | α -helical | α -helical | α -helical and unordered structure |

* Net charge on protein under current experimental conditions.

### 4.2.2 Electrophoresis characterization for the DNA and protein damage

We have demonstrated that the CPEs and OPEs can cause severe damage inside the Gram-negative bacteria in the presence of UV-light.[14] To better understand the nature of the changes, we investigated the effect of the oligomeric EO-OPE-1(C3) under UV-irradiation on two classes of potential targets in *E. coli*, proteins and plasmid DNA. As shown in Figure 4.4A, SDS-PAGE of *E. coli* cells under different exposure conditions to EO-OPE-1(C3) showed no significant differences in the electrophoretic mobilities or intensities of protein bands from cells treated with EO-OPE-1(C3) in the dark (Lane A2) or UV-irradiation alone (Lane A3) compared to untreated cells (Lane A1), indicating that the proteins did not undergo covalent modifications, such as cross linking or degradation. In contrast, protein bands from *E. coli* cells incubated with EO-OPE-1(C3) under UVA irradiation show significantly decreased intensities (Figure 4.4, Lane A4), indicating that $^1O_2$ and ROS generated by the irradiation of EO-OPE-1(C3) had induced significant covalent modifications to the proteins that either caused the formation of insoluble aggregates that are too large to enter the electrophoresis gel or degradation of proteins into fragments too small to be detected by the technique. Similarly, the ROS sensitized by EO-OPE-1(C3) caused considerable decreases to the intensities of the *E. coli* plasmid DNA bands (Lane B5) compared to untreated cells (Lane B2), whereas the bands remained relatively unchanged from *E. coli* cells incubated with EO-OPE-1(C3) for an hour in the dark (Lane B3) or irradiated for an hour (Lane B4). Cross-linking and subsequent aggregation are the primary protein chemical degradations induced by $^1O_2$ and secondary ROS.[4] Likewise, $^1O_2$ and secondary ROS could also induce the formation of covalent DNA-protein complexes.[15] However, protein-DNA complexes and aggregates

may not be soluble in water or identified from electrophoresis. In addition, ROS can also induce protein backbone fragmentation and DNA cleavage, which may also contribute to the changes observed in protein and plasmid DNA gel electrophoresis and the toxic functions of EO-OPE-1(C3). In addition to disrupting membrane lipid bilayer structure, damage to the proteins in bacterial cytoplasmic membranes by light-induced ROS, which serve critical functions, also compromise the membrane integrity and promote the release of cell content as well as the entrance of the CPEs and OPEs.

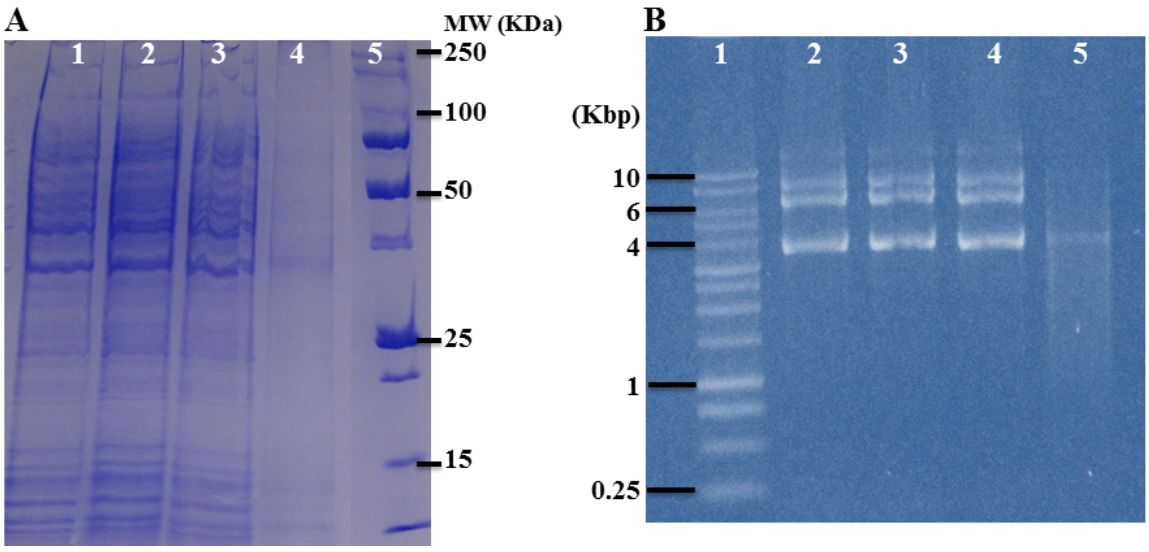


**Figure 4.4**. (A) SDS-PAGE gels of the *E. coli* ($4\times10^8$ CFU/mL) cells incubated with EO-OPE-1(C3) (25 μg/mL) for 1 hour. Lane A1: *E. coli* in the dark; Lane A2: *E. coli* incubated with EO-OPE for 1 hour in the dark; Lane A3: *E. coli* irradiated with UVA for 1 hour; Lane A4: *E. coli* incubated with EO-OPE under UVA-irradiation for 1 hour; Lane A5: Protein ladder. (B) Agarose-gel of the pET-20b plasmid extracted from *E. coli* BL21(DE3) ($1\times10^8$ CFU/mL) incubated with EO-OPE-1(C3) (1 μg/mL) for 1 hour. Lane B1: DNA ladder; Lane B2: *E. coli* in the dark; Lane B3: *E. coli* incubated with EO-OPE in the dark for 1 hour; Lane B4: *E. coli* irradiated with UVA for 1 hour; Lane B5: *E. coli* incubated with EO-OPE under UVA-irradiation for 1 hour.

### 4.3 Conclusions

To further investigate the toxicity pathway of the CPEs and OPEs upon their association to the bacterial surface, we have evaluated whether CPEs and OPEs affect

model protein structures. Herein, we characterized the effect of CPEs and OPEs on the conformation of model proteins bovine serum albumin (BSA), lysozyme and Cytochrome C using circular dichroism. PPE-Th and PPE-DABCO caused the significant losses to the BSA's secondary structures. Moreover, under UV-irradiation, all of the tested antimicrobial compounds can cause damage to the cytoplasm of the Gram-negative *E. coli* cells, including oxidative and covalent modifications of proteins and plasmid DNA.

### 4.4 References


1. Lu, L.; Rininsland, F. H.; Wittenburg, S. K.; Achyuthan, K. E.; McBranch, D. W.; Whitten, D. G., Biocidal activity of a light-absorbing fluorescent conjugated polyelectrolyte. *Langmuir* **2005,** *21* (22), 10154-9.

2. Wang, Y.; Canady, T. D.; Zhou, Z. J.; Tang, Y. L.; Price, D. N.; Bear, D. G.; Chi, E. Y.; Schanze, K. S.; Whitten, D. G., Cationic Phenylene Ethynylene Polymers and Oligomers Exhibit Efficient Antiviral Activity. *ACS Appl. Mater. Interfaces* **2011,** *3* (7), 2209-2214.

3. Wang, Y.; Jett, S. D.; Crum, J.; Schanze, K. S.; Chi, E. Y.; Whitten, D. G., Understanding the dark and light-enhanced bactericidal action of cationic conjugated polyelectrolytes and oligomers. *Langmuir* **2013,** *29* (2), 781-92.

4. Davies, M. J., Singlet oxygen-mediated damage to proteins and its consequences. *Biochem. Biophys. Res. Commun.* **2003,** *305* (3), 761-770.

5. Rabek, J. F., *Photochemistry and Photophysics*. CRC Press: Boca Raton, **1991**; Vol. 3.

6. Wu, M. H.; Maier, E.; Benz, R.; Hancock, R. E. W., Mechanism of interaction of different classes of cationic antimicrobial peptides with planar bilayers and with the

cytoplasmic membrane of Escherichia coli. *Biochemistry* **1999,** *38* (22), 7235-7242.

7. He, X. M.; Carter, D. C., Atomic-Structure and Chemistry of Human Serum-Albumin. *Nature* **1992,** *358* (6383), 209-215.

8. Charbonneau, D. M.; Tajmir-Riahi, H. A., Study on the interaction of cationic lipids with bovine serum albumin. *J. Phys. Chem. B* **2010,** *114* (2), 1148-55.

9. Peters. T. All about Albumin. Biochemistry, Genetics and Medical Applications; Academic Press: San Diego, CA, **1996**.

10. Razumovsky, L.; Damodaran, S., Surface activity-compressibility relationship of proteins at the air-water interface. *Langmuir* **1999,** *15* (4), 1392-1399.

11. White, F. H., Studies on Secondary Structure in Chicken Egg-White Lysozyme after Reductive Cleavage of Disulfide Bonds. *Biochemistry* **1976,** *15* (13), 2906-2911.

12. Aravind, U. K.; Mathew, J.; Aravindakumar, C. T., Transport studies of BSA, lysozyme and ovalbumin through chitosan/polystyrene sulfonate multilayer membrane. *J. Membr. Sci.* **2007,** *299* (1-2), 146-155.

13. Corbitt, T. S.; Ding, L. P.; Ji, E. Y.; Ista, L. K.; Ogawa, K.; Lopez, G. P.; Schanze, K. S.; Whitten, D. G., Light and dark biocidal activity of cationic poly(arylene ethynylene) conjugated polyelectrolytes. *Photochem. Photobiol. Sci.* **2009,** *8* (7), 998-1005.

14. Wang, Y.; Corbitt, T. S.; Jett, S. D.; Tang, Y.; Schanze, K. S.; Chi, E. Y.; Whitten, D. G., Direct visualization of bactericidal action of cationic conjugated polyelectrolytes and oligomers. *Langmuir* **2012,** *28* (1), 65-70.

15. Meffert, R.; Dose, K.; Rathgeber, G.; Schefer, H. J., Ultraviolet crosslinking of DNA protein complexes via 8-azidoadenine. *Methods Mol. Biol.* **2009,** *543*, 389-402.

# Chapter 5. Bactericidal Activities of the CPEs and OPEs

## 5.1 Introduction

Investigations of the biocidal mechanisms of the CPEs and OPEs revealed that these cationic and amphiphilic compounds are membrane-active, capable of inducing disruptions to the membrane structure.[1] For example, the small oligomeric EO-OPE-1(C3) (Scheme 1.3) can disrupt model bacterial membranes and induce a phase transition from a lamellar to a hexagonal phase. In general, these CPE and OPE materials exhibit broad spectrum and rapid light-enhanced biocidal activities and moderate killing efficiencies in the dark. Furthermore, both the light-activated and dark biocidal activities of CPEs and OPEs are believed to be initiated by their interactions with the bacterial outer envelopes. Therefore, the main focus of the work in this chapter is to understand the lethal effect of the CPEs and OPEs against bacteria in the dark and under UV-irradiation, which is also a part of our structure-activity relationship study.

The biocidal activity and selectivity of the CPE, OPE and other antimicrobial compounds can be related to their membrane perturbation ability. However, for some of the biocidal materials, their antimicrobial activity may also stem from the interaction with other bacterial outer envelope components, such as membrane embedded proteins and lipopolysaccharides (LPS).[2-4] In other words, their membrane activity may only partially account for the antimicrobial ability. Although some insights have been gained about CPE and OPE's biocidal and membrane activities, little is known about their mechanism or mode of binding to the bacterial outer envelope or the subsequent key toxicity-inducing events.

Since the cell surface serves as the first point of contact for biocidal agents, the

structure of the cell envelope is important in determining bacterial susceptibility to the CPEs and OPEs. There are significant structural differences between the outer envelopes of Gram-negative and Gram-positive microorganisms. The outer envelope of Gram-negative bacteria is composed of an outer membrane and a cytoplasm membrane (or inner membrane), which are separated by a thin intermittently cross-linked peptidoglycan network. The outer leaflet of Gram-negative bacterial outer membrane contains high levels of LPS (Scheme 3.1). On the other hand, Gram-positive bacteria only have one lipid membrane (cytoplasm membrane) covered by a thick layer of heavily cross-linked peptidoglycan (Scheme 3.1).[5] In both cases, the peptidoglycan layer does not provide an efficient barrier against diffusion of hydrophilic solutes (the peptidoglycan layer of Gram-positive cell wall is accessible to molecules of molecular weight in the range of 30000 to 57000 Da). Moreover, proteins are another essential component for both Gram-negative and Gram-positive bacterial outer envelopes. Generally, Gram-negative bacteria exhibit higher resistance to antimicrobial agents than Gram-positive microorganisms, which is attributed to the more complicated outer envelope structure of the Gram-negative bacteria.[6] Specifically, the presence of the efflux pumps on the outer membrane of Gram-negative bacteria significantly impairs the penetration ability of antimicrobial agents into the cell (Efflux pumps are proteinaceous transporters localized in the cytoplasmic membrane of all kinds of cells. efflux is a mechanism responsible for moving out of toxic substances and antibiotics outside the cell. From Wikipedia). One important common characteristic of both Gram-negative and Gram-positive bacterial cell envelopes is the net negative charge, which is provided by LPS for Gram-negative bacteria, teichoic acids for Gram-positive bacteria and the anionic phospholipids from

bacterial cytoplasm membrane and/or outer membrane, such as phosphatidylglycerol (PG) and cardiolipin (CL) (Scheme 2.1).[7] For Gram-negative bacteria, the negatively charged outer membrane serves as the first point of contact for the cationic antimicrobial compounds. Furthermore, the amphiphilic nature of the CPEs and OPEs may enhance their ability to denature membrane proteins and perturb lipid membranes via hydrophobic interactions. The biological functions of teichoic acids from Gram-positive bacteria are not fully understood; some of their proposed functions include (ⅰ) binding of divalent cations (particularly $Mg^{2+}$), (ⅱ) regulation of autolytic enzymes, and (ⅲ) barrier to control the diffusion of nutrients and wastes.[8-9] Although the cell wall of Gram-positive bacteria is believed to be an open network and accessible to solutes with a broad range of molecular weights,[10] the cationic CPEs and OPEs may bind with the negatively charged cell wall components, thus reducing their penetration through the cell envelope. As such, dark toxicity of CPEs and OPEs against Gram-positive bacteria may stem from a different mechanism than those towards Gram-negative bacteria. In summary, the bacterial outer envelope should be one of the main sites of attack for the CPEs and OPEs, due to the favorable electrostatic and hydrophobic interactions.

**Scheme 3.1**. Structures of peptidoglycan and LPS on the bacterial cell wall.

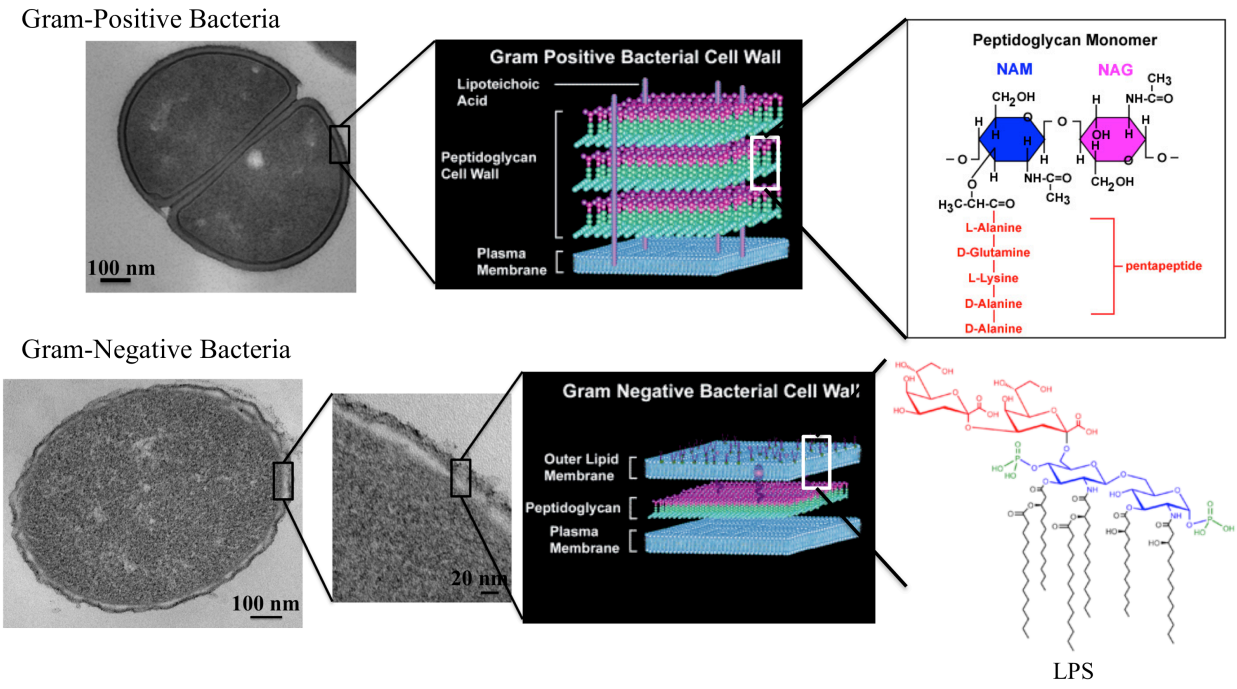


In addition, since there are no advanced organelles in the bacteria, the cell wall and membrane serve many essential biological functions, including structural support against osmotic pressure gradients, nutrient and waste transport, metabolic reactions, and synthesis.[9] Therefore, compromises to the structural integrity of the bacterial cell envelope may trigger a lethal effect. For example, ethylenediaminetetraacetic acid (EDTA) has been demonstrated to cause the release of LPS molecules from *E. coli* outer membrane by chelating $Mg^{2+}$ or $Ca^{2+}$ ions, which destabilizes the LPS assembly and increases the permeability of the bacterial outer envelope.[11]

Some PPE-based cationic compounds with different structures, which exhibited various toxicity against *Escherichia coli* (*E. coli*), were chosen for the initial study to explore the structure-antimicrobial activity relationship (Scheme 1.3). Due to large differences in molecular weight and spatial arrangement of the positively charged side

and end groups, the interactions of these antimicrobial compounds with the bacterial outer envelope were expected to be different, and it was anticipated that these differences could result in different mechanisms of action against Gram-negative bacteria. In this study, we examined the toxicity mechanisms of these antimicrobial materials. In particular, direct visualization of damages to the bacterial outer envelope and changes to bacterial morphology were found via scanning and transmission electron microscopy (SEM and TEM) imaging of *E. coli* cells exposed to the selected materials. Laser scanning confocal microscopy (LSCM) gives additional detailed information on the antimicrobial mechanism of OPE-1.

$^1O_2$ and the secondary ROS sensitized by the CPE and OPE materials have shown to be to be highly toxic to bacteria by possibly inducing damages to proteins, RNA, DNA, and unsaturated lipids.[12-13] Due to the different structures and components of the bacterial cell envelopes, Gram-positive and Gram-negative bacteria have been found to exhibit different susceptibilities towards chemical damages induced by pure $^1O_2$.[14] Briefly, for Gram-negative bacteria, $^1O_2$ can react with the components of the outer membrane (e.g., LPS) and generate secondary ROS so that the damage to the bacteria is the culmination of $^1O_2$ damage of the cytoplasmic membrane and the lethal effect caused by the ROS products on the outer membrane. However, for Gram-positive bacteria, $^1O_2$ can rapidly diffuse through the cell wall and cause lethal damages directly on the cytoplasmic membrane. Aside from the intrinsic diffusing rate and reactivity of $^1O_2$, the light-enhanced biocidal activity of CPEs and OPEs is also expected to be highly dependent on the penetrating ability or the location of the compounds in bacteria.

Damages to the morphology of the Gram-negative *E. coli* and Gram-positive

*Staphylococcus epidermidis* (*S. epi*) cells exposed to the biocidal compounds were visualized by scanning and transmission electron microscopies (SEM and TEM).

## 5.2 Results and Disscussion

Previously, we have shown that the PPE-based cationic conjugated polymers (CPEs) and oligomers (OPEs) with different side chains and repeat units exhibit a range of toxicities against bacteria and different perturbation abilities against model membranes.[1] Generally, the amphipathic properties, molecular size, aggregation state, and charge density are factors modulating the interactions between CPEs and OPEs and their biological targets. The motivation of the current study is to elucidate the mechanistic origin of the different killing abilities among different CPEs and OPEs. SEM imaging and the cytoplasmic membrane permeability assays are used to elucidate the interactions between a CPE or an OPE with bacterial cell walls and membranes. The minimum inhibitory concentration (MIC) and hemolytic concentration (HC) values serve as useful parameters to evaluate the selectivity the compound, i.e., antimicrobial activity against bacteria compared to cytotoxicity against mammalian cells.

### 5.2.1 CPEs and OPEs can disrupt bacterial cell walls and membranes

The addition of different CPE and OPE materials caused different visual changes to ATCC 11303 *E. coli* cells. As shown in Figure 5.1, the addition of PPE-DABCO, PPE-Th and OPE-3 caused the *E. coli* cells to aggregate and precipitate (Figures 5.1D, G and H). No visible changes occurred with the addition of OPE-1 or melittin (Figure 5.1B and C). On the other hand, after the addition of two EO-OPE-1 compounds, the turbidity of the *E. coli* cell suspension decreased (Figure 5.1E and F), implying that the EO-OPE-1s

may have caused cell lysis. The same effects of the CPEs and OPEs on BL21(DE3)pLysS *E. coli* cells were observed (data not shown).

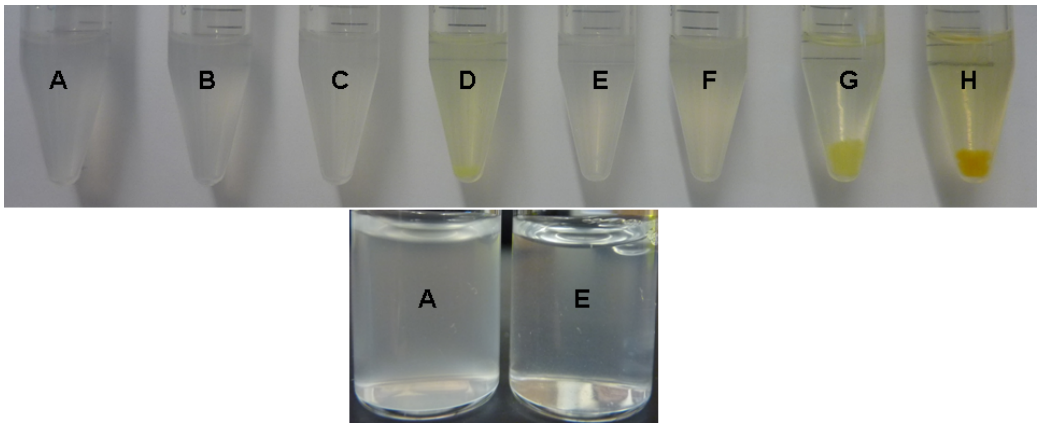


**Figure 5.1**. Images of *E. coli* cells (ATCC 11303, ~$10^8$ CFU/ml) exposed to 10 μg/ml of antimicrobials at 37℃ for one hour in the dark. A, *E coli* cells alone; B, Melittin; C, OPE-1; D, OPE-3; E, EO-OPE-1(C3); F, EO-OPE-1(Th); G, PPE-DABCO; H, PPE-Th. The bottom figure is a close up of *E. coli* suspensions in glass vials of A and E.

The effect of the different CPEs and OPEs on *E. coli* cell viability was determined by counting the colony forming units of *E*. coli cells after exposure to 10 μg/ml for one hour in the dark. Results are presented in Figures 5.2, 5.3 and 5.4. As shown, OPE-1 and melittin did not exert significant toxicity. In contrast, all other CPEs and OPEs show significant antimicrobial activities against the *E. coli* cells For example, the oligomer EO-OPE-1(C3) induced close to 100% cell death in both *E*. coli strains (Figure 5.2B).

Previously, we have shown that the dark biocidal activity of the CPE and OPE is associated with damages to bacterial cell walls and membranes by the direct contact between these materials and bacteria. When the cell walls and membranes are perturbed, cytoplasm contents, such as nucleic acids and proteins can leak out and these materials can be detected by measuring the absorbance of the soluble fraction of the cell suspension at 260 nm.[15] Table 5.1 summarizes absorbance measurements of the supernatant of *E.*

*coli* cells after incubating with the antimicrobial compounds. As shown, EO-OPE-1(C3) causes the highest level of leakage from both *E. coli* strains, which correlates with its bacteriolysis effect (Figure 5.1E) and high toxicity (Figure 5.2A and B). However, a direct correlation between toxicities and level of soluble cell content caused by the CPEs and OPEs cannot be drawn at this time primarily because the interaction between the antimicrobial compounds and *E. coli* cell content (i.e., DNA and proteins) is not fully understood. For example, polyvalent cations can readily precipitate DNA.[16] Therefore, low absorbance readings do not necessarily correlate with low levels of cell content leakage. Nonetheless, some meaningful comparisons can be made from the absorbance measurements. Figure 5.2, and results from our previous study, shows that OPE-3 exhibits much higher dark antimicrobial activity than OPE-1. OPE-3 is also known to interact much more strongly with DNA compared to OPE-1.[17] Therefore, DNA released from the *E. coli* cells may form stable complexes with OPE-3 that can be pelleted during centrifugation, resulting in a lower absorbance at 260 nm in the cell supernatant compared to OPE-1 (Table 5.1).

**Table 5.1**. Absorbance at 260 nm for the antimicrobial compounds and their mixture with soluble materials released from bacteria. The concentration of the antimicrobial materials and *E. coli* cells are 10 μg/ml and $10^8$ CFU/ml respectively. All samples were incubated at 37℃ for 1 hour in 10 mM PBS, followed by centrifuging at 10000 rpm for 10 min. All experiments were done in the dark.

| Antimicrobial Agents | Antimicrobial compounds alone | *E. coli* BL21(DE3)pLysS | *E. coli* (ATCC 11303) |
|---|---|---|---|
| Control | 0.06* | 0.20** | 0.17** |
| Melittin | 0.06 | 0.63 | 0.46 |
| OPE-1 | 0.15 | 0.33 | 0.31 |
| OPE-3 | 0.14 | 0.20 | 0.19 |
| EO-OPE-1(C3) | 0.16 | 1.30 | 0.88 |
| EO-OPE-1(Th) | 0.19 | 0.26 | 0.31 |
| PPE-DABCO | 0.13 | 0.80 | 0.79 |
| PPE-Th | 0.17 | 0.20 | 0.22 |

* PBS buffer alone; ** *E. coli* cells alone in the PBS buffer

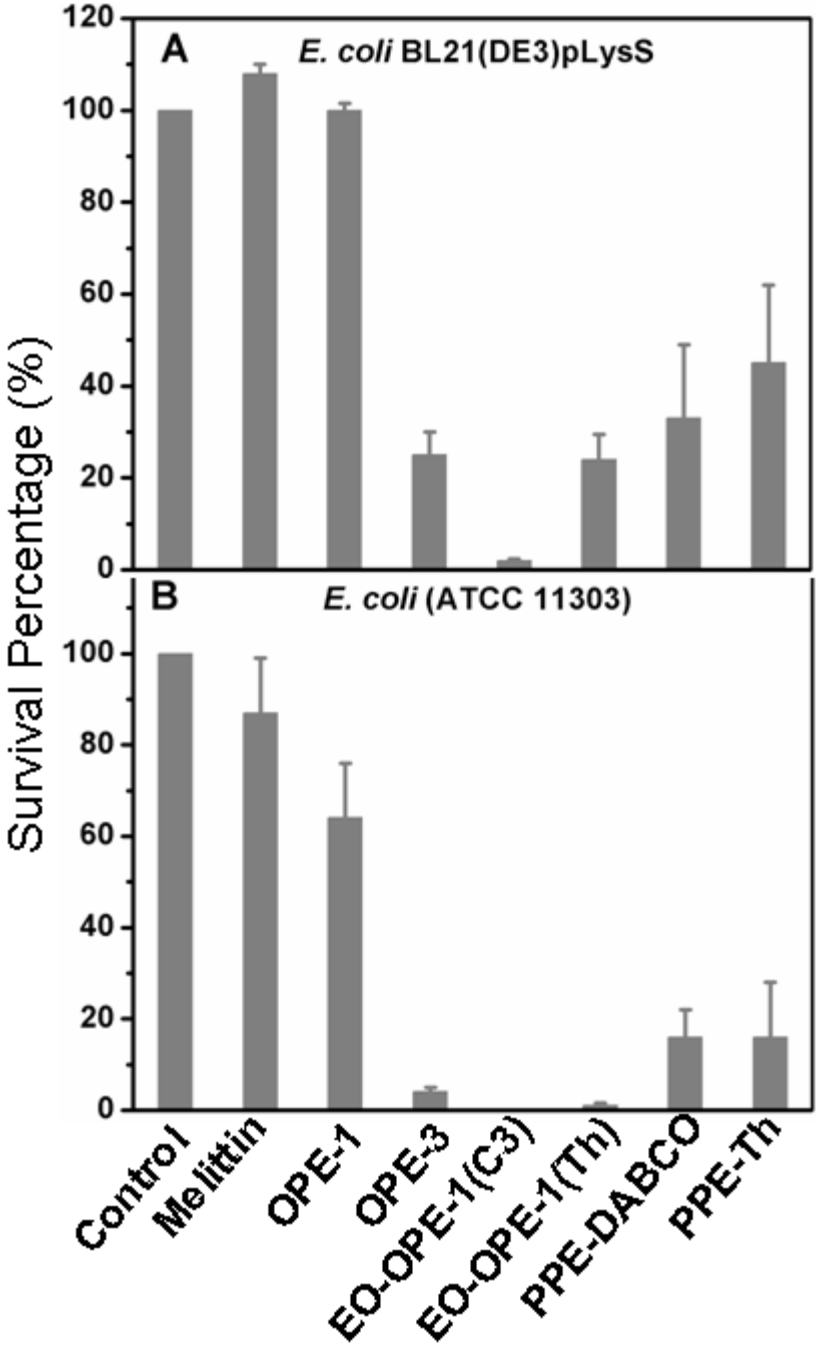


**Figure 5.2**. Antimicrobial activities of CPEs and OPEs against *E. coli* cells. Exponential growth phase *E. coli* cells (~$10^8$ CFU/ml) were incubated with 10 μg/ml CPEs or OPEs at 37℃ for one hour in the dark followed by $10^6$ fold dilution. The diluted samples were loaded on Luria broth plates. The reported survival percentage is the average of two independent experiments and normalized to the control.

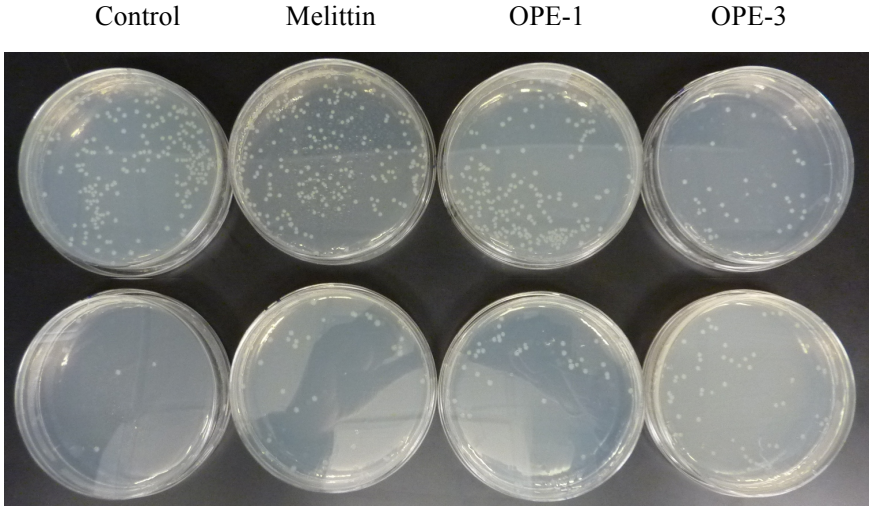


**Figure 5.3**. CFU counting for the antimicrobial activities of CPEs and OPEs against *E. coli* BL21(DE3)pLysS. Exponential growth phase *E. coli* cells (~$10^8$ CFU/ml) were incubated with 10 μg/ml CPE or OPE at 37℃ for one hour in the dark followed by $10^6$ fold dilution. The diluted samples were loaded on Luria broth agar plates.

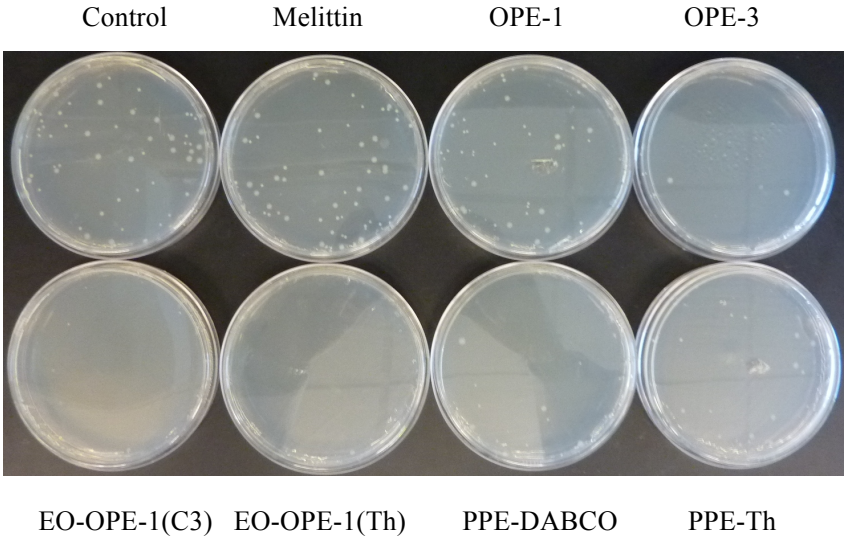

**Figure 5.4**. CFU counting for the antimicrobial activities of CPEs/OPEs against *E. coli* (ATCC 11303). Exponential growth phase *E. coli* cells (~$10^8$ CFU/ml) were incubated with 10 μg/ml CPEs/OPEs at 37℃ for one hour in the dark followed by $10^6$ fold dilution. The diluted samples were loaded on Luria broth agar plates.

The ability of OPEs and melittin to depolarize the cytoplasmic membrane is determined by using the cationic membrane potential-sensitive cyanine dye diSC3-5. The distribution of diSC3-5 between cell membrane and periphery medium is dependent on the cytoplasmic membrane potential gradient.[18] This cationic dye readily partitions into the bacterial cell membrane and aggregates within the membrane, causing self-quenching.[19] If the antimicrobial compounds perturb the cell membrane, it can lead to the loss of the membrane potential gradient, causing the dye to release into the medium. As a result, the fluorescence intensity of the dye increases. Hancock *et al.* employed the mutant *E. coli* DC2 cell with increased outer membrane permeability for their cytoplasmic membrane permeability assay. Herein, the laboratory strain *E. coli* BL21(DE3)pLysS cells growing with carbenicillin and chloramphenicol also possess modified loose outer membranes.

After incubating *E. coli* cells in the exponential growth phase with diSC3-5 for one hour, the fluorescence of this membrane potential dye decreased dramatically (Figure 5.5), which indicates that the dye has been taken up by the *E. coli* cells and that the cells have unperturbed membrane potential gradients. As shown in Figure 5.6, these antimicrobial compounds exhibit similar membrane permeability abilities against the two different strains of *E. coli* cells. Melittin strongly interacts with bacterial cytoplasmic membrane, causing dye release from the membrane and increasing the fluorescence of the dye in the sample. Melittin exhibits increased membrane perturbation ability with increased concentration. OPE-1 shows a similar concentration dependent trend, but

fluorescence intensity is much lower than that caused by melittin, indicative of weaker interaction between OPE-1 and bacterial. Surprising, the addition of EO-OPE-1(C3) to both strains of bacteria caused increases in fluorescence at low oligomer concentrations, followed by decreases of diSC3-5's fluorescence at oligomer concentrations higher than 2 μg/ml. One explanation for the observed trend is that EO-OPE-1(C3) exerts its biocidal activity by bacteriolysis. When the bacteria are disintegrated by EO-OPE-1(C3), the bacterial cytoplasm is released and may strongly interact with the cationic membrane potential dye and quench its fluorescence. Figure 5.7 show that DNA is effective at quenching diSC3-5 fluorescence. Therefore the overall fluorescence intensity of diSC3-5 in Figure 5.6 is the result of two competing processes. Upon the perturbation of bacterial cytoplasmic membrane by the antimicrobial agent, the released diSC3-5 initially increases the sample's fluorescent intensity. However, disruption of cell wall and membrane can subsequently release DNA and other contents of the cytoplasm, which effectively quench diSC3-5's fluorescence, resulting in overall decreases in the fluorescence intensity of diSC3-5. A similar trend was observed for OPE-3. Due to the loose outer membrane of *E. coli* BL21(DE3)pLysS, the decrease of diSC3-5's fluorescence occurred at a lower concentration of OPE-3 than that of *E. coli* (ATCC 11303). As concluded by Hancock *et al.,* since there is no correlation between the membrane permeability of antimicrobial compounds and their lethal effect against bacteria, other antimicrobial and inhibitory mechanisms may be involved.[25] The high membrane potential gradient perturbation ability of melittin only accounts for its efficient interaction with bacterial cytoplasmic membrane. Even though the results of this assay are not conclusive, it is clear that the four antimicrobial compounds (mellitin and three

oligomers) used in this assay can interact with bacterial cytoplasmic membrane, although the extent varies

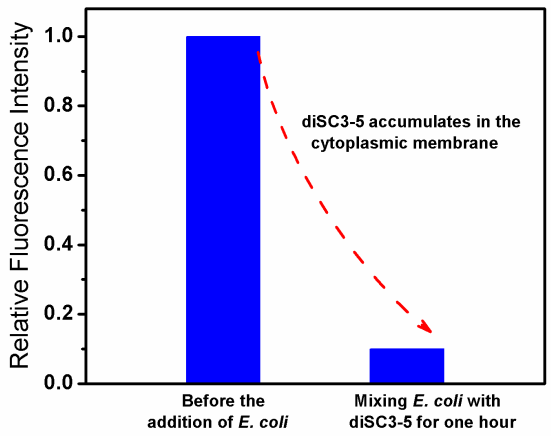


**Figure 5.5**. Fluorescence change of diSC3-5 (0.4 μM) before and after mixing with fresh exponential growth phase *E. coli* BL21(DE3)pLysS cells ($10^7$ CFU/ml) in the HEPES buffer (5 mM HEPES, 5 mM glucose, pH 7.2). The same phenomenon was observed for *E. coli* (ATCC 11303) cells.

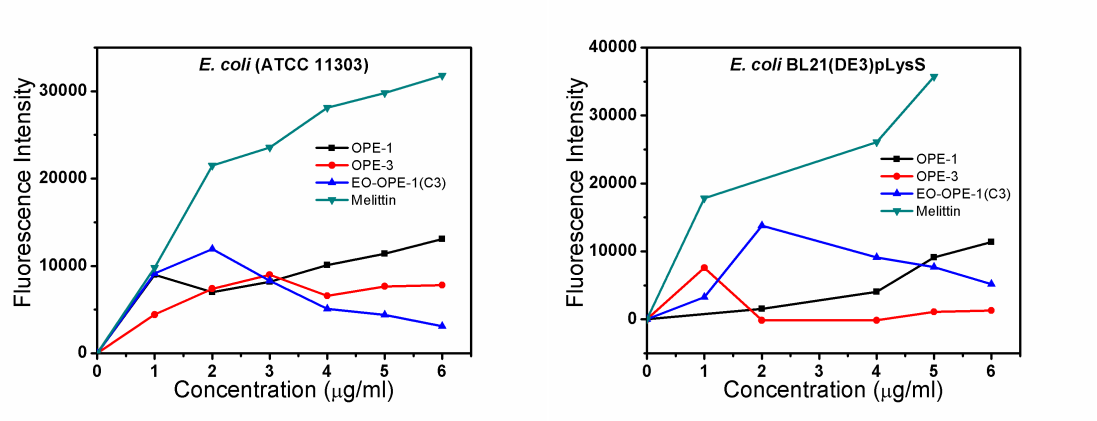


**Figure 5.6**. Cytoplasmic membrane permeability of *E. coli* cells induced by melittin and OPEs. The fluorescence changes of diSC3-5 as a function of antimicrobial compound concentration are plotted.

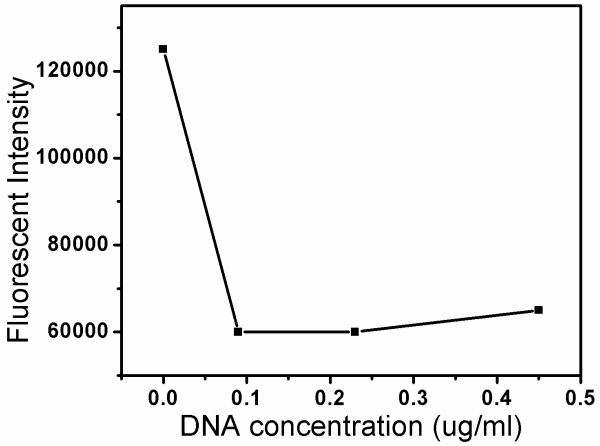


**Figure 5.7**. Effect of DNA (plasmid from *E. coli* BL21(DE3)pLysS) on diSC3-5's (0.4 μM) fluorescence in the HEPES buffer (5 mM HEPES, 5 mM glucose, pH 7.2).

### 5.2.2 CPEs and OPEs selectively exert toxicity towards bacterial cells

We tested the inhibitory activities of CPEs and OPEs against *E. coli* cells in the dark. As shown in Table 5.2, the antimicrobial compounds exhibit very similar inhibitory effect on the two different strains of *E. coli* cells, implying that the physiological differences between these *E. coli* strains have limited influence on their susceptibilities towards CPEs, OPEs and melittin. Therefore, it is reasonable to conclude that the specific resistance strategies the *E. coli* BL21(DE3)pLysS acquired against carbenicillin and chloramphenicol antibiotics are not effective against our novel antimicrobial agents. In particular, OPE-3 and PPE-Th exhibit excellent inhibitory activities against *E. coli* cells (Table 5.2). At relatively low concentrations, the two EO-OPE-1 compounds, PPE-DABCO, and melittin show efficient inhibitory activity against the *E. coli* cells. However, no inhibitory activity is observed for OPE-1 within the tested concentration range.

In order to evaluate the biocidal selectivities of the CPEs and OPEs, we tested their hemolytic activity against human RBCs. The concentrations necessary to cause 50% RBC hemolysis ($HC_{50}$) of OPE-1 and OPE-3 are fairly high (Table 5.2). Thus, no

significant hemolytic activity is observed for OPE-1 and OPE-3 within the tested concentration range. Under the same conditions, the two EO-OPE-1 compounds exhibited moderate hemolytic ability against RBC with $HC_{50}$ values around 20 μg/ml. However, significant blood cell lysis was observed for polymer PPE-DABCO and peptide melittin at relatively low concentrations with $HC_{50}$ values of around 5 μg/ml. We were unable to determine the $HC_{50}$ value for PPE-Th using this method, probably due to the strong interaction of PPE-Th with hemoglobin that precipitated rather than lysed RBCs. A different method to measure hemolysis, based on Coulter Counter (Beckman Coulter, Miami, FL) measurements, was used to determine $HC_{50}$ of PPE-Th and the value is about 1 μg/ml (data not shown).

Overall, the oligomer OPE-3 exhibited the highest selectivity towards bacterial cells while the polymeric PPE-DABCO and PPE-Th and antimicrobial peptide melittin showed poor biocidial selectivity. The latter three compounds show efficient biocidal as well as hemolytic activities.

**Table 5.2**. Minimum inhibitory concentrations and hemolytic concentrations of the antimicrobial compounds in the dark.

| Antimicrobial Agents | $MIC_{90}$ (μg/ml) | | $HC_{50}$ (μg/ml) |
|---|---|---|---|
| | BL21(DE3)pLysS | ATCC 11303 | |
| OPE-1 | >30 | >30 | >100 |
| OPE-3 | 0.5 | 0.5 | >50 |
| EO-OPE-1(C3) | 2 | 2 | 24 |
| EO-OPE-1(Th) | 2 | 1 | 16 |
| PPE-DABCO | 2 | 2 | 4 |
| PPE-Th | 0.3 | 0.5 | N/D* |
| Melittin (70% purity) | 6 | 4 | 5 |

*unable to make measurement

### 5.2.3 CPEs and OPEs can induce changes to bacterial cell morphology

#### 5.2.3.1 Effect of the CPEs and OPEs on Gram-negative bacteria

In order to further elucidate the CPEs and OPEs' effects on bacterial cells, the morphological changes of *E*. coli cells with the addition of the different antimicrobial agents were examined by SEM imaging. As shown in Figures 5.8A and 5.9A, the two strains of *E. coli* cells alone in PBS buffer maintain their integrity with a smooth cell surfaces. *E. coli* cells treated with melittin are still able to maintain the intact cell structures, but some cells now appear more rough and wrinkled (Figures 5.8B and 5.9B, see arrows). *E. coli* cells treated with the polymers PPE-DABCO and PPE-Th exhibit obvious morphological changes compared to the untreated samples (Figure 5.8C, 5.8D, 5.9C, and 5.9D). The surfaces of polymer treated cells appear more rough, with possible formation of circular blebs (Figure 5.9C, see arrows), and the cells appear to be agglomerated.

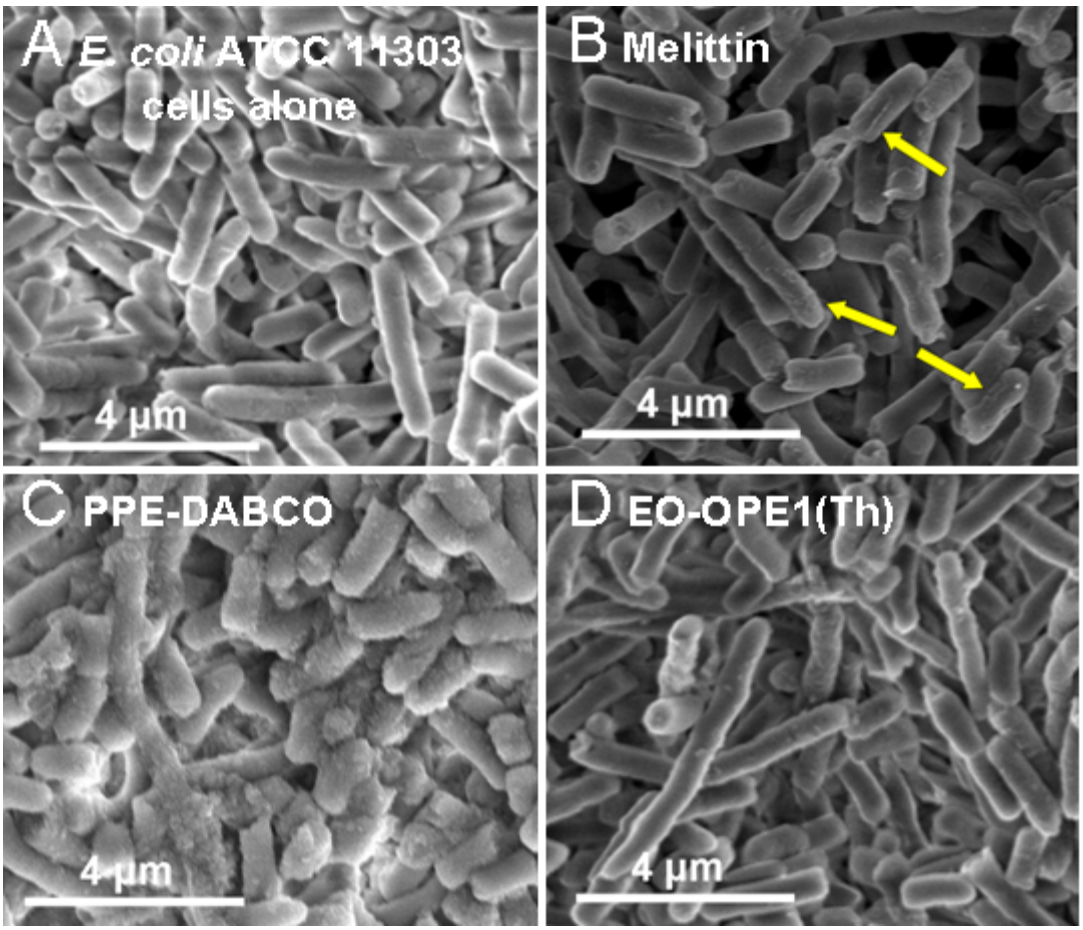


**Figure 5.8**. SEM images of *E. coli* (ATCC 11303) cells ($10^8$ CFU/ml) incubated with 10 µg/ml antimicrobial compounds for one hour in the dark. The scale bars of these images are 4 µm.

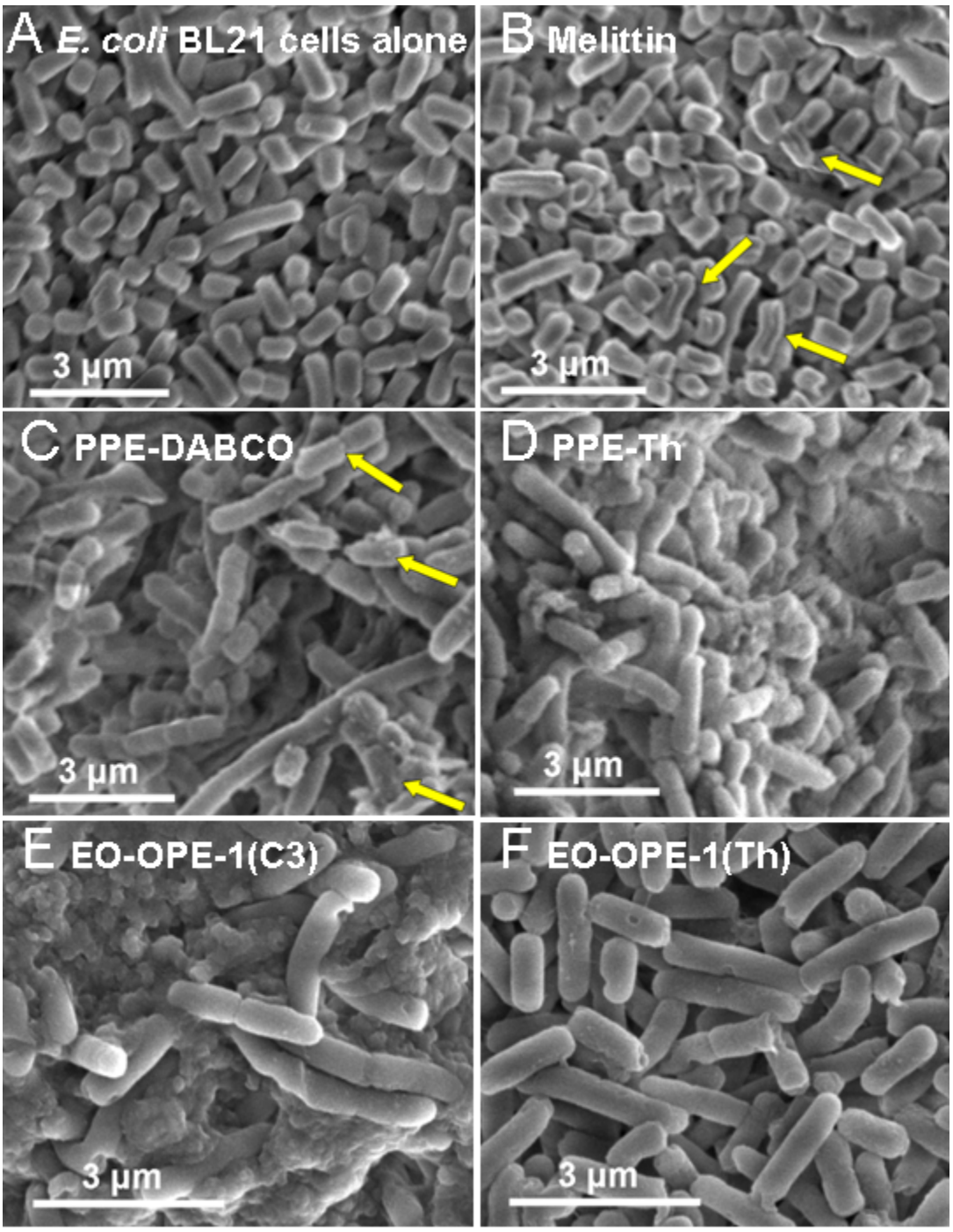


**Figure 5.9**. SEM images of *E. coli* BL21(DE3)pLysS cells ($10^8$ CFU/ml) incubated with 10 μg/ml antimicrobial compounds for one hour in the dark. The scale bars of these images are 3 μm.

The addition of oligomeric EO-OPE-1(Th) and EO-OPE-1(C3) also caused changes to cell morphology. Most BL21(DE3)pLysS cells exposed to EO-OPE-1(C3) became

completely disrupted, appearing as amorphous material rather than cells (Figure 5.9E). ATCC cells exposed to EO-OPE-1(Th) showed roughening of the cell surface (Figure 5.8D) while BL21(DE3)pLysS cells, mostly maintained their integrity with a smooth cell surface (Figure 5.9F).

It is important to note that the molecular size of the antimicrobial compounds is one of the determining factors in their interactions with bacteria. The relatively large sizes of the polymeric CPEs hinder their ability to penetrate into the cell wall and membrane, and as a result, they may only cause damages to the cell surfaces and cause cell aggregation. On the other hand, the smaller and unique linear structures of the oligomeric EO-OPE-1(C3) and EO-OPE-1(Th) compounds enable them to easily penetrate cell walls and membranes without at first causing serious morphological changes to the cell surface. These oligomers may then exert their cytotoxicity by inducing small membrane defects and inhibiting metabolic pathways. This proposed toxicity mechanism of the linear oligomers is supported by our observation that the addition of the two compounds significantly decreases the optical density of *E. coli* cell suspensions (Figures 5.1E and F). Disintegration of bacterial cells is likely caused by the insertion of the linear oligomers into the cell walls and membranes and subsequent disruption of these structures. The more linear of the two oligomers, EO-OPE-1(C3), showed highest cell lysis activity, resulting in a large amount of cell debris that was both detected by absorbance measurements (Table 5.1) and visualized by SEM (Figure 5.9E). Due to the strong lytic activity of EO-OPE-1(C3) against ATCC 11303, no sample was visualized with SEM imaging. In addition, it is worth mentioning that because of the resolution limit of the SEM instrument, neither individual antimicrobial molecules nor their aggregates could be

clearly visualized.

Many naturally occurring and synthetic antimicrobial agents with cationic and amphiphilic properties exert their toxicity by disrupting the integrity of bacterial cells. Moreover, small hydrophilic molecules are able to readily penetrate the bacterial outer membrane and/or peptidoglycan layer. As described above, CPEs and OPEs with different molecular weights may penetrate the bacterial outer envelope to various extents, leading to different toxic mechanisms of action.

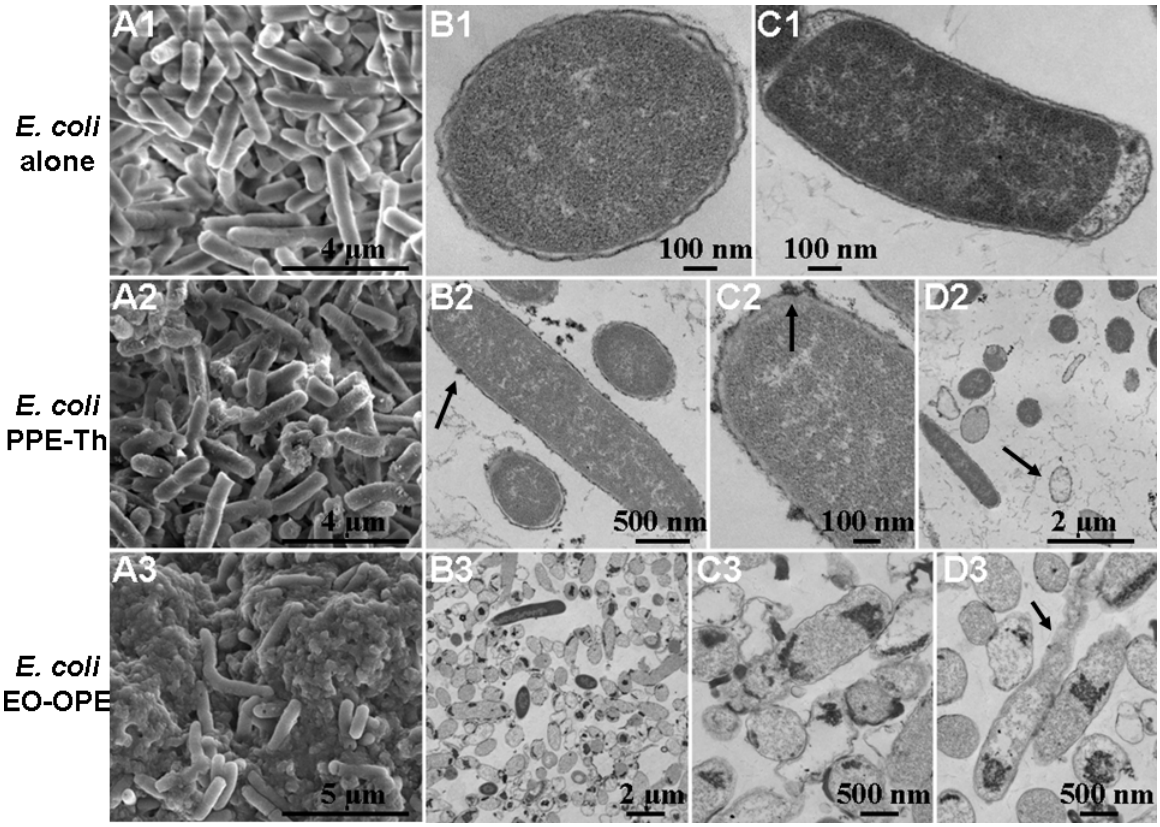


**Figure 5.10**. SEM (A1, A2 and A3) and TEM (B1-D3) micrographs of *E. coli* (ATCC 11303) cells ($10^8$ CFU/ml) alone (A1, B1 and C1), incubated with 10 µg/ml PPE-Th (A2, B2, C2 and D2) and EO-OPE-1(C3) (A3, B3, C3 and D3) for one hour in the dark.

TEM was also used to image the structural changes on *E. coli* cells upon incubation with the antimicrobial agents. As shown in Figure 5.10 (A1, B1 and C1), the *E. coli* cells alone maintain their integrity with a smooth cell surface, and the intact bacterial outer

envelopes are clearly seen. After 1 hour incubation in the dark, the *E. coli* cells ($10^8$ CFU/ml) exposed to PPE-Th or EO-OPE-1(C3) (10 μg/ml) show striking, but different structural damages. The surfaces of PPE-Th treated cells appear to be rougher (Figure 5.10 A2), and the cell outer membrane is significantly remodeled by the polymer, possibly leading to the formation of blebs on the bacteria surface (see arrows in Figure 5.10 B2 and C2). In addition, an obvious, but small population of the PPE-Th treated cells is empty (see arrow in Figure 5.10 D2), which implies that these cells have released their content as a result of compromised cell integrity. A remarkable characteristic feature of the EO-OPE-1(C3) treated cells is the appearance of abundant amorphous material, presumably cell content (Figure 5.10 A3). TEM images confirm the collapse of bacterial structure induced by EO-OPE-1(C3) as a large number of empty or partially empty cells with debris are observed (Figures 5.10 B3 and C3). Moreover, TEM imaging also captured the site and process of the release of internal cell content from some bacteria (see arrow in Figure 5.10 D3).

OPE-1 and EO-OPE-1(C3) share the same molecular backbone and are of similar size, but have different spatial arrangements of the cationic functional groups (Scheme 1.3), which may result in different antimicrobial activities and mechanisms of action. Generally, OPE-1's dark biocidal activity is not as high compared with other CPEs or OPEs.[19-20] Herein, the lethal effect of OPE-1 on two Gram-negative bacteria is examined by LSCM imaging, which is capable of tracking real-time changes to the structure of bacteria. As shown in Figures 5.11 A1 and A2, most of the untreated bacteria were live. However, a significant number of bacteria were killed and agglomerated by the addition of OPE-1 under the specific experimental condition (Figures 5.11 B1 and B2).

Interestingly, the release of fibrous and threadlike materials, probably cell content, from dead bacteria is clearly observed (Figures 5.11 D1 and D2, see arrows). As described earlier, OPE-1 can induce membrane depolarization in *E. coli*, which implies the cell transmembrane electrochemical gradient is perturbed by OPE-1. As a result, the microorganisms may not be able to generate energy, and the water and ion flow across the membrane may become disregulated, leading to possible cell swelling and/or lysis. Moreover, for both *E. coli* and PAO1, some of the dead bacteria (Figures 5.11 D1 and D2) seem to be larger than the corresponding live bacteria (Figures 5.11 C1 and C2), which may result from a single swelling dead bacterium and/or the aggregation of dead bacteria. TEM imaging also confirms the loss of cell content from *E. coli* induced by OPE-1 (Figure 5.12).

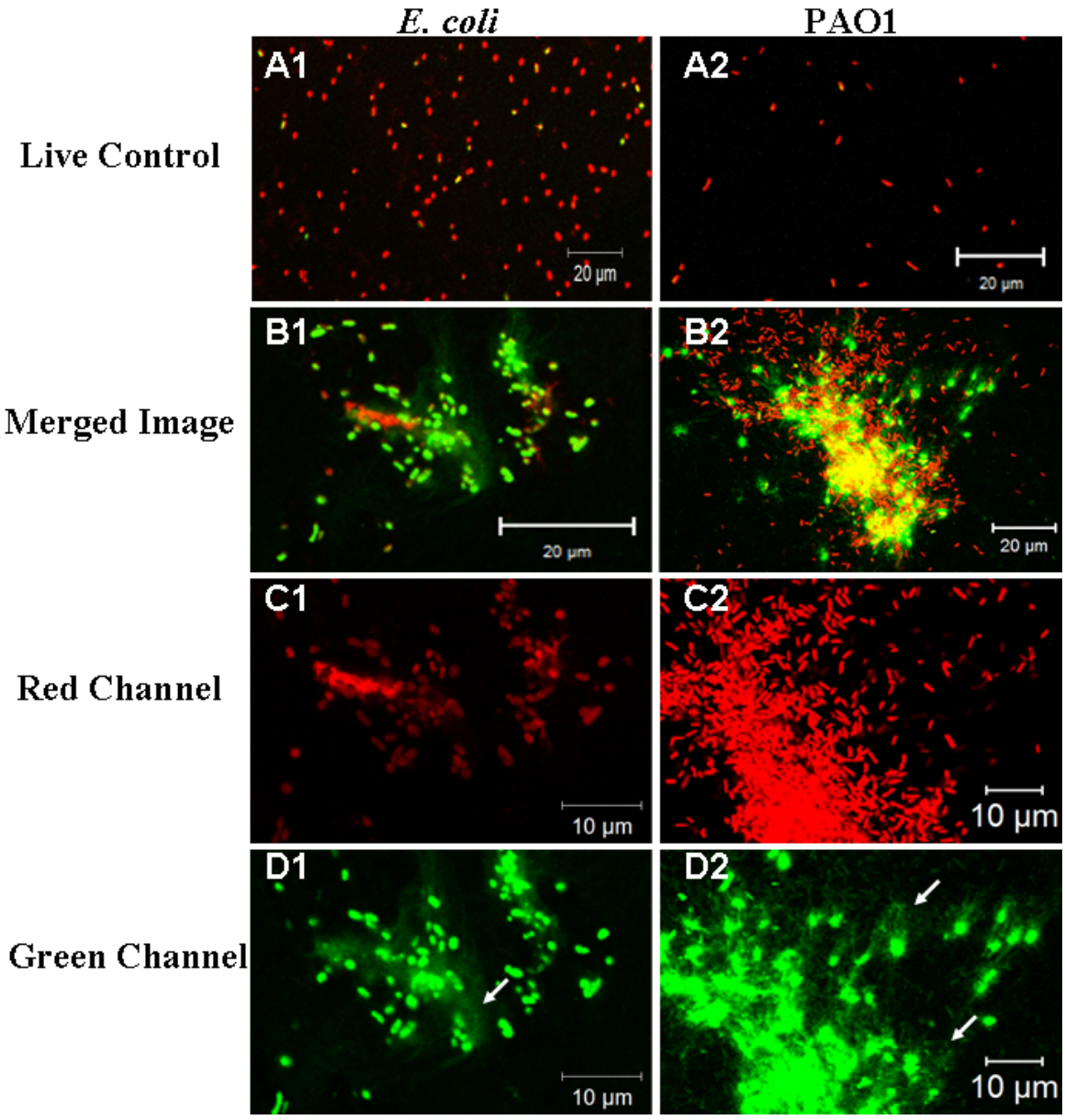


**Figure 5.11**. LSCM imaging of *E. coli* (ATCC 29425) and PAO1 cells (~$10^8$/ml) alone (A1 and A2) and treated with 42.5 μg/ml OPE-1 (B1 and B2) in the dark. The merged images are further split into red channel (C1 and C2, live bacteria) and green channel (D1 and D2, dead bacteria).

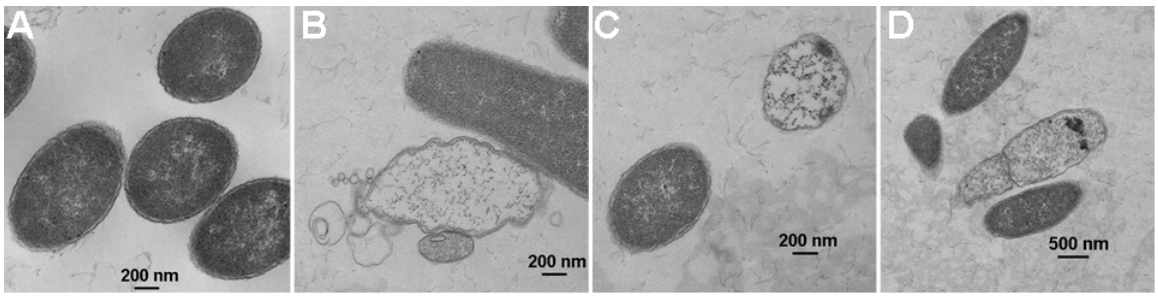

**Figure 5.12**. TEM micrographs of *E. coli* cells alone (A) and incubated with 10 μg/ml OPE-1 (B, C and D) for one hour in the dark.

So far, we have shown that the cytoplasmic membrane in Gram-negative bacteria is one of the main targets for oligomeric OPEs. Although the penetration ability of the polymeric CPEs through the outer membrane and peptidoglycan layer in *E. coli* cell is largely hindered by their bulky sizes, these compounds may still interact with the bacterial cytoplasmic membrane. Herein, further characterizations on the biocidal mechanisms have been performed with representative CPEs and OPEs against model *E. coli* cells. Although interactions with the plasma membrane are necessary in the bactericidal actions of CPE and OPE compounds, interactions of these compounds with the bacterial cell envelope are also crucial since the cell envelope serves as the first point-of-contact for exogenous materials.

As described earlier, the cell envelopes of Gram-positive and Gram-negative bacteria are compositionally and structurally different. Understanding the interactions of the CPE and OPE compounds with the different cell surfaces will not only provide a deeper and more complete understanding of the toxicity mechanism, but will also give us insights to the susceptibilities of the two different classes of bacteria. The complexities of the cell envelopes make such biological entities difficult to mimic with model systems.

As shown in Figure 5.13, the untreated *E. coli* cells ($1\times10^8$ CFU/mL) in PBS appear structurally intact and the outer envelopes are clearly visible (Figure 5.13 A1, A2, and

A3). After 1 hour incubation with OPE-3 or EO-OPE-1(C3) in the dark, the *E. coli* cells show remarkable structural damages (Figure 5.13 B and C). The attachment of OPE-3 to the bacterial cells extensively remodeled the outer membrane, leading to the roughening of the cell surface and formation of blebs (Figure 5.13 B). In addition, the cytoplasm density of the majority of OPE-3 treated cells decreased, which implies that the cytoplasm contents were being released during incubation through damaged cell envelopes. Disruption and permeabilization of the cell envelope can also lead to the penetration of OPE-3 into the bacteria cytoplasm. The cationic and amphiphilic oligomer can then bind to and disrupt other cellular components, for example, proteins and nucleic acids. Likewise, incubation with the oligomeric EO-OPE-1(C3) also led to significant disruptions to the cell envelope (Figure 5.13 C), which is consistent with previous findings that EO-OPE-1(C3) can permeabilize cell envelopes and cause cell lysis Furthermore, the TEM images in of cells incubated with EO-OPE-1(C3) (Figure 5.13 C) also showed time-dependent release of the cell cytoplasm, where only a small population of the cells show partial cytoplasm leakage/damage after exposure to the oligomer for 10 min (Figure 5.13 C1), whereas most cells were empty and/or collapsed after one hour (Figure 5.13 C3). This finding is consistent with a previous observation that EO-OPE-1(C3) exerts time-dependent biocidal activity against *E. coli* cells in the dark.[20]

The outer membrane of Gram-negative bacteria, such as *E. coli*, is permeable to solutes with a molecular weight smaller than 600 Da due to the presence of porin channels.[21] In terms of molecular weight and chain length, PPE-Th and EO-OPE-1(C3) represent two extremes in our current antimicrobial agent library (Scheme 1.3), whereas OPE-3 falls in between. PPE-Th, with a high molecular weight, is believed to exert toxicity towards

Gram-negative bacteria by disrupting the outer membrane (LPS assembly) through an "ion-exchange" process.[2, 11] However, PPE-Th is not expected to penetrate through the bacterial envelop and get into the cytoplasm due to its high molecular weight. In contrast, EO-OPE-1(C3) with its needlelike structure may easily penetrate through the outer membrane and the thin peptidoglycan layer in the bacteria without causing serious structural damages. Subsequently, it can reach, perturb and even penetrate the bacterial cytoplasmic membrane, leading to cell lysis. The molecular weight of the intermediate sized OPE-3 exceeds the permeability limit of the porin channel. Thus, similar to PPE-Th, the oligomer may exert toxicity against *E. coli* by disrupting the outer membrane. However, due to its rod-like structure and moderate molecular weight, OPE-3 may penetrate through the peptidoglycan layer, disturb the cytoplasmic membrane and trigger the release of cell content. Therefore, both molecular weight and architecture of the CPEs and OPEs are key factors controlling their interactions and toxicities with *E. coli* cells.

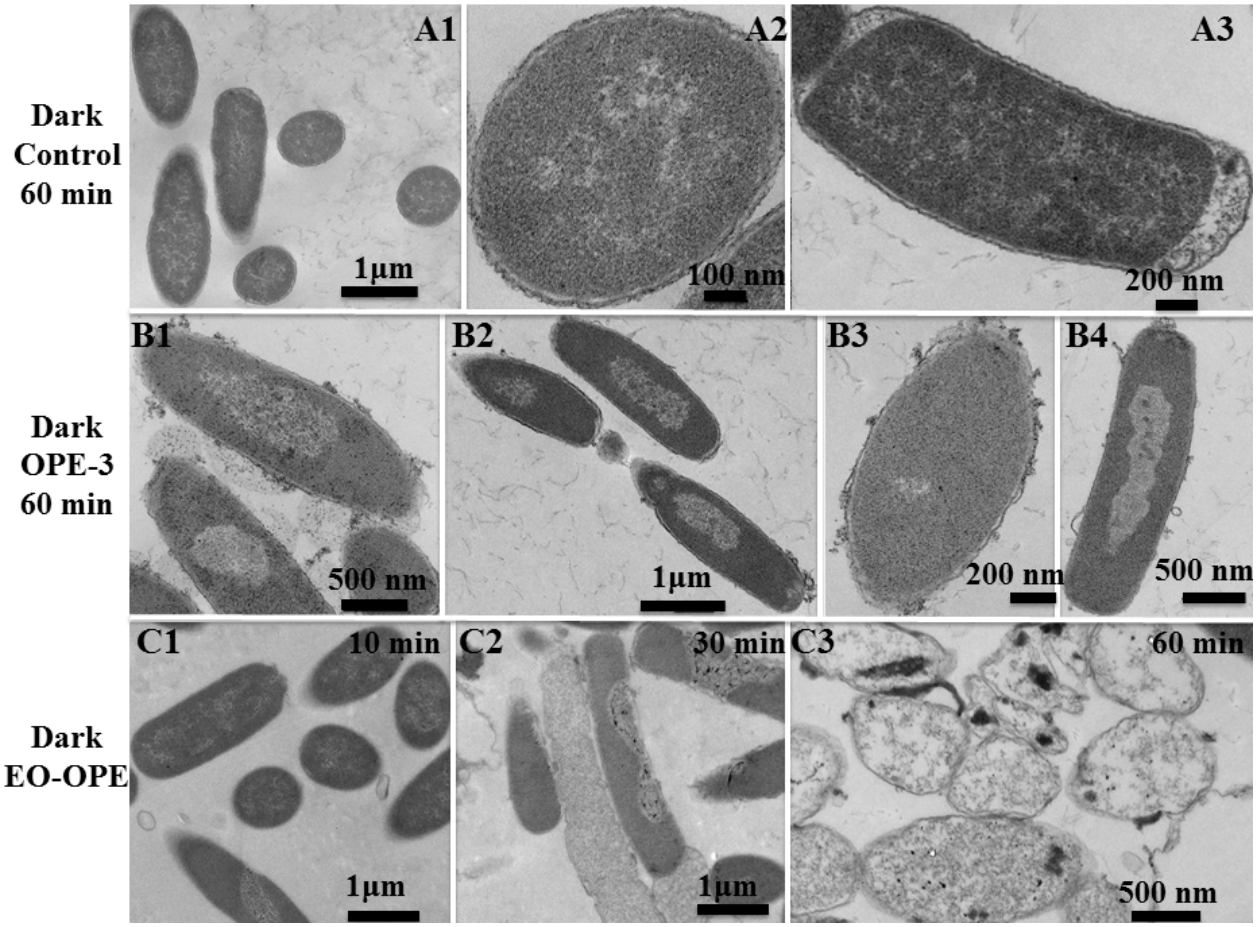


**Figure 5.13**. TEM micrographs of Gram-negative *E. coli* (ATCC 11303) cells ($10^8$ CFU/mL) alone (A1, A2 and A3), incubated with 10 µg/mL OPE-3 (B1, B2, B3 and B4) and EO-OPE-1(C3) (C1, C2 and C3) for different time intervals in the dark.

Generally, the antimicrobial activities of CPE and OPE materials are greatly enhanced with the irradiation of UV or visible light such that they exhibit rapid and efficient toxicities at very low doses. The light-enhanced toxicities of the compounds are in part contributed by the dark biocidal mechanisms of the CPE and OPE compounds, such as those visualized in Figure 5.13. Light enhanced biocidal actions of CPEs and OPEs, however, have not been directly visualized. In this study, Gram-negative *E. coli* cells incubated with oligomeric OPE-3 and EO-OPE-1(C3) and polymeric PPE-DABCO under UV-irradiation have been imaged with TEM and SEM.

Similar to untreated cells (Figure 5.13A), a control sample of *E. coli* cells irradiated for 30 min without the addition of biocidal compounds appeared intact with unperturbed cytoplasm (Figure 5.14A). Thus UV-irradiation alone did not cause obvious damages to cell morphology, consistent with our previous findings that UV-irradiation alone causes very low-level toxicity to *E. coli* cells. However, the addition of OPE-3 or EO-OPE-1(C3) with UV-irradiation caused catastrophic damages to the bacteria (Figure 5.14 B and C). In addition to the disruptions to the cell surfaces similar to those seen in cells incubated with the oligomers in the dark (Figure 5.13 B and C), the cytoplasm of the UV-irradiated cells is also clearly damaged. In the OPE-3 and UV-light treated sample, a large amount of amorphous materials outside the cells was observed, which may be complexes of OPE-3 with cell envelope components such as LPS and/or released cell content. In contrast to the cells incubated with EO-OPE-1(C3) in the dark (Figure 5.13 C1) where the cytoplasm remained relatively intact after 10 minutes, UV-irradiation in the presence of EO-OPE-1(C3) for the same duration of time caused significant damages to the cell, including decreased density of the cytoplasm. However, the time dependent bacteriolytic effect as observed by the loss of cell cytoplasm, was not observed under UV irradiation (Figure 5.14 C). This may be partly explained by the appearance of the dark, therefore dense, features in the UV-irradiated cells. Although the nature of these dark inclusions is not known, they could be oxidatively damaged and cross-linked cytoplasm components, such as proteins and nucleic acids. It is important to note that there was less leakage of the bacterial cytoplasm caused by the oligomers under UV-irradiation compared to their dark actions, which implies that the bacteria can be killed by the oligomers without releasing toxic debris.

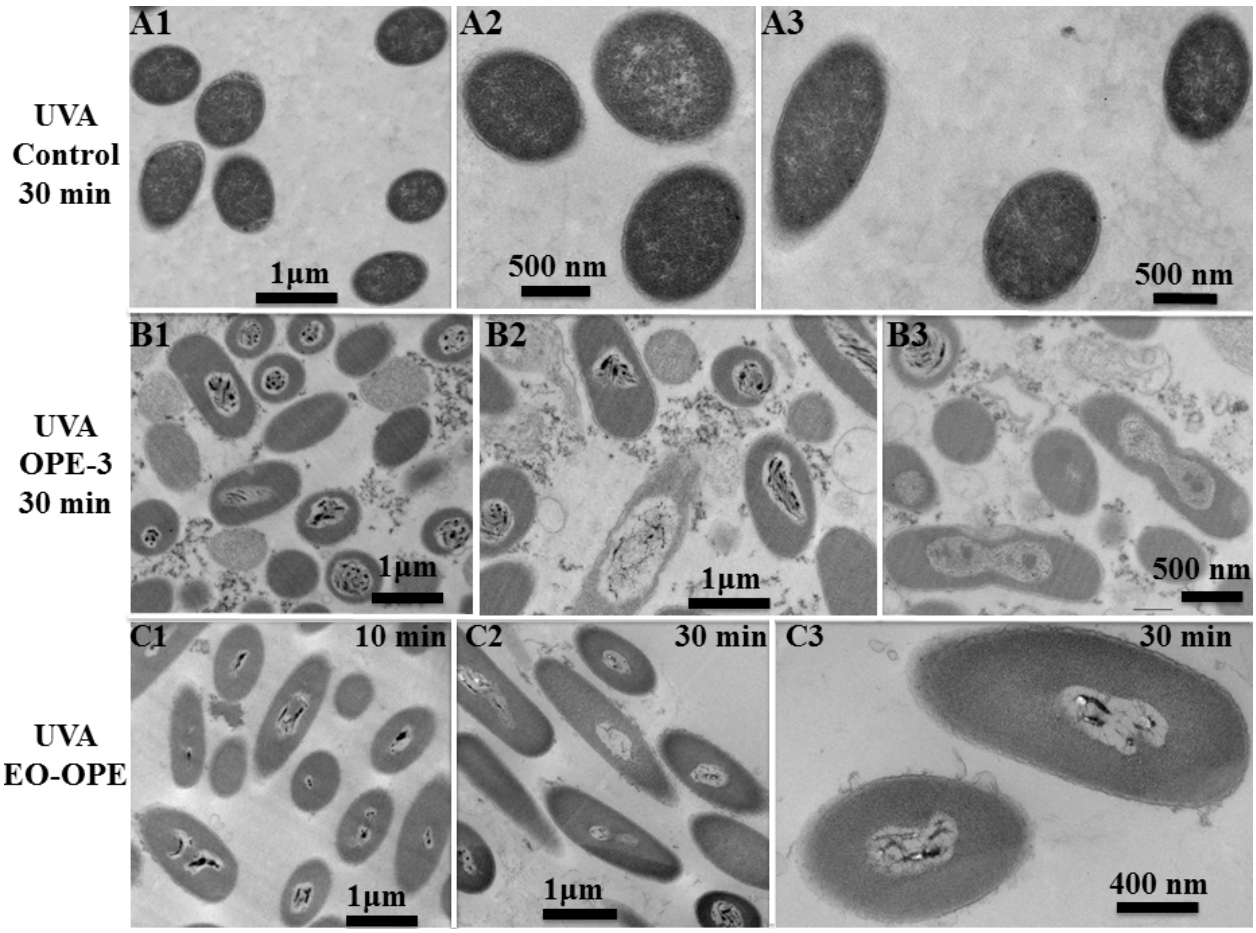


**Figure 5.14**. TEM micrographs of Gram negative *E. coli* (ATCC 11303) cells ($10^8$ CFU/mL) alone (A1, A2 and A3), incubated with 10 µg/mL OPE-3 (B1, B2 and B3) and EO-OPE-1(C3) (C1, C2 and C3) for different time intervals under UVA irradiation.

Polymeric CPEs have been observed to strongly bind to and remodel the outer membrane (previous findings of TEM imaging) of *E. coli* cells in the dark. Although their high molecular weights attenuate their ability to penetrate through the cell envelope, the oxygen radicals generated by the CPE compounds under UV-irradiation may cause sufficient damages and defects on the cell envelope to allow these polymeric agents to reach the cell interior and/or cell cytoplasm to be released. Similar to OPE-3, under UV-light irradiation, PPE-DABCO caused catastrophic damages to the bacteria cell envelope as well as induced the leakage of cell cytoplasm as evidenced by the empty (lighter

colored) cells and the appearance of amorphous materials outside the cells (Figure 5.15 B and C). These morphological changes are induced by the biocidal polymer as cells irradiated by UV-light alone are intact and smooth (Figure 5.15 A). Damages induced to the cell envelope by PPE-DABCO under UV-irradiation are further confirmed by the drastic roughening of the cell surface imaged by SEM. Additionally, SEM imaging also confirmed the presence of amorphous materials outside the cells, which could be leaked cytoplasm and material complexed with the polymer (Figure 5.15 D and E).

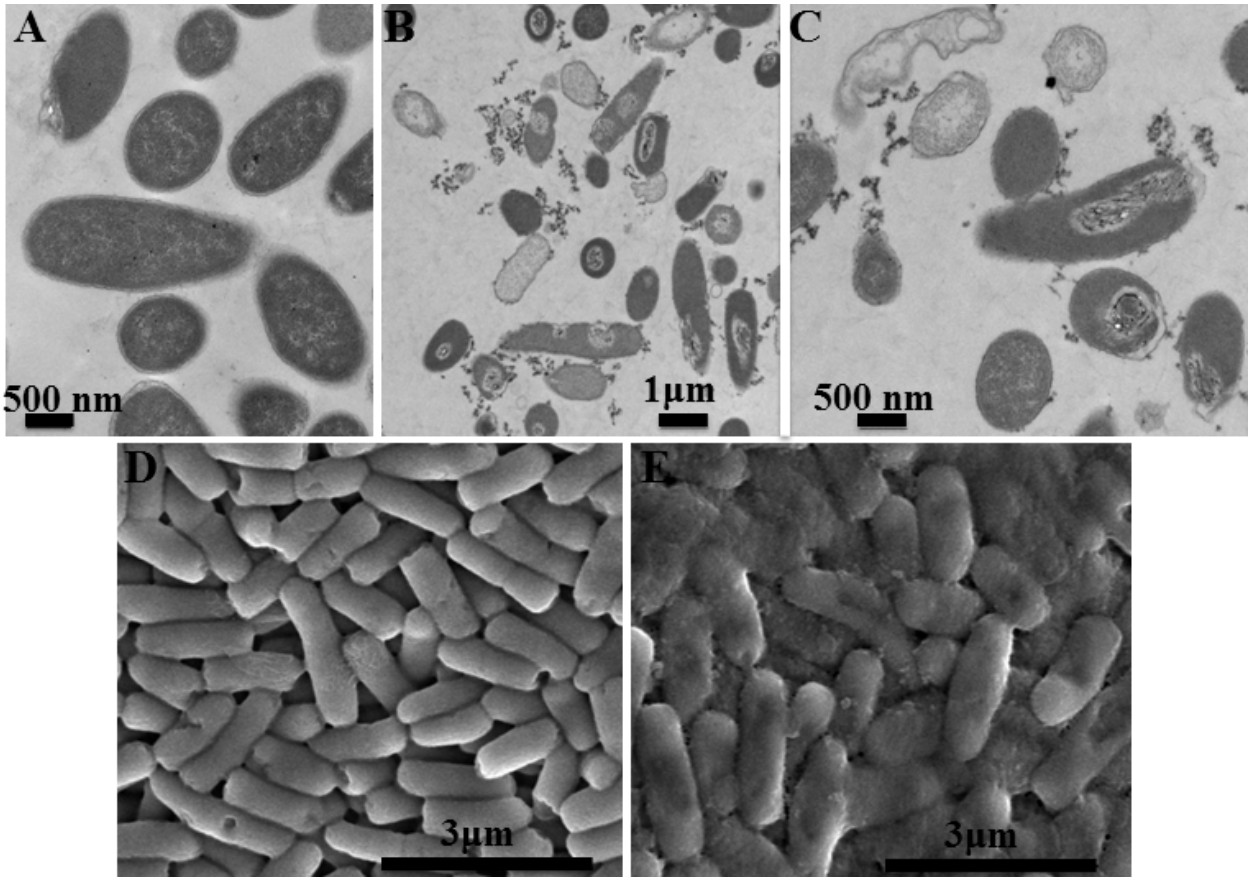


**Figure 5.15**. TEM (A, B and C) micrographs of Gram-negative *E. coli* (ATCC 11303) cells ($10^8$ CFU/mL) alone (A), incubated with 10 µg/mL PPE-DABCO (B and C) under UV-420 irradiation for 30 min. SEM (D and E) micrographs of *E. coli* cells alone (D) and incubated with 1 µg/mL PPE-DABCO (E) under UV-420 irradiation for 60 min.

It is evident from our results that UV-irradiation causes further damages to the *E. coli* cell morphology in the presence of oligomeric and polymeric compounds. $^1O_2$ has a

relatively long lifetime ($10^{-6}$-$10^{-5}$s) and diffusion distance in pure water. However, in cells, both lifetime and diffusion range of $^1O_2$ must be significantly reduced due to its high reactivity towards biomolecules in the cytoplasm.[12, 22] As a result, the damage caused by $^1O_2$ may be related to the positions of the sensitizers in the cells, whether at the cell surface or in the cell interior. Likewise, locations of damage of the bacteria under UV-irradiation also confirm the presence of the CPEs or OPEs, either at the cell surface or inside the cells. This "self-promoted uptake" mechanism,[23] which has been extensively studied for antimicrobial peptides, may also apply for the CPE and OPE compounds where defects created by the CPEs and OPEs on the bacterial outer membrane facilitate their entrance into the cell interior.

Results from these studies reveal some mechanistic insights to the different biocidal efficiencies and selectivities of the CPE and OPE materials. The following are three important modulating factors for the observed biocidal and hemolytic activities of the tested compounds. First, the molecular size, shape, and aggregation state determine whether the compounds can penetrate the bacterial outer membrane and reach the cytoplasmic membrane. This factor explains the toxicities and cell lytic activity of the CPEs and OPEs. In general, the oligomeric OPEs and oligo-peptide melitin appear to be small enough to penetrate the bacterial outer membrane once they bind to cell surfaces due to attractive electrostatic interactions. However, the penetrating ability of the polymers is compromised due to their large sizes.[24] Second, a compound's ability to perturb bacterial and mammalian cytoplasmic membranes determines its biocidal selectivity. Because OPE-3's perturbation ability against model bacterial membrane is rather effective compared to model mammalian membrane (made of cholesterol and 1,2-

dioleoyl-*sn*-glycero-3-phosphocholine),[25] OPE-3 possesses high biocidal selectivity. In contrast to OPE-3, PPE-DABCO perturbs both model bacterial and mammalian membranes, leading to a poor biocidal selectivity. Even though the two EO-OPE-1 compounds and OPE-3 can cause similar levels of damage to model bacterial membrane, the high perturbation ability against model mammalian membranes endows the two EO-OPE-1 compounds relative high hemolytic activities. Third, the ability of a compound to interact and denature membrane proteins provides another pathway for toxicity. The ability of CPEs to complex and denature the native protein conformation of BSA gives us an explanation for its high antimicrobial activity when the compound does not exhibit significant lytic or membrane perturbation abilities. For example, the high inhibitory ability of PPE-Th against *E. coli* cells is believed to derive from its high lipophilicity property to efficiently damage bacterial cell wall and membrane, including membrane proteins. In addition, since the exponential growth phase *E. coli* cells, which are undergoing fast propagation, was employed in the antimicrobial investigations, other antimicrobial and inhibitory mechanisms may be involved, such as interference with bacterial metabolic pathways.

It has been previously observed that the addition of polymeric PPE-Th can cause *E. coli* cells to aggregate and precipitate. In contrast, EO-OPE-1(C3) was found to decrease the optical density of a *E. coli* cell suspension and induce the release of 260 nm absorbing materials (e.g. DNA and protein), which may be caused by the lysis of the cells. The polymeric PPE-Th is large, fairly hydrophobic and tends to form large aggregates in aqueous solution.[26] However, EO-OPE-1(C3) with the functional cationic groups on the molecular termini is a small needle-like molecule. Jérôme *et al*. proposed that

antimicrobial polycationic compounds with relatively high molecular weights may exert toxicity against Gram-negative bacteria via binding strongly to LPS and leading to the disruption of the cell outer membrane.[2] Because of the attractive electrostatic and/or hydrophobic interactions, PPE-Th may bind strongly to the bacterial outer membrane, but its penetrating ability through the outer membrane and peptidoglycan layer may be limited by its large molecular size. As a result, the polymeric PPE-Th binds to bacterial surface and causes damage predominately to the surface of bacteria, including inducing cell agglomeration; after that, PPE-Th may also further damage the bacterial cytoplasm membrane and induce cell content release. On the other hand, the small and needle-like features of EO-OPE-1(C3) may provide the oligomer the ability to permeate through the outer membrane and peptidoglycan layer and allow it to disrupt the cytoplasm membrane, leading to the lysis of the bacteria. Taken together, a general bactericidal action scheme for the polymeric CPEs and oligoermic OPEs is proposed in Figure 5.16, and it is reasonable to apply this model to other antimicrobial agents with similar structures.

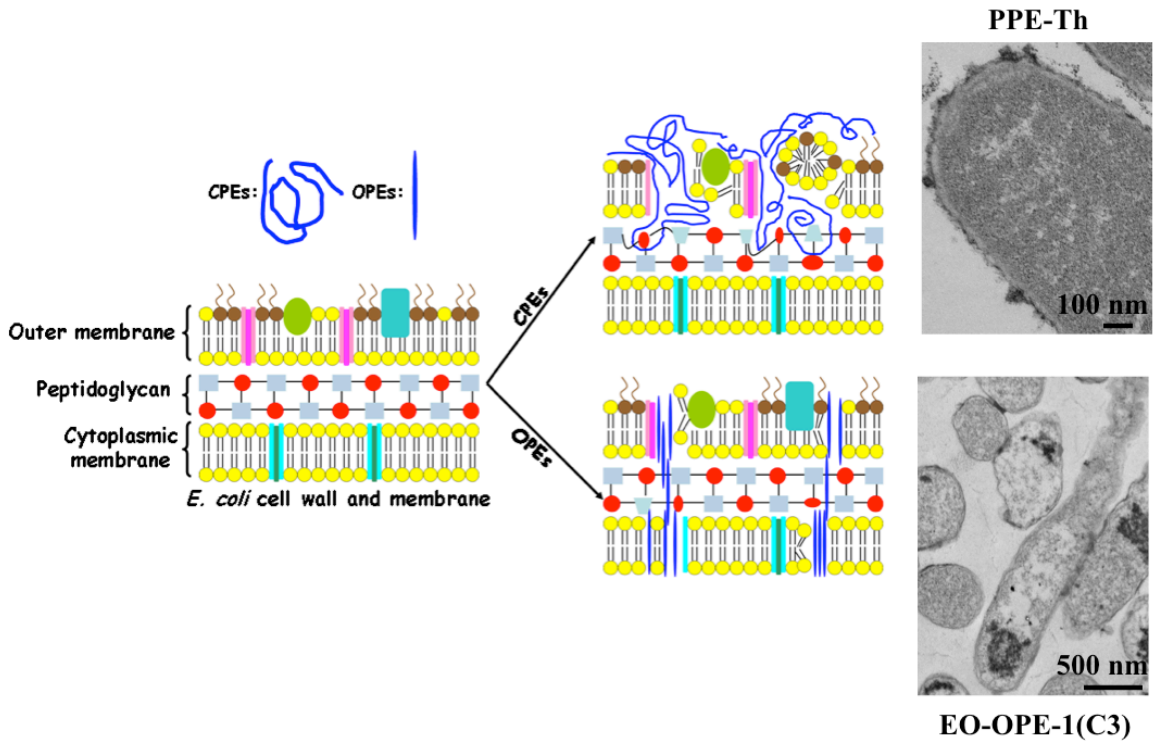


**Figure 5.16**. Proposed antimicrobial mechanism for CPEs and OPEs in the dark.

### 5.2.3.2 Effect of the CPEs and OPEs on Gram-positive bacteria

The CPE and OPE materials have been shown to exert toxicity towards both Gram-negative (e.g., *E coli*.) and Gram-positive bacteria, which have compositionally and structurally different cell envelopes as described above. Bactericidal actions of the compounds on Gram-positive bacteria have not been directly visualized previously. In this study, the dark and light-enhanced antimicrobial actions of oligomers and polymers on the Gram-positive *S. epi* bacteria were visualized for the first time via TEM and SEM imaging. *S. epi* cells incubated with oligomeric EO-OPE-1(C3) in the dark for 10-60 minutes do not appear damaged, with intact cell envelope and cytoplasm, compared with the control sample (Figure 5.17A). UV-irradiation alone also did not cause any obvious damages to the cells (Figure 5.17B1). However, UV-irradiation in the presence of CPE and OPE compounds caused obvious damage to the cell surfaces with PPE-DABCO

inducing the highest level of roughness to the cell surface (Figure 5.17B2, B3, and B4). In contrast to extensive damage induced in Gram-negative *E. coli* cells, however, damage induced by the biocidal compounds in the Gram-positive *S. epi* cells under UV irradiation seems to be localized only to the cell surface. The compounds do not appear to have caused sufficient defects that extend through the cell envelope to cause leakage of the cytoplasm, for example. SEM imaging further verifies the cell surface damage caused by PPE-DABCO in similar conditions (Figure 5.18).

It has been determined that the CPEs and OPEs exhibit both dark and light-enhanced antimicrobial activities against Gram-positive bacteria at concentrations lower than that used for the electron microscopy experiments in this study. In addition, at similar concentrations of the CPE and OPE compounds, UV irradiation always increases the toxicities of the compounds. As shown in Figure 5.17B, the cytoplasm of the *S. epi* cells do not appear damaged, even under UV-irradiation with the biocidal compounds, which implies that the tested compounds were not capable of penetrating through the Gram-positive cell envelop. Boix and co-workers have found that the eosinophil cationic protein can induce significant morphological damages to the Gram-negative *E. coli* cells, but the protein does not induce any damage to the morphology of Gram-positive *Staphylococcus aureus* (*S. aureus*) cells under the same conditions.[27] One explanation of this phenomenon is that the eosinophil protein can penetrate the *E. coli* cell envelope via the "self-promoted uptake" mechanism and then release the cell content. However, the thick and tough peptidoglycan layer in the Gram-positive bacterial cell walls provides a sufficient barrier to prevent damage to the cytoplasm. Meanwhile, the eosinophil protein exhibits high affinity toward bacterial peptidoglycan. The same principle may also

account for the similar observations of the effect of the CPEs and OPEs on Gram-positive *S. epi* cells. The thick and negatively charged Gram-positive bacteria cell wall serves as the main binding site for the cationic CPE and OPE compounds but can also prevent the penetration of the compounds into the cell interior which may cause further damages to the cell. However, since the CPE and OPE compounds are toxic toward Gram-positive bacteria, disruption of the structure, and thereby function, of the peptidoglycan layer and anionic teichoic/lipoteichoic acid, seems to be sufficient for inducing cell death and serves as the toxicity mechanism for these compounds against Gram-positive bacteria.

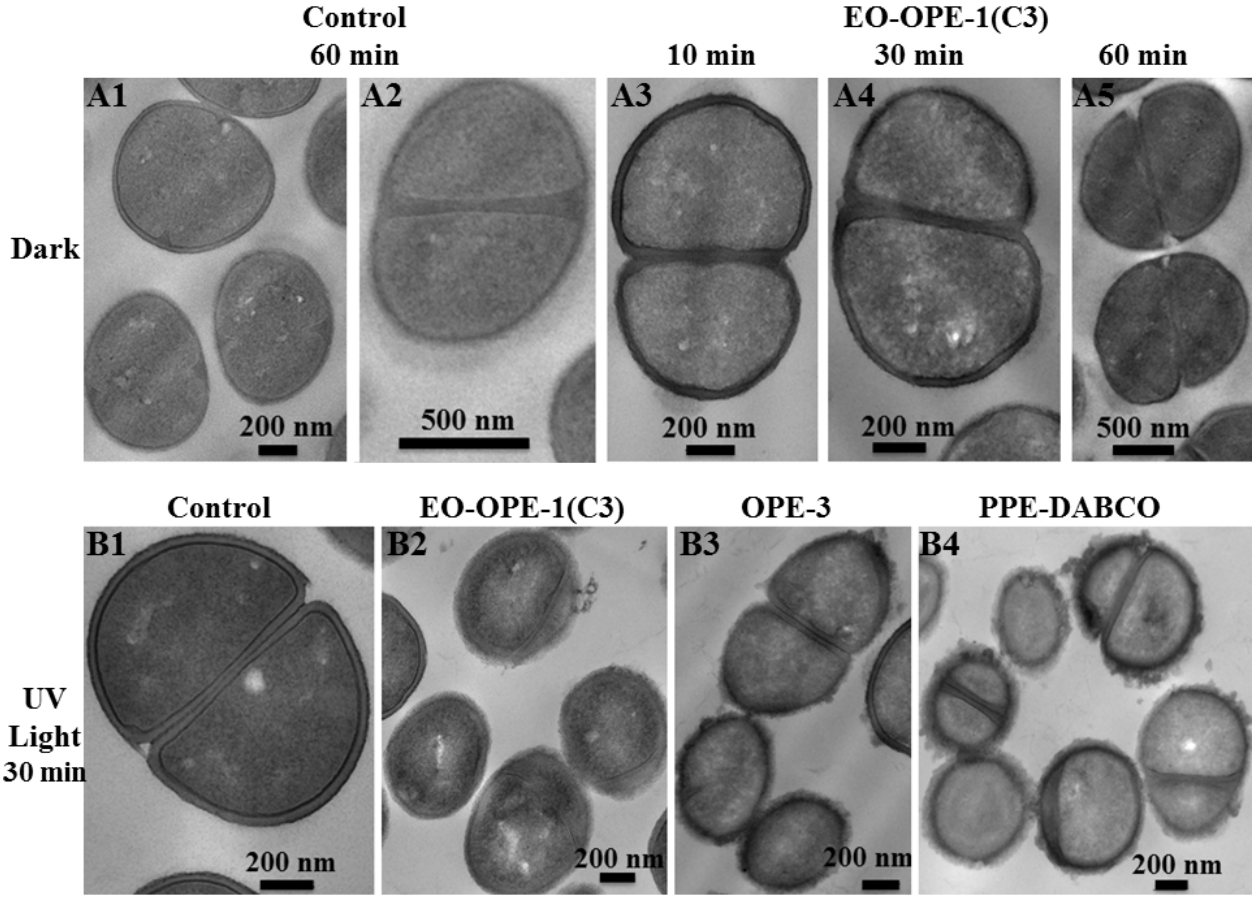


**Figure 5.17**. TEM micrographs of *S.epi* (ATCC 14990) cells ($4\times10^8$ CFU/mL) alone incubated with 25 μg/mL antimicrobial agents in the dark or under UV-light irradiation for various periods.

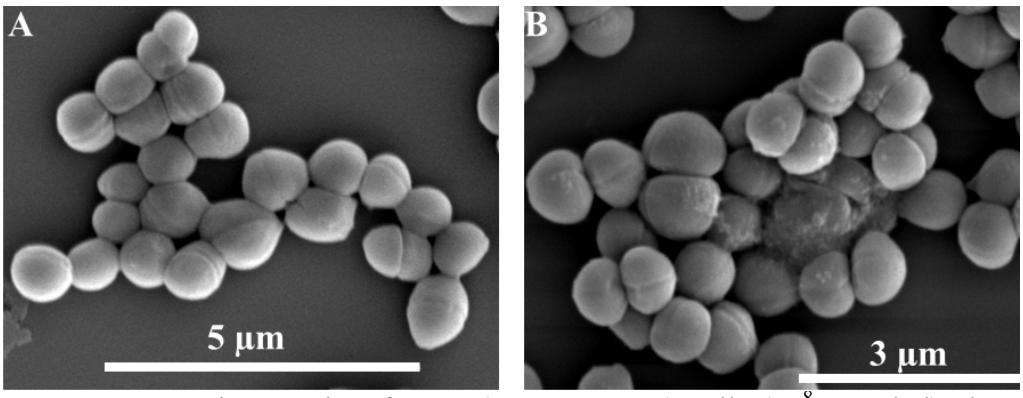


**Figure 5.18**. SEM micrographs of *S.epi* (ATCC 14990) cells ($10^8$ CFU/ml) alone (A), incubated with 10 μg/ml PPE-DABCO (B) under UV-420 irradiation for 60 min.

### 5.2.4 Summary

It is clear from our results that the polymeric CPE and oligomeric OPE materials exert toxicity towards Gram-negative and Gram-positive bacteria through different mechanisms. While the materials cause visible damage toward only the cell walls of Gram-positive bacteria, they damage the cell wall, plasma membrane, proteins, and plasmid DNA in Gram-negative bacteria. Our results indicate that the structures of the antimicrobial agents and bacterial outer envelope control their interactions as well as the biocidal mechanisms. In terms of bacteria cell envelope structures, the relatively thin and soft cell envelope in Gram-negative *E. coli* cells does not serve as an efficient barrier for the oligomeric OPEs in the dark, but can impair the penetrating ability of bulky polymeric CPEs. Under UV-irradiation, all of the tested antimicrobial compounds can cross the cell envelope of the Gram-negative *E. coli* cells and cause damage to the cytoplasm, including oxidative and covalent modifications of proteins and plasmid DNA. In contrast, the thicker and tougher cell envelope in Gram-positive bacteria seems to be an efficient permeability barrier for the CPEs and OPEs both in the dark and under UV-irradiation. The cell envelope is also the main target of the CPEs and OPEs.

Damages to *E. coli* cells in the dark reveal the important role molecular structure of the CPE and OPE compounds play toward their toxicity mechanism. The large polymeric CPEs with high charge density may sequester and remove molecules from the bacterial surface and destabilize the cell envelope and outer membrane through an "ion-exchange" process, while the small oligomeric EO-OPE-1(C3) may easily cross the outer membrane without causing serious damages and directly disturb the cytoplasmic membrane and cytoplasm. The intermediate sized OPE-n compounds can induce damages to both bacterial surface and cytoplasm. In summary, the membrane activity of the CPEs and OPEs are affected by many factors, such as molecular conformation, size, side functional groups, and membrane composition.

### 5.3 References


1. Wang, Y.; Jett, S. D.; Crum, J.; Schanze, K. S.; Chi, E. Y.; Whitten, D. G., Understanding the dark and light-enhanced bactericidal action of cationic conjugated polyelectrolytes and oligomers. *Langmuir* **2013,** *29* (2), 781-92.

2. Lenoir, S.; Pagnoulle, C.; Galleni, M.; Compere, P.; Jerome, R.; Detrembleur, C., Polyolefin matrixes with permanent antibacterial activity: preparation, antibacterial activity, and action mode of the active species. *Biomacromolecules* **2006,** *7* (8), 2291-6.

3. Palermo, E. F.; Kuroda, K., Structural determinants of antimicrobial activity in polymers which mimic host defense peptides. *Appl. Microbiol. Biotechnol.* **2010,** *87* (5), 1605-1615.

4. Wang, Y.; Zhou, Z. J.; Zhu, J. S.; Tang, Y.; Canady, T. D.; Chi, E. Y.; Schanze, K. S.; Whitten, D. G., Dark Antimicrobial Mechanisms of Cationic Phenylene Ethynylene Polymers and Oligomers against Escherichia coli. *Polymers* **2011,** *3*, 1199-1214.

5. Graham, J. M.;Higgins, J. A. Membrane Analysis; Springer; New York, **1997**.

6. McDonnell, G.; Russell, A. D., Antiseptics and disinfectants: activity, action, and resistance. *Clin. Microbiol. Rev.* **1999,** *12* (1), 147-79.

7. Timofeeva, L.; Kleshcheva, N., Antimicrobial polymers: mechanism of action, factors of activity, and applications. *Appl. Microbiol. Biotechnol.* **2011,** *89* (3), 475-92.

8. Schäffer, C.; Messner, P., The structure of secondary cell wall polymers: how Gram-positive bacteria stick their cell walls together. *Microbiology* **2005,** *151* (3), 643-651.

9. Cowan, M. K.; Talaro, K. P., *Microbiology: A Systems Approach*. 2 ed.; McGraw-Hill Science: New York, **2008**.

10. Lambert, P. A., Cellular impermeability and uptake of biocides and antibiotics in Gram-positive bacteria and mycobacteria. *J. Appl. Microbiol.* **2002,** *92 Suppl*, 46S-54S.

11. Amro, N. A.; Kotra, L. P.; Wadu-Mesthrige, K.; Bulychev, A.; Mobashery, S.; Liu, G. Y., High-Resolution Atomic Force Microscopy Studies of the Escherichia coli Outer Membrane: Structural Basis for Permeability. *Langmuir* **2000,** *16* (6), 2789-2796.

12. Davies, M. J., Singlet oxygen-mediated damage to proteins and its consequences. *Biochem. Biophy. Res. Commum.* **2003,** *305* (3), 761-770.

13. Xing, C. F.; Xu, Q. L.; Tang, H. W.; Liu, L. B.; Wang, S., Conjugated Polymer/Porphyrin Complexes for Efficient Energy Transfer and Improving Light-Activated Antibacterial Activity. *J. Am. Chem. Soc.* **2009,** *131* (36), 13117-13124.

14. Dahl, T. A.; Midden, W. R.; Hartman, P. E., Comparison of killing of gram-negative and gram-positive bacteria by pure singlet oxygen. *J. Bacteriol.* **1989,** *171* (4), 2188-94.

15. Broxton, P.; Woodcock, P. M.; Gilbert, P., A Study of the Anti-Bacterial Activity of Some Polyhexamethylene Biguanides Towards Escherichia-Coli Atcc-8739. *J. Appl. Bacteriol.* **1983,** *54* (3), 345-353.

16. Toma, A. C.; de Frutos, M.; Livolant, F.; Raspaud, E., DNA Condensed by Protamine: A "Short" or "Long" Polycation Behavior. *Biomacromolecules* **2009,** *10* (8), 2129-2134.

17. Tang, Y. L.; Achyuthan, K. E.; Whitten, D. G., Label-free and Real-Time Sequence Specific DNA Detection Based on Supramolecular Self-assembly. *Langmuir* **2010,** *26* (9), 6832-6837.

18. Wu, M. H.; Maier, E.; Benz, R.; Hancock, R. E. W., Mechanism of interaction of different classes of cationic antimicrobial peptides with planar bilayers and with the cytoplasmic membrane of Escherichia coli. *Biochemistry* **1999,** *38* (22), 7235-7242.

19. Tang, Y. L.; Corbitt, T. S.; Parthasarathy, A.; Zhou, Z. J.; Schanze, K. S.; Whitten, D. G., Light-Induced Antibacterial Activity of Symmetrical and Asymmetrical Oligophenylene Ethynylenes. *Langmuir* **2011,** *27* (8), 4956-4962.

20. Zhou, Z. J.; Corbitt, T. S.; Parthasarathy, A.; Tang, Y. L.; Ista, L. F.; Schanze, K. S.; Whitten, D. G., "End-Only" Functionalized Oligo(phenylene ethynylene)s: Synthesis, Photophysical and Biocidal Activity. *J. Phys. Chem. Lett.* **2010,** *1* (21), 3207-3212.

21. Epand, R. M.; Epand, R. F., Lipid domains in bacterial membranes and the action of antimicrobial agents. *Bba-Biomembranes* **2009,** *1788* (1), 289-294.

22. Redmond, R. W.; Kochevar, I. E., Spatially resolved cellular responses to singlet oxygen. *Photochem. Photobiol.* **2006,** *82* (5), 1178-86.

23. Powers, J.-P. S.; Hancock, R. E. W., The relationship between peptide structure

and antibacterial activity. *Peptides* **2003,** *24* (11), 1681–1691.

24. Lienkamp, K.; Kumar, K. N.; Som, A.; Nusslein, K.; Tew, G. N., "Doubly Selective" Antimicrobial Polymers: How Do They Differentiate between Bacteria? *Chem. Eur. J.* **2009,** *15* (43), 11710-11714.

25. Wang, Y.; Tang, Y. L.; Zhou, Z. J.; Ji, E.; Lopez, G. P.; Chi, E. Y.; Schanze, K. S.; Whitten, D. G., Membrane Perturbation Activity of Cationic Phenylene Ethynylene Oligomers and Polymers: Selectivity against Model Bacterial and Mammalian Membranes. *Langmuir* **2010,** *26* (15), 12509-12514.

26. Corbitt, T. S.; Ding, L. P.; Ji, E. Y.; Ista, L. K.; Ogawa, K.; Lopez, G. P.; Schanze, K. S.; Whitten, D. G., Light and dark biocidal activity of cationic poly(arylene ethynylene) conjugated polyelectrolytes. *Photochem. Photobiol. Sci.* **2009,** *8* (7), 998-1005.

27. Torrent, M.; Navarro, S.; Moussaoui, M.; Nogues, M. V.; Boix, E., Eosinophil cationic protein high-affinity binding to bacteria-wall lipopolysaccharides and peptidoglycans. *Biochemistry* **2008,** *47* (11), 3544-55.

# Chapter 6 Antifungal Activities of the CPEs and OPEs

## 6.1 Introduction

Fungal infection is one of the most pressing public healthcare concerns worldwide.[1] The increased emergence of fungal infections especially associated with immunocompromised patients and medical devices and the shortage of efficient treatments has prompted the discovery and development of new antifungal agents.[2] The CPEs and OPEs with controlled chain lengths and functional groups have been demonstrated to exhibit significant light-activated biocidal activities against a broad range of clinically relevant pathogens, including Gram-positive and Gram-negative bacteria, viruses and biofilms.[3-5]

Because of the general mechanism(s) by which CPEs and OPEs inactivate bacteria and viruses, we investigated in this study the utility of the compounds as antifungal agents. The antifungal activities of a set of antimicrobial CPEs and OPEs against the vegetative eukaryotic *Saccharomyces cerevisiae* (*S. cerevisiae*) cells and ascospores/asci were measured. *S. cerevisiae* is a common opportunistic human pathogen and has long been used as a model fungal organism.[6] Because the cell envelope serves as the first point-of-contact for biocidal agents, the structure of the *S. cerevisiae* cell envelope has been the focus of many antibiotic development studies.[2] Ultrastructural and biochemical analyses reveal that the *S. cerevisiae* cell wall has a thick (100-200 nm) and layered structure and is largely composed of polysaccharides and proteins, with chitin being a minor component (Scheme 6.1).[7-9] The outer layer of the cell wall is comprised primarily of glycosylated mannoproteins and serves as an impermeable barrier to macromolecules due to the presence of the branched carbohydrate side chains of the mannoproteins. In

addition, these carbohydrate side chains contain many phosphodiester bridges, which give rise to a negatively charged cell surface at physiological pH.[8] The inner layer of the cell wall is permeable and comprised of glucans and chitin; this fibrillar layer provides mechanical strength to the cell wall. Beneath the cell wall is the cytoplasmic membrane, which is about 7.5 nm thick and contains polar lipids and proteins.[10] The lipids are distributed asymmetrically in the membrane, where the inner leaflet is largely composed of anionic phosphatidylserine (PS) and phosphatidylinositol (PI), zwitterionic phosphatidylethanolamine (PE), while the outer leaflet is enriched in zwitterionic phosphatidylcholine (PC) and sphingolipids of varying charges.[10]

Some yeast cells produce ascospores when they encounter certain environmental stresses, such as a lack of nutrients.[11] The spores are in a dormant state, which enables them to survive for long periods in unfavorable environments.[12] Ascospores are resistant to ambient stresses, such as antibiotics, alcohols, and moderate heat. Extreme conditions, such as strong oxidants, high heat, and γ-radiation, can efficiently inactivate bacterial and fungal spores. However, these treatments are neither environmentally friendly nor practical to use in the treatment of patients. Once spores are exposed to suitable conditions, they can germinate and become pathogenic. Unlike bacterial endospores, yeast ascospores form through a meiotic process.[11] Ascospores have an unique multilayered wall, which enables them to be more resistant to environmental stresses and damages compared to vegetative cells (Scheme 6.1).[11] The two inner layers of the ascospore wall are composed of polysaccharides mannan and glucan.[11] On top of the glucan layer is a layer of chitosan and a layer of cross-linked dityrosine.[13-14] Multiple ascospores are enclosed by the ascal coat, which is derived from the cytoplasmic

membrane and cell wall of the vegetative mother cell,[11] to form an ascus. These thick protective structures make the inert ascospores highly resistant to the antibiotics. A 2% glucose solution has been shown to be an excellent germinating agent for the yeast ascospores.[15] And, applying antimicrobial agents under conditions that induce germination has been proven to be an efficient strategy to inactivate bacterial spores.[16]

**Scheme 6.1.** Models of yeast vegetative cell wall and spore wall organization

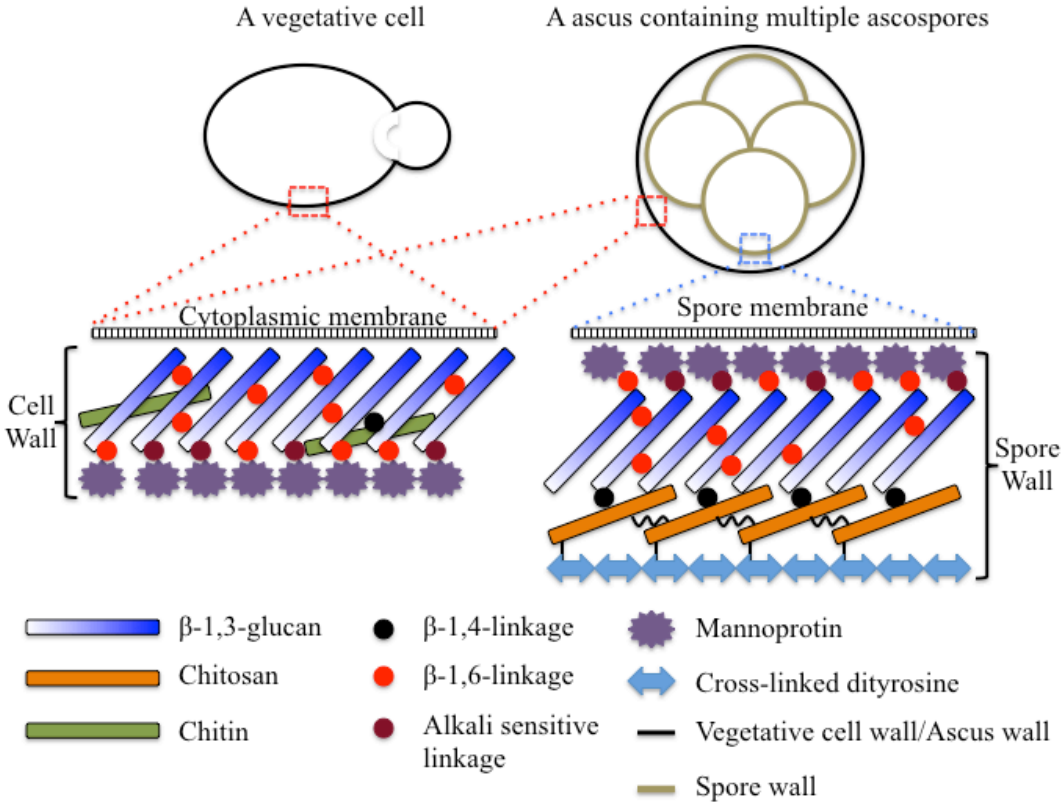


Because of the cationic nature of the PPE-based polymers and oligomers, the materials are expected to readily associate with anionic groups on the surfaces of vegetative yeast cells and asci. After exposure to UV/visible light, singlet oxygen and secondary ROS species generated by the bound CPEs and OPEs could cause severe damages to the outer envelopes of these cells.

In the current study, we investigated the antifungal activities of a series of CPEs and

OPEs (Scheme 1.3) in the dark and under UV-irradiation against *S. cerevisiae* vegetative cells, germinated ascospores and asci. The exact molecular weights of PPE-DABCO and PPE-Th are currently unavailable, but the number average molar mass (Mn) values are estimated to be within the range of 20-30 kD. As a comparison, the Food and Drug Administration (FDA)-approved, broad-spectrum antifungal agent Amphotericin B (AmB), was used as a benchmark antibacterial agent. It has been proposed that AmB exerts its toxicity by penetrating the fungal cell wall and binding to ergosterols, thereby perturbing the function of the fungal cytoplasmic membrane.[2] In this study, the viability of cells exposed to CPEs and OPEs under different conditions were determined. Additionally, cellular damages induced by the CPEs and OPEs on the morphological level were visualized by scanning electron microscopy (SEM).

## 6.2 Results and Discussion

The vast majority of antibiotics that have been developed to control bacterial infections are not effective against fungi or spores.[17] In addition, growing attention is being paid to the need to decontaminate environments contaminated by spores. Here, we report the antifungal and sporicidal activities of a class of synthetic arylene-ethynylene-based polymers and oligomers.

### 6.2.1 CPEs and OPEs exhibit efficient dark and light-enhanced antifungal activities

Figure 6.1 summarizes the biocidal effects of different CPEs and OPEs in the dark (blue bars) or with UV/visible light irradiation (red bars) against fresh *S. cerevisiae* vegetative cells (ATCC 9763) prepared in the YPD medium for 4 hours. As shown, in the absence of irradiation, the polymeric PPE-DABCO exhibited significant antifungal

activity against the vegetative cells in 60 min, reducing the number of CFU by more than 2 orders of magnitude. By comparison, the oligomeric EO-OPE-1(DABCO), OPE-3 and EO-OPE-1(C3) induced approximately a 10-fold decrease in CFU in the dark, on the same order as AmB. However, limited dark inactivation activities were observed for EO-OPE-1(Th, C2) and PPE-Th. UV irradiation significantly enhanced the inactivation activities of all CPEs and OPEs against the yeast vegetative cells relative to the activities obtained in the dark. After just 30 min of irradiation, no living cells were detected. Interestingly, AmB's biocidal activity decreased with UV-irradiation compared to its activity in the dark and is comparable to the inactivation caused by the UV-light alone (Figure 6.1). This is likely due to: 1) damages caused by the UV-light to the polyene rings of the AmB molecules, thus compromising its antifungal activity and/or 2) the shorter incubation time (30 min) employed with the UV-light irradiation experiment as compared to the dark incubation experiment (60 min).

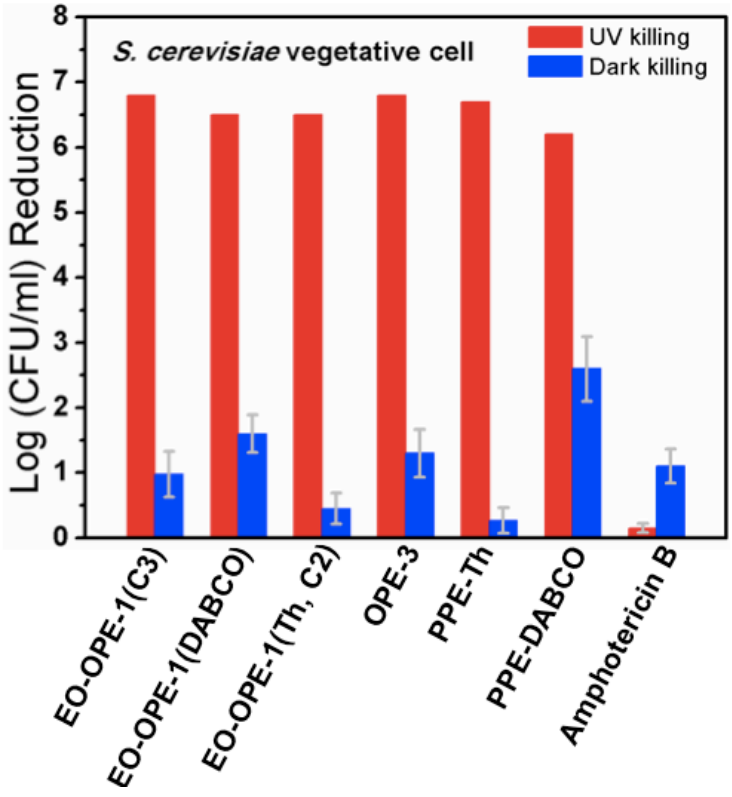


**Figure 6.1**. Inactivation of the *S. cerevisiae* vegetative cells (ATCC 9763) (~$2\times10^6$ CFU/ml) at exponential phase by CPEs or OPEs (10 μg/ml) in the dark (blue bars, 60 min incubation) or with UV-light irradiation (red bars, 4 UV-lamps and 30 min incubation). The detection limit for the assay is 6 to7 logs of CFU/ml. UVA and LZC-420 irradiation alone causes about 0.16 and 0.17 log of inactivation, respectively.

It has been shown previously that CPEs and OPEs can bind to and denature anionic protein assemblies in the dark[18] and covalently modify cytoplasmic proteins under UV/visible light irradiation. PPE-DABCO and EO-OPE-1(DABCO), which are both functionalized with DABCO-based quaternary ammonium groups (Scheme 1.3), exhibited the highest dark fungal inactivation activities among the tested agents. The high activities are likely due in part to the unique structural features of the compounds. The DABCO-based quaternary ammonium groups possess the highest positive charge density on its side chains among the CPEs and OPEs used in this study, which may enable these compounds to most strongly associate with the negatively charged cell surface and induce

the greatest degree of disruption of the self-assembled protein structures on the cell wall. This could cause the integrity of the cell envelope to be compromised. Moreover, the proteins on the cell surface could readily react with singlet oxygen and secondary ROS species generated by the CPEs and OPEs under UV-irradiation, leading to a higher extent of inactivation.

Microorganisms always exhibit various biological characters during their life cycle,[19] such as viability and metabolic activity, thus the cells at different growth phases may show different susceptibilities to the biocidal agents. Figure 6.2 shows that the susceptibility of vegetative *S. cerevisiae* cells to the dark antifungal activity of EO-OPE-1(Th, C2) varies with growth phase. Yeast cells grow exponentially for the first 12 hours in the YPD medium, after which the cells shift to diauxic and postdiauxic phases.[19] After continuous growth for about 1 week in the same medium, the cells enter the stationary phase.[19] The level of nutrients is one of the main factors controlling the cell cycle and the stationary phase has been recognized as a dormancy state in response to nutrient starvation.[19] As shown in Figure 6.2, EO-OPE-1(Th, C2) exhibited growth phase-dependent dark antifungal activities, where the inactivation activity increased during the first 24 hours of incubation, during which the yeast cells had undergone rapid growth with high metabolism and are highly susceptible to EO-OPE-1 (Th, C2)-induced toxicity. When glucose becomes exhausted, cells switch from fermentative growth to respiratory metabolism and grow at a much lower rate.[19] As shown, the metabolically inactive yeast cells were more resistant to the biocidal activity of EO-OPE-1(Th, C2) after 24 hours in YPD medium (Figure 6.2). These results imply that the dark antifungal activities of the CPEs and OPEs are dependent on the metabolism of the yeast cells, and the cells are

more susceptible when they are metabolically active. It is also important to note that the light-enhanced activity of EO-OPE-1(Th, C2) were growth phase-independent under the conditions tested. After exposure to the UV-light (4 lamps, 30 min), 10 μg/ml EO-OPE-1(Th, C2) completely inactivated the vegetative cells (~$10^6$ CFU/ml) at all of the tested growth phases. Thus in addition to damage caused to the cell envelope, it is possible that the CPEs and OPEs may be taken up by the yeast cells and interfere with metabolic pathways, thereby contributing to cell death. This seems particularly plausible in the case of damage caused in the dark, given that killing in the dark was dependent on the metabolic state of the cells.

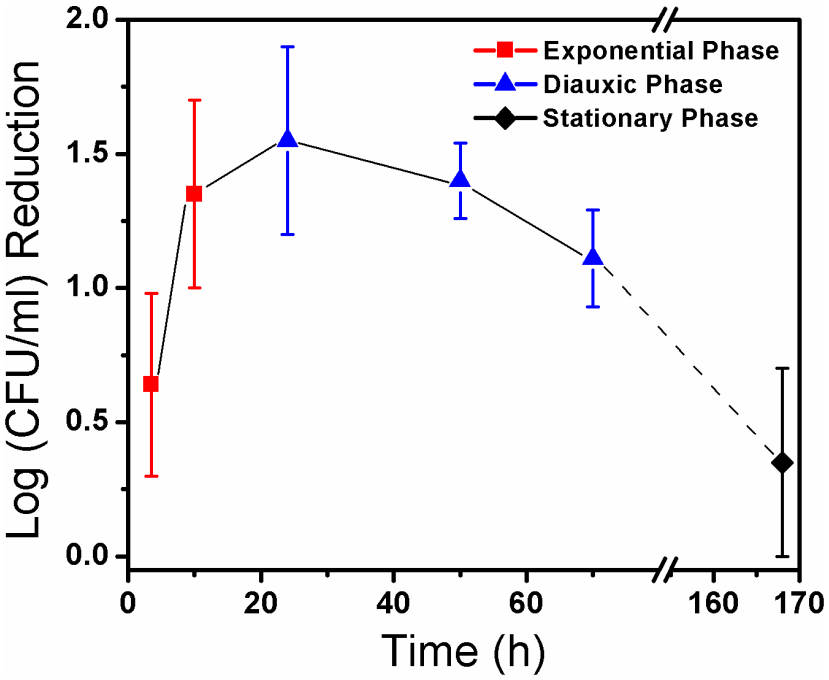


**Figure 6.2**. Inactivation of vegetative *S. cerevisiae* cells (ATCC 9763) (~$10^6$ CFU/ml) at different growth phases by 10 μg/ml EO-OPE-1(Th, C2) in the dark for 60 min. Only ~$10^5$ CFU/ml of the yeast cells were alive after 168 hours continuous incubation. The growth phases are determined based on Ref. 19.

### 6.2.2 CPEs and OPEs exhibit limited sporicidal activities

Inactivation of bacterial and fungal spores is widely recognized as being more difficult

than the killing of vegetative cells, and therefore spores present a special challenge to human health. As described, ascospores have a multilayered protective coat and moreover, ascospores are covered by an additional layer of ascal membrane and wall (Scheme 6.1). These structures enable ascospores to be highly resistant to environmental stresses and damages and the inactivation of these organism requires damages to and penetration through both the ascal layer as well as the spore coat.

As shown in Figure 6.3, in the absence of UV-light, none of the tested oligomers or polymers was effective at inactivating ascospores after 60 minutes of incubation. The viability of ascospores did not decrease after treatment with OPE-3 (30 μg/ml) for 5 hours in the dark (data not shown). In contrast, upon treatment with EO-OPE-1(Th, C2) and strong UV-irradiation (10 lamps), ascospore viability decreased about 95% within 1 hour (Figure 6.3). No increased sporicidal efficiency was observed for EO-OPE-1(Th, C2) after extended UV-light exposure (3 hours). All other tested oligomers and polymers were essentially inactive with UV-light irradiation under the current experimental conditions. Our results indicate that, except EO-OPE-1(Th, C2), other tested biocidal agents may not be able to disrupt or penetrate through the ascal coat or spore coat.

Working with *Bacillus* spores, Kane and coworkers showed that upon germination, spores become more susceptible to biocidal agents.[16] In the presence of germinant, that can trigger the spore germination program, the ascal and spore coats could be removed and the spore re-entries into the vegetative cell cycle.[11] Herein, we tested the effect of germination on the susceptibility of yeast ascospores to the CPEs and OPEs. The ascospores were first treated with 2% glucose and 0.37% $NH_4Cl$ for 20 hours to promote germination. Then the germinated spores were incubated with a CPE or OPE in the dark

or under UV-irradiation for 1 hour. As shown in Figure 6.4, in the dark, 30 μg/ml of EO-OPE-1(C3), EO-OPE-1(Th, C2) and OPE-3 resulted in more than 50% reduction in the viability of germinated spores. Moreover, all of the tested agents became effective at reducing spore viability with UV light irradiation. EO-OPE-1(Th, C2) inactivated more than 95% of the germinated spores and showed the highest light-enhanced biocidal efficacy compared to other polymers or oligomers. It is interesting to note that PPE-DABCO and EO-OPE-1(DABCO) did not exhibit any biocidal effect agains the germinated ascospores in the dark, while they were fairly active against the vegetative cells (Figure 6.1). This could be due to the existence of the extra ascus coat outside the ascospores. The ascus coat is derived from the envelope of the vegetative mother cell, and thereby has similar characteristics, such as chemical components and net charge, to those of the mother cell envelope. Since the DABCO functionalized oligomers and polymers readily associate to the vegetative cell envelope, they are expected to bind to the ascus coat with high affinity. Once bound to the coat, the polymer or oligomer molecules can become hindered from binding to and damaging the germinated spores underneath the coat.

The EO-OPE-1(Th, C2) oligomer exhibited efficient biocidal activity against both dormant and germinated ascospores under UV-light irradiation, probably due to its ability to sensitize singlet oxygen species with a high quantum yield in addition to its high solubility in water.[5, 20] However, none of the tested agents reduced the number of CFU by more than 2 orders of magnitude against the germinated ascospores. Even when the germinated spores were treated with 30 μg/ml OPE-3 for extended periods (2 to 3 hours) with UV-light exposure, no improvement in biocidal activity was observed. Rine and co-

workers have reported that 2% glucose can germinate 95% of the yeast spores (~$10^7$/ml) within 12 hours. Although the ascospores samples employed in our study were incubated for 20 hours in 2% glucose to promote complete germination, viewing the ascospores under a light microscope showed that a number of the spores did not undergo germination (data not shown). Incomplete germination of the spores can account the low inactivation levels shown in Figure 6.4. Additionally, although YPD is an excellent germination medium, bio-macromolecules in this rich medium, such as proteins and nucleic acids, may bind to the CPEs and OPEs, attenuating their biocidal activities.

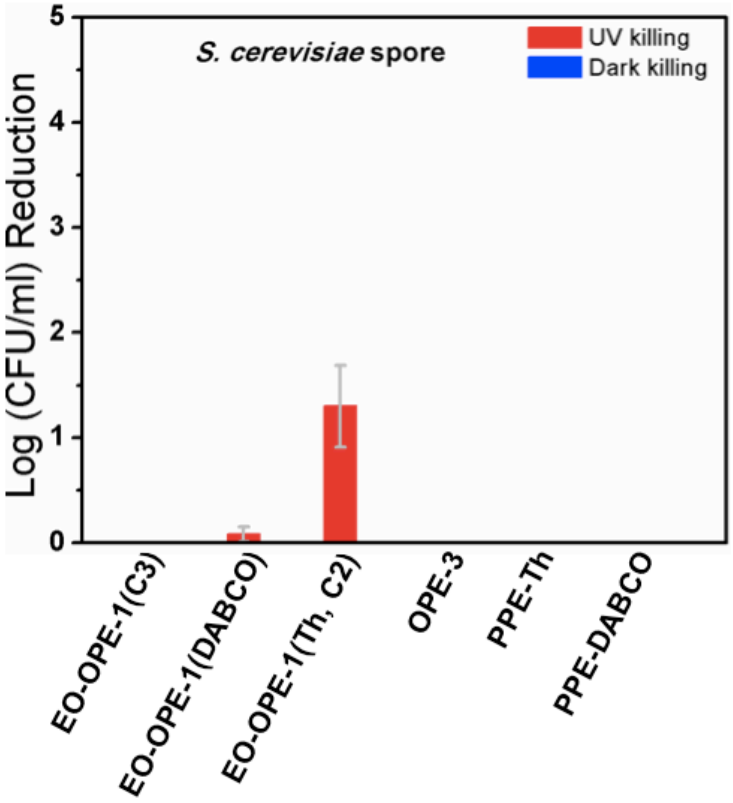


**Figure 6.3**. Inactivation of *S. cerevisiae* ascospores (ATCC 204722) (~$2\times10^6$ CFU/ml) by CPEs or OPEs (30 μg/ml) in the dark (blue bars) or with UV-light irradiation (red bars, 10 UV-lamps) for 60 min. UVA and LZC-420 irradiation alone did not cause spore inactivation under the experimental conditions.

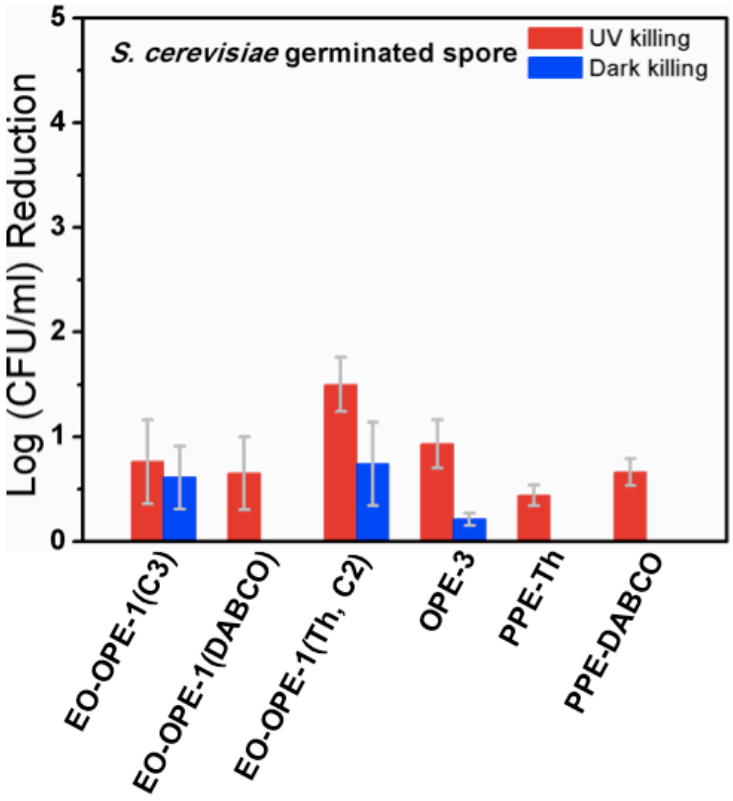


**Figure 6.4**. Inactivation of the germinated *S. cerevisiae* ascospores (ATCC 204722) (~$2\times10^6$ CFU/ml) by CPEs or OPEs (30 μg/ml) in the dark (blue bars) or with UV-light irradiation (red bars, 10 UV lamps) for 60 min. UVA and LZC-420 irradiation alone did not cause obvious spore inactivation under these current experimental conditions.

### 6.2.3 CEPs and OPEs induced morphological damages to *S. cerevisiae* vegetative cells and asci

In order to gain some insights to the antifungal and sporicidal activities of the CPEs and OPEs, morphological changes of yeast cells and ascospores in response to exposure to the different agents were examined by SEM imaging. As shown in 6.5A, the vegetative cells alone in PBS buffer maintained their integrity with smooth cell surfaces. Yeast cells treated with EO-OPE-1(C3) in the dark remained intact, but cell surfaces appeared rough and wrinkled (Figures 6.5B). Some of the PPE-Th treated cells exhibited obvious morphological damages (Figure 6.5C) compared to the untreated samples, and significant

cell envelope defects were observed. PPE-Th has been demonstrated to associate strongly with and denature anionic proteins, and it may bind to the anionic groups on the yeast cell surface and induce lethal defects. The sample preparation process for SEM imaging may amplify these defects and result in large holes on the cell surface.[21] Similar to the untreated cells (Figure 6.5A), control yeast cells irradiated by the UV-light for 30 min without the addition of biocidal agents appeared intact with smooth surfaces (Figure 6.6A), consistent with our findings that UV-irradiation alone caused low-levels of toxicity to the vegetative cells (Figure 6.1). However, the addition of oligomeric EO-OPE-1(C3) or EO-OPE-1(Th, C2) with UV-irradiation caused significant changes to the cell envelope (Figure 6.6B and D). Similar to the damage seen in the dark, PPE-Th disrupted the cell envelope and created large defects on the cell surface (Figure 6.6C). However, roughening and wrinkling of the cell surface were not observed. The polymeric PPE-Th and oligomeric EO-OPEs induced different types of damages to the yeast cells both in the dark and with UV-irradiation, which may be due to the permeability of the cell wall top layer. The glycosylated mannoproteins with branched carbohydrate side chains on the cell surface can render the cell wall impermeable to the polymeric PPE-Th. As a result, the relatively hydrophobic PPE-Th chains may aggregate[22] and act to create defects on the cell surface. However, the EO-OPEs with a nearly linear conformation may penetrate deeper into the cell envelope and reorganize the layered structure of the cell envelope. It is important to note that the yeast cells seem to be damaged to different extents by the biocidal compounds (Figure 6.5 and 6.6), which probably is due to the non-uniform binding of these compounds toward the yeast cells.

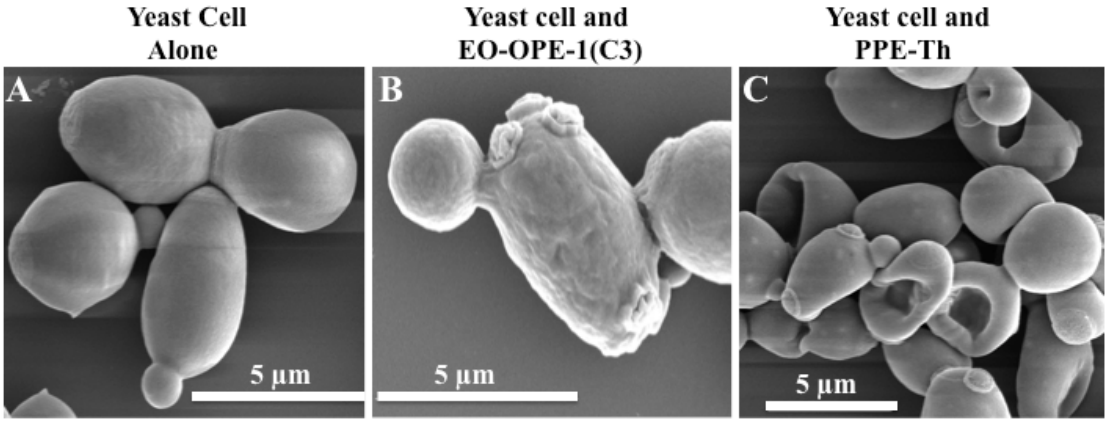


**Figure 6.5**. SEM images of *S. cerevisiae* vegetative cells alone (ATCC 9763) (~$2\times10^6$ CFU/ml) (A) and incubated with 10 µg/ml antimicrobial EO-OPE-1(C3) (B) or PPE-Th (C) for one hour in the dark.

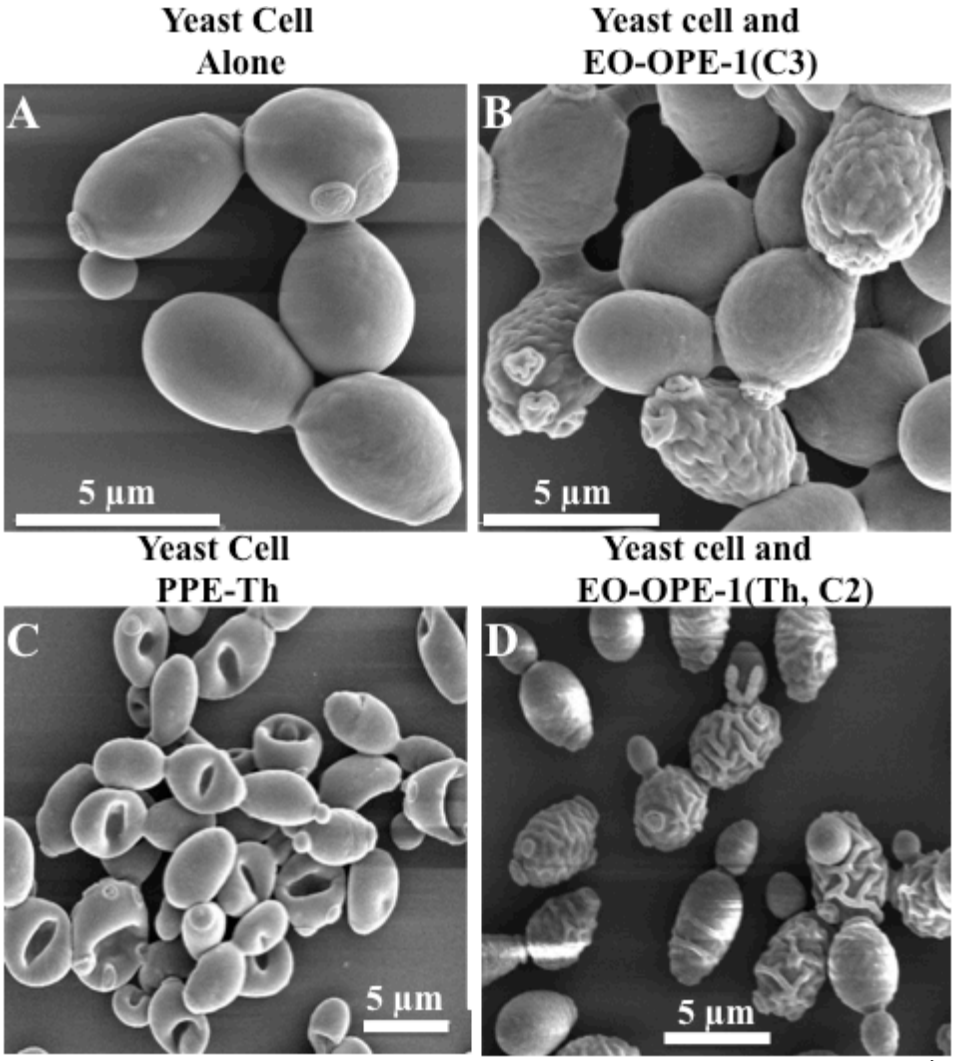


**Figure 6.6**. SEM images of *S. cerevisiae* vegetative cells (ATCC 9763) (~$2\times10^6$ CFU/ml)

alone (A) and incubated with 10 μg/ml EO-OPE-1(C3) (B) or PPE-Th (C) or EO-OPE-1(Th, C2) (D) for 30 min with UV-light irradiation (4 lamps).

EO-OPE-1(Th, C2) was shown to inactivate more than 95% of dormant and germinated yeast ascospores (Figures 6.3 and 6.4). As shown in Figure 6.7A, the ascus exhibits a classic tetrahedral shape with a smooth coat and each individual ascospore is clearly seen in the ascus. With UV-light irradiation alone, the ascus coat became ridged in appearance, while maintaining its structural integrity and continued to enclose the ascospores (Figure 6.7B). After treatment with EO-OPE-1(Th, C2) in the presence of UV-light (Figure 6.7D), asci exhibited similar structural features as shown in Figure 6.7B and no further morphological damage could be observed to the asci, implying that the oligomer may use other mechanisms to inactivate the ascospores.

In contrast to the asci, germinated ascospores have a distinctive appearance and a smaller size (Figure 6.7C), indicating that the ascus coat may be partially removed during the germination process. The addition of EO-OPE-1(Th, C2) with UV-irradiation caused obvious damages to the surface of the germinated spores with the vegetative cell wall (Figure 6.7E, see arrows), which appeared very similar to the vegetative cells treated by the oligomer with UV-light (Figures 6.6B and 6.6D).

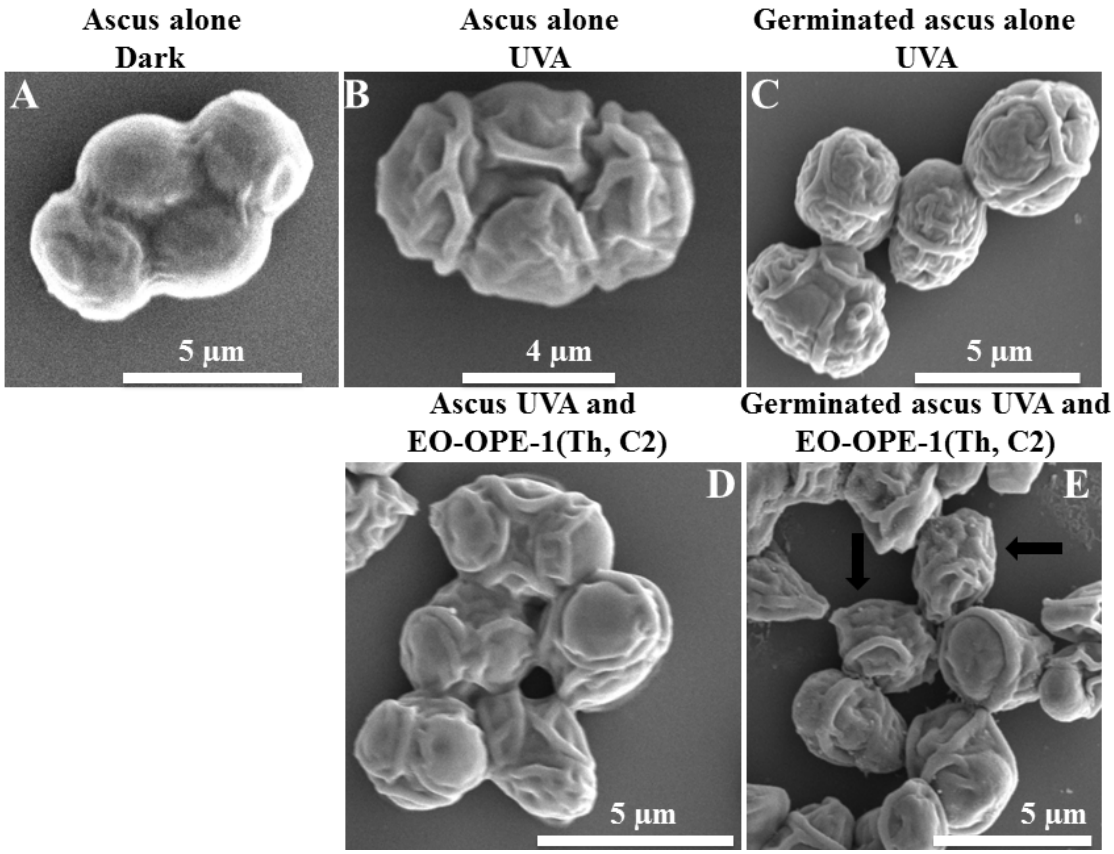


Figure 6.7. SEM images of A. an *S. cerevisiae* ascus containing four ascospores (ATCC 204722) (~$10^6$ CFU/ml), B. an ascus irradiated with UV-light, C. germinated asci irradiated with UV-light, D. asci incubated with 30 µg/ml EO-OPE-1(Th, C2) and irradiated with UV-light for 1 hour, and E. germinated asci incubated with 30 µg/ml EO-OPE-1(Th, C2) and irradiated with UV-light for 1 hour. All UV-irradiation experiments were carried out with 10 lamps.

### 6.3 Conclusions

This study explored the antifungal and sporicidal activities of the arylene-ethynylene-based CPEs and OPEs using *S. cerevisiae* as a model pathogen toward the goal of extending the utility of these polymers and oligomers as biocidal agents. In the dark, the CPEs and OPEs exhibited moderate inactivation of vegetative yeast cells. In particular, PPE-DABCO, EO-OPE-1(DABCO) and OPE-3 showed comparable or higher antifungal activities compared to the widely-used antibiotic AmB. With UV-irradiation, all of the tested agents induced more than 6-log reductions in yeast cell viability. Moreover,

antifungal activities of the compounds were shown to be dependent on the growth phase of the yeast cells where cells in growth phases that correspond to higher metabolic activities were more susceptible to the biocidal activities of CPEs and OPEs. These materials showed limited inactivation activities towards ascospores. In the dark, all compounds tested were not effective at reducing spore viability and with UV irradiation, only EO-OPE-1(Th, C2) was active, inactivating more than 95% of the yeast ascospores. The compounds were more effective at inactivating ascospores once they undergo germination, where the tested agents showed inactivation activity with UV-light irradiation. SEM imaging revealed that the envelopes of the vegetative cell and germinated ascospore are targets of the CPEs and OPEs.

### 6.4 References


1. Wisplinghoff, H.; Bischoff, T.; Tallent, M.; Seifert, H.; Wenzel, R. P.; Edmond, M. B., Nosocomial bloodstream infections in US hospitals: analysis of 24,179 cases from a prospective nationwide surveillance study. *Clin. Infect. Dis.* **2004,** *39* (7), 1093-1093.

2. Odds, F. C.; Brown, A. J. P.; Gow, N. A. R., Antifungal agents: mechanisms of action. *Trends Microbiol.* **2003,** *11* (6), 272-279.

3. Tang, Y. L.; Corbitt, T. S.; Parthasarathy, A.; Zhou, Z. J.; Schanze, K. S.; Whitten, D. G., Light-Induced Antibacterial Activity of Symmetrical and Asymmetrical Oligophenylene Ethynylenes. *Langmuir* **2011,** *27* (8), 4956-4962.

4. Wang, Y.; Canady, T. D.; Zhou, Z. J.; Tang, Y. L.; Price, D. N.; Bear, D. G.; Chi, E. Y.; Schanze, K. S.; Whitten, D. G., Cationic Phenylene Ethynylene Polymers and Oligomers Exhibit Efficient Antiviral Activity. *ACS Appl. Mater. Interfaces* **2011,** *3* (7),

2209-2214.

5. Dascier, D.; Ji, E.; Parthasarathy, A.; Schanze, K. S.; Whitten, D. G., Efficacy of End-Only-Functionalized Oligo(arylene-ethynylene)s in Killing Bacterial Biofilms. *Langmuir* **2012,** *28* (31), 11286-11290.

6. Goldstein, A. L.; McCusker, J. H., Development of Saccharomyces cerevisiae as a Model Pathogen: A System for the Genetic Identification of Gene Products Required for Survival in the Mammalian Host Environment. *Genetics* **2001,** *159* (2), 499-513.

7. Lesage, G.; Bussey, H., Cell wall assembly in Saccharomyces cerevisiae. *Microbiol. Mol. Biol. R* **2006,** *70* (2), 317-343.

8. Klis, F. M.; Mol, P.; Hellingwerf, K.; Brul, S., Dynamics of cell wall structure in Saccharomyces cerevisiae. *FEMS Microbiol. Rev.* **2002,** *26* (3), 239-256.

9. Osumi, M., The ultrastructure of yeast: Cell wall structure and formation. *Micron* **1998,** *29* (6), 207-233.

10. Vanderrest, M. E.; Kamminga, A. H.; Nakano, A.; Anraku, Y.; Poolman, B.; Konings, W. N., The Plasma-Membrane of Saccharomyces-Cerevisiae - Structure, Function, and Biogenesis. *Microbiol. Rev.* **1995,** *59* (2), 304-322.

11. Coluccio, A.; Neiman, A. M., Interspore bridges: a new feature of the Saccharomyces cerevisiae spore wall. *Microbiology* **2004,** *150*, 3189-3196.

12. Feofilova, E. P.; Ivashechkin, A. A.; Alekhin, A. I.; Sergeeva, Y. E., Fungal spores: Dormancy, germination, chemical composition, and role in biotechnology (review). *Appl. Biochem. Micro+* **2012,** *48* (1), 1-11.

13. Briza, P.; Ellinger, A.; Winkler, G.; Breitenbach, M., Chemical-Composition of the Yeast Ascospore Wall - the 2nd Outer Layer Consists of Chitosan. *J. Biol. Chem.*

**1988,** *263* (23), 11569-11574.

14. Neiman, A. M., Sporulation in the Budding Yeast Saccharomyces cerevisiae. *Genetics* **2011,** *189* (3), 737-765.

15. Herman, P. K.; Rine, J., Yeast spore germination: a requirement for Ras protein activity during re-entry into the cell cycle. *EMBO J.* **1997,** *16* (20), 6171-6181.

16. Banerjee, I.; Mehta, K. K.; Dordick, J. S.; Kane, R. S., Light-activated porphyrin-based formulations to inactivate bacterial spores. *J. Appl. Microbiol.* **2012,** *113* (6), 1461-1467.

17. Cowan, M. K.; Talaro, K. P., *Microbiology: A Systems Approach*. 2 ed.; McGraw-Hill Science: New York, **2008**.

18. Wang, Y.; Zhou, Z. J.; Zhu, J. S.; Tang, Y.; Canady, T. D.; Chi, E. Y.; Schanze, K. S.; Whitten, D. G., Dark Antimicrobial Mechanisms of Cationic Phenylene Ethynylene Polymers and Oligomers against Escherichia coli. *Polymers* **2011,** *3*, 1199-1214.

19. Wernerwashburne, M.; Braun, E.; Johnston, G. C.; Singer, R. A., Stationary-Phase in the Yeast Saccharomyces-Cerevisiae. *Microbiol. Rev.* **1993,** *57* (2), 383-401.

20. Zhou, Z. J.; Corbitt, T. S.; Parthasarathy, A.; Tang, Y. L.; Ista, L. F.; Schanze, K. S.; Whitten, D. G., "End-Only" Functionalized Oligo(phenylene ethynylene)s: Synthesis, Photophysical and Biocidal Activity. *J. Phys. Chem. Lett.* **2010,** *1* (21), 3207-3212.

21. Bozzola, J. J.; Russell, L. D., *Electron Microscopy: Principles and Techniques for Biologists* 1ed.; Jones & Bartlett Pub: London, **1992**.

22. Corbitt, T. S.; Ding, L. P.; Ji, E. Y.; Ista, L. K.; Ogawa, K.; Lopez, G. P.; Schanze, K. S.; Whitten, D. G., Light and dark biocidal activity of cationic poly(arylene ethynylene) conjugated polyelectrolytes. *Photochem. Photobiol. Sci.* **2009,** *8* (7), 998-

1005.

# Chapter 7 Antiviral Activity of the CPEs and OPEs

## 7.1 Introduction

The work discussed in previous chapters has shown that the cationic PPE-based polymers and oligomers display significant photoinducible antimicrobial activity in both Gram-positive and Gram-negative bacteria. The direct contact between these antimicrobial compounds and microorganisms followed by the generation of corrosive reactive oxygen species (ROS) after exposure to UV-visible light appears to account for the high bactericidal activity of these cationic PPE-based materials.

In addition to health threats caused by bacterial infections, many serious diseases are caused by viruses. The most notable example is human immunodeficiency virus induced Acquired Immune Deficiency Syndrome (HIV-AIDS), which has infected an estimated 33.3 million people.[1] Current interferon-based treatments for virus-caused diseases and current wastewater treatments against viral-contamination are inadequate.[2] The development of new antiviral agents is a critical worldwide healthcare need. Given our increased understanding of the mechanism of dark and light-induced inactivation of bacteria by the PPE polymers and oligomers, we suspected that these materials might also be effective against viruses. Here, we investigate the antiviral activities of a series of CPEs and OPEs against two model viruses, the MS2 and T4 bacteriophages. The structures and compositions of these bacteriophages have been extensively investigated.[3-5] Bacteriophage MS2 is a non-enveloped, ~27 nm RNA virus with a small single-stranded RNA genome of ~3600 nucleotides. Its structure is very similar to some members of the picornavirus family, which are important human and animal viral pathogens.[6] Bacteriophage T4 is a relative large, non-enveloped 170 kbp double-stranded

DNA virus with a 120 by 86 nm head and a 100 nm tail. These two bacteriophages are commonly used as model systems for environmental pollution and virus detection studies.[7]

The isoelectric points of the MS2 and T4 phage particles are 3.9 and 4~5, respectively,[8] which render them slightly negatively charged in neutral buffers. Thus, our cationic CPEs and OPEs are expected to readily associate with the phage particles and possibly attenuate their recognition and binding to host cells. Previously, we proposed that after exposure to UV-visible light, the CPEs and OPEs can generate singlet oxygen species followed by the formation of more corrosive reactive oxygen intermediates.[9] This property of the CPEs and OPEs is due to the conjugated $\pi$ bonding system in the backbone of the compounds, which allows for efficient intersystem crossing to a triplet state that sensitizes the formation of singlet oxygen $^1O_2$. $^1O_2$ and the subsequent ROS intermediates are known to be highly damaging to biomolecules, including proteins, RNA and DNA.[10] In addition, the association of CPEs and OPEs with biological structures, in the absence of any irradiation, has been shown to disrupt non-covalent biomolecular assemblies, including the lipid membrane,[11] and folded protein structures. The major components of viruses are proteins, RNA or DNA. Moreover, the virus capsid, which encloses the genetic material of the virus, is made of non-covalently assembled proteins.

In the current study, we evaluate the antiviral activities of a number of CPE and OPE compounds against two model viruses in the presence and absence of UV or short wavelength visible light using biological (infectivity) and morphological structural (TEM) assays. SDS-PAGE provides additional insights into the mechanism of the light-induced

inactivation mechanism of CPEs and OPEs.

## 7.2 Results and Discussion

The phage titer assay was carried out by a serial dilution of phage-CPE/OPE mixture and incubating each diluted sample with the corresponding *E. coli* host cells within molten soft LB agar. Since our previous work demonstrated that the CPEs/OPEs can efficiently inactivate *E. coli* cells,[12-14] which may interfere with the plaque assay, it is necessary to study the effect of residual CPEs/OPEs on the *E. coli* host cells. For the control experiment without phage and CPEs/OPEs, *E. coli* forms a confluent cell sheet on the soft agar after 6 hours of incubation at 37°C. Under the current experimental conditions, 0.33 μg/ml was the maximum concentration of residual CPEs/OPEs in the soft agar (100 μl inactivated phage sample by 10 μg/ml CPEs/OPEs was mixed with 3 ml melted soft agar), which did not cause any obvious defects in the bacterial cell sheet.

### 7.2.1 CPEs and OPEs exhibit efficient phage inactivation ability

Figure 7.1 summarizes T4 and MS2 phage inactivation induced by different CPE and OPE compounds in the dark (black bars) or with UV/visible irradiation (blue bars). The effect of irradiation alone (red bars) on phage inactivation was also determined. Even in the absence of UV or visible light, PPE-DABCO and EO-OPE-1(Th) exhibit significant antiviral activities against the T4 phage, reducing the number of PFU by 6 and 3 orders of magnitudes, respectively. In comparison, PPE-Th, OPE-1 and EO-OPE-1(C3) are less active in the dark, albeit inducing *ca*. 1 order of magnitude of inactivation. No dark inactivation activity is observed for OPE-3 against the T4 phage. UV irradiation enhanced the inactivation of the T4 phage induced by all CPEs and OPEs. For example,

UV light enhanced PPE-Th and EO-OPE-1(C3)-induced inactivation by about 5 and 3 orders of magnitude compared to inactivation by the compounds in the dark. Whereas OPE-3 was ineffective in the dark, a 3 order of magnitude decrease in PFU was observed with UV irradiation.

Compared with the inactivation of T4 phage, all CPEs and OPEs tested were more efficient at inactivating the MS2 phage in the dark (Figure 7.1B). All compounds, except OPE-1 and EO-OPE-1(C3), induced more than 6-log inactivation against MS2 phage in the dark. With UV irradiation, OPE-1 and EO-OPE-1(C3) became very efficient at inactivating the MS2 phage.

Of the materials tested, PPE-DABCO exhibited the highest virus inactivation activity, inducing more than 6 orders of magnitude of inactivation of both model viruses in the dark and with UV irradiation. The high antivirial activity of PPE-DABCO is likely due in part to its unique structural features. The polymer possesses the highest positive charge density on its side chains among the CPEs and OPEs tested in this study, which gives PPE-DABCO the ability to easily associate with the negatively charged viruses. In addition, the bulky side chains with highly hydrophobic yet positively charged groups of the PPE-DABCO prevent self-aggregation thus making more of the polymer available to associate with the phage particles.

Our results also showed that all of the oligomers exhibit more efficient dark inactivation activity against the MS2 phage than the T4 phage. This could be due in part to the presence of 32 pores[15] (1.8 nm in diameter) on the MS2 capsid that provide easier access for the oligomers to interact with the packaged phage genome. It is also worth noting that long wavelength UV-visible light (LZC-420) alone produces negligible

inactivation of the viruses (UV control data for polymeric PPE-DABCO and PPE-Th samples in Figure 7.1). In contrast, UVA irradiation alone in the absence of the oligomers causes measurable inactivation of both viruses (UV control data for oligomeric OPE-1, OPE-3, EO-OPE-1(C3), and EO-OPE-1(Th) samples in Figure 7.1). Moreover, UVA irradiation caused a higher level of virus inactivation of T4 compared to MS2. The different effects of UV light on the model viruses could be explained by T4's higher susceptibility to chemical damage. Upon exposure to UVA irradiation, adjacent thymidine residues in the T4 phage DNA genome can covalently link to form thymidine dimers,[16] and can to a lesser extent also induce protein-DNA photocrosslinking leading the inactivation of T4 phage. While UVA can cause protein-RNA photocrosslinking, RNA does not contain thymine, and uracil photodimerization is very rare.

It is clear from our data that the cationic CPE and OPE compounds tested show efficient inactivation activity against the two model viruses. The first step in viral infection is the recognition and binding of the viruses to the surface of the host cells. The T4 bacteriophage infection is initiated by the recognition of the lipopolysaccharides and the OmpC protein on the surface of host *E. coli* cells and followed by release of the phage genome into the host for replication.[17] Although the exact infection pathway of the MS2 phage is not clear, it is believed that the pilus of *E. coli* cells is a potential receptor for the MS2 phage.[18] The cationic CPEs and OPEs are expected to bind to the slightly negatively charged T4 and MS2 virus surfaces through electrostatic interactions. Thus, it is reasonable to assume that the antiviral activities of the PPE and OPE compounds are due in part from their ability to shield the virus particles from the host cells. Meanwhile, it is worth noting that since the sorption of the CPEs and OPEs to the viral particles is not

fully understood, it is possible for the absorbed antiviral compounds to be desorbed with a change in the environmental conditions (such as solution pH and ionic strength) without causing lethal damage to the bacteriophages. We have shown previously that the CPE and OPE compounds can disrupt non-covalent biomolecular assemblies and generate reactive oxygen species with UV-visible light exposure, which can strongly damage biomolecules, including proteins that make up the virus capsid.[10, 19] We examined below if the binding of the compounds to virus particles results in further capsid damage.

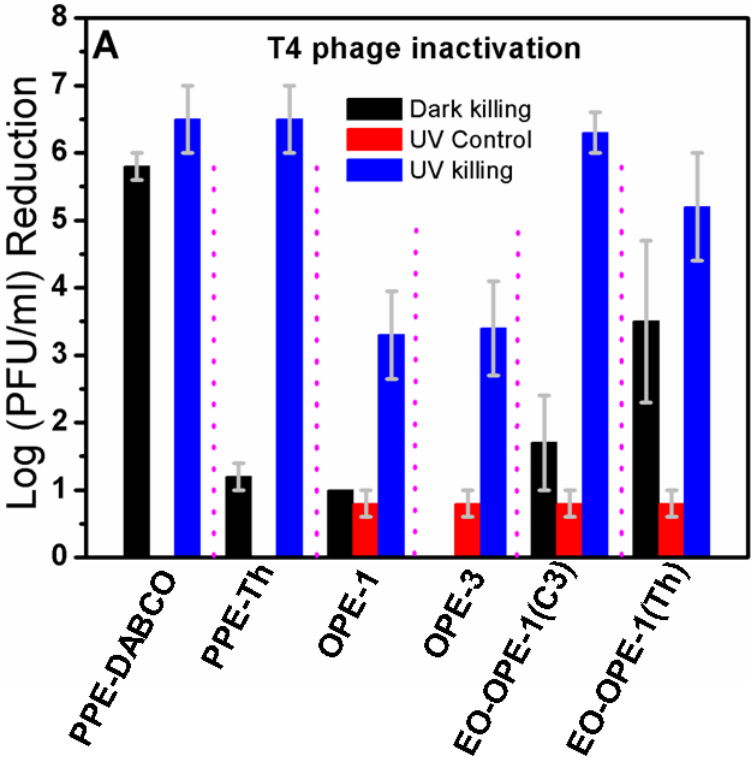

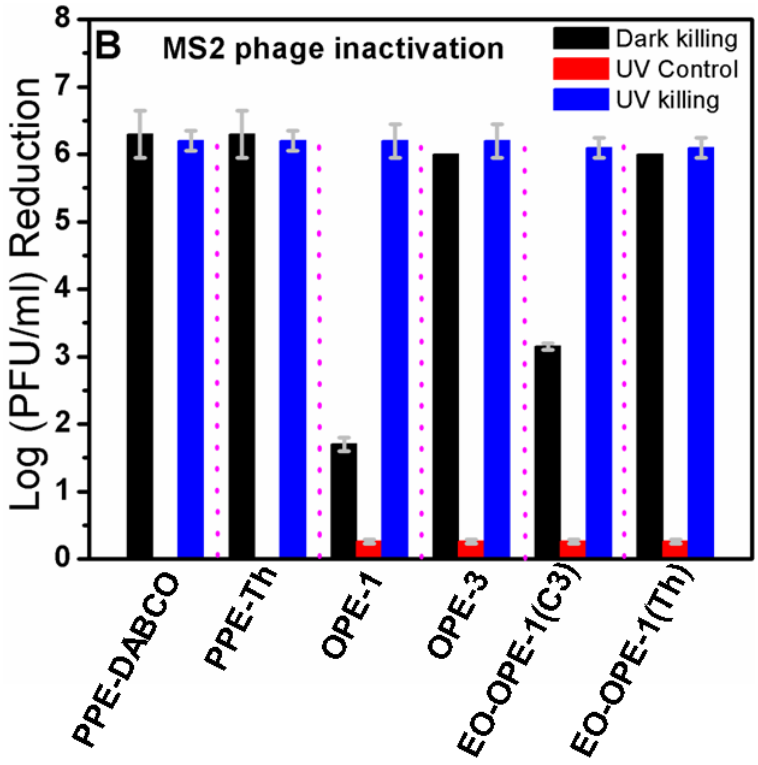


**Figure 7.1**. Inactivation of the T4 (A) and MS2 (B) bacterialphages by CPEs or OPEs in the dark (black bars) or with UV-light irradiation (blue bars). UV control samples (red bars) were those exposed to irradiation alone. The detection limit for the assay is 6 to7 logs of PFU/ml.

### 7.2.2 PPE-DABCO and EO-OPE-1(Th) disrupt viral morphology

To visualize the changes in viral morphology induced by PPE-DABCO and EO-OPE-1(Th), virus samples exposed to the compounds were imaged by TEM. Representative images (out of more than 10 collected) are shown in Figure 7.2. As a control, the untreated T4 phage shows its classic morphology with intact icosahedral head and tail structure (Figure 7.2 A1). In contrast, when exposed to PPE-DABCO or EO-OPE-1(Th), both in the dark as well as with UV-light exposure, significant changes to the virus morphology are observed. As shown in Figure 7.2 B1, the tail of the T4 phage is detached from the head in the presence of PPE-DABCO in the dark. Significant damage

is also observed to the head of the T4 phage with the addition of PPE-DABCO in the light or with EO-OPE-1(Th) in the dark and under irradiation (Figure 7.2C1, D1 and E1). Likewise, the untreated MS2 phage are uniformly sized and spherically shaped (Figure 7.2 A2). When exposed to PPE-DABCO and EO-OPE-1(Th) in the dark, the surface of the phage particles became rough and wrinkled (Figure 7.2 B2 and D2). MS2 phage treated with PPE-DABCO or EO-OPE-1(Th) with UV light irradiation exhibited significant disruption (Figure 7.2 C2 and E2).

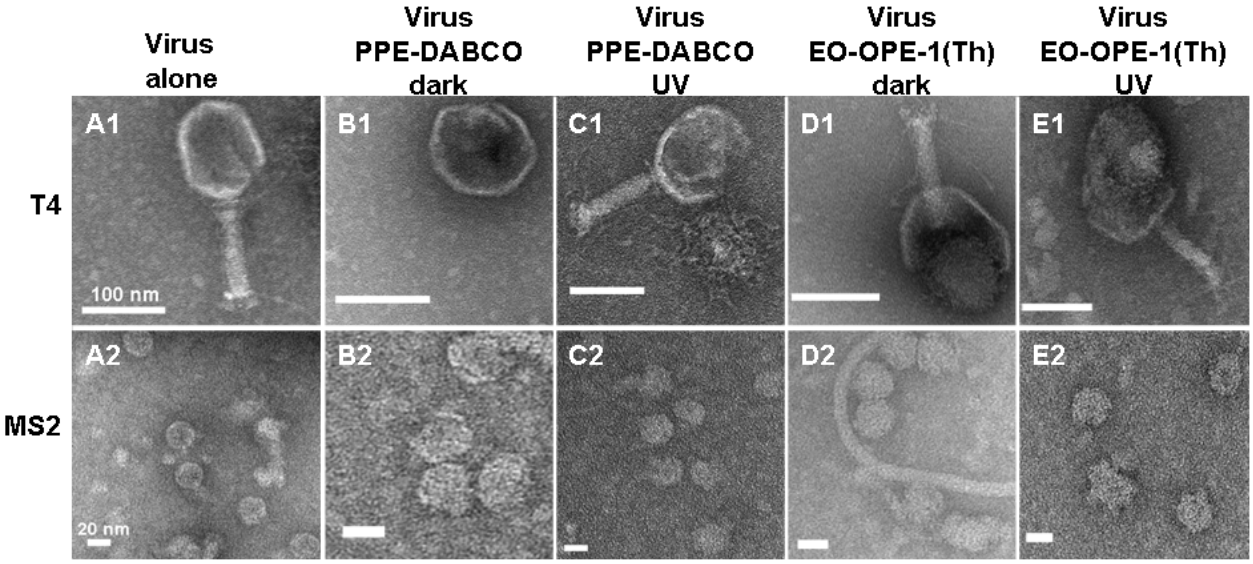


**Figure 7.2**. TEM images of the T4 and MS2 viruses alone (A1 and A2) and incubated with PPE-DABCO (B1 and B2, in the dark; C1 and C2, with UV irradiation) or EO-OPE-1 (Th) (D1 and D2, in the dark; E1 and E2, with UV irradiation) for one hour. The scale bars of the T4 images are 100 nm and the scale bars of the MS2 images are 20 nm.

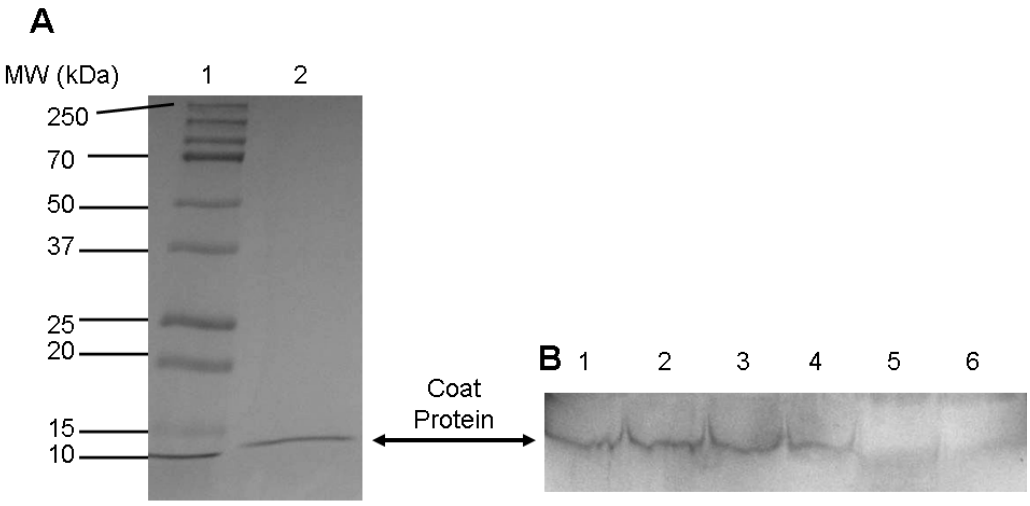


**Figure 7.3**. SDS-PAGE gels of the MS2 phage capsid. Lane A1: protein marker (BIO-RAD); Lane A2 and B1: phage alone in the dark; Lane B2: phage irradiated with UVA; Lane B3: phage with 20 μg/ml EO-OPE-1(Th) in the dark; Lane B4: phage with 40 μg/ml EO-OPE-1(Th) in the dark; Lane B5: phage with 20 μg/ml EO-OPE-1(Th) irradiated with UVA; Lane B6: phage with 40 μg/ml EO-OPE-1(Th) irradiated with UVA.

### 7.2.3 EO-OPE-1(Th) damages MS2 capsid protein with UV irradiation

To assess the extent of damage to the virus capsid induced by the CPE and OPE compounds, the capsid proteins of the MS2 bacteriophage were analyzed with SDS-PAGE. The MS2 capsid is comprised of 180 copies of a coat protein with a molecular weight of ~ 13.7 kDa and one copy of the maturase protein with a molecular weight of ~ 44 kDa.[3, 20] The band in lane 2 in Figure 7.3A from isolated MS2 phage particles is in agreement with expected molecular weight of the phage coat protein. Lanes 2-4 in Figure 7.3B show the coat protein band of viruses exposed to UVA irradiation alone and with EO-OPE-1(Th) in the dark. UV irradiation alone (Figure 7.3B, band 2) or the presence of EO-OPE-1(Th) in the dark (band 3 and 4) did not cause any significant changes to the coat protein band, indicating that these two conditions did not cause either aggregation or cleavage to the virus coat proteins. In contrast, the coat protein bands of MS2 in the

presence of EO-OPE-1(Th) with UVA irradiation showed a band with significantly decreased intensity (Figure 7.3B, bands 5 and 6), indicating that the reactive oxygen species generated by the irradiation of EO-OPE-1(Th) has caused almost complete modification of the coat protein. However, the degradation products have not been characterized in the present study.

MS2 phage inactivation data in Figure 7.1B show that the oligomer EO-OPE-1(Th) is very potent at inactivating the virus both in the dark and with UV irradiation, reducing the number of plaques by over 6 orders of magnitude. Our gel electrophoresis results show that virus inactivation in the dark and with UV irradiation proceeds through different mechanisms. No damage to the monomeric coat protein occurred with the virus particles exposed to the oligomer alone, implying that EO-OPE-1(Th) exerts its dark phage inactivation activity through physical binding to the phage particles, followed by possible remodeling of capsid architecture. Meanwhile, UV irradiation in the presence of the oligomer induced almost complete degradation of the virus coat protein. Thus, the mechanism of the antiviral properties of the CPEs and OPEs may be comprised of at least three parts: (1) Association of these cationic compounds with the virus particles attenuates virus recognition and binding to host cells. (2) The compounds disrupt the architecture or morphology of the virus capsid, and (3) UV-induced generation of reactive oxygen species by the PPE-based compounds has the potential ability to covalently modify the capsid coat proteins.

### 7.3 Conclusions

In summary, the current study expands upon the utility of the PPE-based CPEs and OPEs as antimicrobials and it underscores that (1) most of these compounds exhibited

high dark inactivation activity against the MS2 phage and moderate dark inactivation ability against the T4 phage through the inhibition of their infection pathway and/or the destruction of the virus structures, and (2) the UV light-enhanced antiviral activity of the CPEs and OPEs is achieved by the generation of corrosive reactive oxygen species, which can chemically damage the capsid protein of the model viruses.

### 7.4 References


1. World Health Organization, Global Summary of the AIDS Epidemic, **2009**.

2. Moradpour, D.; Penin, F.; Rice, C. M., Replication of hepatitis C virus. *Nat. Rev. Microbiol.* **2007,** *5* (6), 453-463.

3. Kuzmanovic, D. A.; Elashvili, I.; Wick, C.; O'Connell, C.; Krueger, S., Bacteriophage MS2: Molecular weight and spatial distribution of the protein and RNA components by small-angle neutron scattering and virus counting. *Structure* **2003,** *11* (11), 1339-1348.

4. Rao, V. B.; Black, L. W., Structure and assembly of bacteriophage T4 head. *Virol. J.* **2010,** *7*, 356.

5. Leiman, P. G.; Arisaka, F.; van Raaij, M. J.; Kostyuchenko, V. A.; Aksyuk, A. A.; Kanamaru, S.; Rossmann, M. G., Morphogenesis of the T4 tail and tail fibers. *Virol. J.* **2010,** *7*, 355.

6. Norder, H.; De Palma, A. M.; Selisko, B.; Costenaro, L.; Papageorgiou, N.; Arnan, C.; Coutard, B.; Lantez, V.; De Lamballerie, X.; Baronti, C.; Sola, M.; Tan, J.; Neyts, J.; Canard, B.; Coll, M.; Gorbalenya, A. E.; Hilgenfeld, R., Picornavirus non-structural proteins as targets for new anti-virals with broad activity. *Antivir. Res.* **2011,** *89* (3), 204-218.

7. Pasloske, B. L.; Walkerpeach, C. R.; Obermoeller, R. D.; Winkler, M.; DuBois, D. B., Armored RNA technology for production of ribonuclease-resistant viral RNA controls and standards. *J. Clin. Microbiol.* **1998,** *36* (12), 3590-3594.

8. Brady-Estevez, A. S.; Schnoor, M. H.; Kang, S.; Elimelech, M., SWNT-MWNT hybrid filter attains high viral removal and bacterial inactivation. *Langmuir* **2010,** *26* (24), 19153-8.

9. Chemburu, S.; Corbitt, T. S.; Ista, L. K.; Ji, E.; Fulghum, J.; Lopez, G. P.; Ogawa, K.; Schanze, K. S.; Whitten, D. G., Light-induced biocidal action of conjugated polyelectrolytes supported on colloids. *Langmuir* **2008,** *24* (19), 11053-11062.

10. Davies, M. J., Singlet oxygen-mediated damage to proteins and its consequences. *Biochem. Biophys. Res. Commum.* **2003,** *305* (3), 761-770.

11. Wang, Y.; Tang, Y. L.; Zhou, Z. J.; Ji, E.; Lopez, G. P.; Chi, E. Y.; Schanze, K. S.; Whitten, D. G., Membrane Perturbation Activity of Cationic Phenylene Ethynylene Oligomers and Polymers: Selectivity against Model Bacterial and Mammalian Membranes. *Langmuir* **2010,** *26* (15), 12509-12514.

12. Corbitt, T. S.; Ding, L. P.; Ji, E. Y.; Ista, L. K.; Ogawa, K.; Lopez, G. P.; Schanze, K. S.; Whitten, D. G., Light and dark biocidal activity of cationic poly(arylene ethynylene) conjugated polyelectrolytes. *Photochem. Photobiol. Sci.* **2009,** *8* (7), 998-1005.

13. Zhou, Z. J.; Corbitt, T. S.; Parthasarathy, A.; Tang, Y. L.; Ista, L. F.; Schanze, K. S.; Whitten, D. G., "End-Only" Functionalized Oligo(phenylene ethynylene)s: Synthesis, Photophysical and Biocidal Activity. *J. Phys. Chem. Lett.* **2010,** *1* (21), 3207-3212.

14. Tang, Y. L.; Corbitt, T. S.; Parthasarathy, A.; Zhou, Z. J.; Schanze, K. S.; Whitten,

D. G., Light-Induced Antibacterial Activity of Symmetrical and Asymmetrical Oligophenylene Ethynylenes. *Langmuir* **2011,** *27* (8), 4956-4962.

15. Hooker, J. M.; Kovacs, E. W.; Francis, M. B., Interior surface modification of bacteriophage MS2. *J. Am. Chem. Soc.* **2004,** *126* (12), 3718-3719.

16. Goodsell, D. S., The molecular perspective: Ultraviolet light and pyrimidine dimers. *Oncologist* **2001,** *6* (3), 298-299.

17. Furukawa, H.; Kuroiwa, T.; Mizushima, S., DNA Injection during Bacteriophage-T4 Infection of Escherichia-Coli. *J. Bacteriol.* **1983,** *154* (2), 938-945.

18. Date, T., Kinetic Studies of the Interaction between Ms2-Phage and F-Pilus of Escherichia-Coli. *Eur. J. Biochem.* **1979,** *96* (1), 167-175.

19. Davies, M. J., Reactive species formed on proteins exposed to singlet oxygen. *Photochem. Photobiol. Sci.* **2004,** *3* (1), 17-25.

20. Peabody, D. S., A Viral Platform for Chemical Modification and Multivalent Display. *J. Nanobiotechnology* **2003,** *1* (1), 5.

# Chapter 8 Summary and Future Directions

## 8.1 Summary

In this dissertation, I have summarized findings from multiple investigations of the interactions of CPEs and OPEs with potential pathogens such as Gram-negative and Gram-positive bacteria, model viruses, and fungi, and fungus spore. We have also discussed the interactions of these synthetic materials with model membrane systems and cell components such as proteins, nucleic acids and cellulose materials in a effort to better understand the interactions on a molecular scale.

We examined the interactions of biocidal CPE and OPE materials with model membrane systems in an effort to understand the underlying mechanism and selectivity of their biocidal activity. Electrostatic interactions are important for the initial binding between the CPEs and OPEs with lipid membranes and the presence of lipids with negative intrinsic curvature can facilitate membrane disruption or phase transition induced by CPEs and OPEs. In addition, the membrane activity of these materials is also dependent on molecular conformation and size, as well as the structure of side chains. Since *in vitro* membrane activity measurements of the synthetic antimicrobial agents correlates well with their biocidal activity and selectivity, these studies may guide the rational design of more efficient synthetic antimicrobial materials.

Our studies have also shown that for most CPE/OPE-biological systems investigated, there are two pathways for pathogen inactivation: a dark process in which the CPE/OPE associates with and/or penetrates the outer envelope of the pathogen and a light-activated process in which a reactive oxygen species, initially singlet oxygen in most cases, is generated either at or within the envelope of the pathogen. Both dark and light activated

pathways induce disruptions to the physical and chemical stabilities, and thereby functions, of biological targets, thus inducing toxicity. These toxicity mechanisms are non-specific and underlie the remarkable broad-spectrum biocidal activity observed. Importantly, our findings support the development and use of these materials as novel antimicrobial agents that are unlikely to induce resistance. Furthermore, these materials are relatively easy to synthesize, stable, and amenable to be processed into different materials, including coatings and fibers, which could greatly expand their applications into antiseptic materials for preventing and limiting the spread of infections, including sterile clothing and paints, biocompatible medical materials such as catheters, sutures, and implants.

## 8.2 Future directions

### 8.2.1 Membrane perturbation mechanisms

As described previously, more experimental studies are necessary to construct a more complete picture describing the membrane perturbation mechanisms and the structure–function relationships of the CPEs and OPEs.

To evaluate the effect of CPE/OPE-membrane interactions on membrane stability and permeability, we have proposed to measure the effects of the materials on the molecular structure and permeabilization of model lipid membranes. On the molecular level, destabilization of supported lipid bilayers will be assessed by neutron reflectivity (NR) (LANSCE, LANL, Los Alamos, NM).[1] Briefly, a lipid bilayer will be prepared on a quartz surface using a Langmuir-Blodgett/Langmuir-Schaefer (LBLS) deposition method. This preparation method yields bilayers with near complete surface coverage so that the

effect of membrane disruption by the biocides can be resolved. The bilayer will then be sealed in a solid-liquid interface fluid cell and NR data will be collected before and after the injection of a CPE/OPE sample. Different hydrogen-deuterium schemes will be tested for optimal contrast. From our experience, hydrogenated lipids and polymers with $D_2O$ superphase provide excellent contract for detecting membrane structure, while the deuterated oligomer with hydrogenated lipids and superphase will allow us to easily determine the location of the biocide. Changes in lipid membrane phase will continue to be determined by small angle X-ray scattering (SSRL, SLAC National Accelerator Laboratory, Menlo Park, CA).[2] Changes in lipid bilayer structure and morphology will be evaluated by AFM imaging of supported bilayer patches formed by rupturing unilamellar vesicle on mica surface in a fluid cell before and after incubation with a CPE/OPE. Bilayer patch height, area, edge appearance, and possible surface deformation and resulting biocide/lipid structures will be imaged and determined to assess the mechanism of membrane destabilization.

### 8.2.2 Interaction of the CPEs and OPEs with live pathogen in aqueous environment

The morphological damage to the model pathogens have been routinely visualized by conventional SEM and TEM in our study. But the sample preparation process for these imaging techniques may create artifacts[3] and the interactions of the CPEs and OPEs with living pathogens can not be visualized by these techniques. The atomic force microscopy (AFM) has been applied in the studies of dynamic biological process, for example, the growth and septum formation of S. aureus have been imaged by AFM in aqueous environment.[4] Real-time investigation of the interactions between the PPE-based antimicrobial materials and a single living pathogen cell in the aqueous environment via

AFM will provide more insights into the biocidal mechanisms of the CPEs and OPEs.

### 8.2.3 Antimicrobial selecity of the CPEs and OPEs and their delivery

To fully realize the potential of these PPE-based materials as new antibiotics and novel antiseptic materials, rational design of the materials to optimize activity and selectivity for different applications need be guided by a fundamental understanding of the antimicrobial mechanisms and the structure-function relationship of these materials.

As discussed in the preceding chapters, there may be both important concerns and opportunities in the ability of CPE/OPE materials to damage mammalian cells. Thus future work will be targeted to render CPE/OPE materials more selective in some cases so that they can be used perhaps in the presence of mammalian cells without damaging them. Since in general the concentration of CPE or OPE materials sufficient to damage bacterial cells is usually much lower than that necessary for damaging mammalian cells, it might be useful to develop formats where the CPE or OPE materials are loaded on nanoparticles such as Laponite,[5] that have been proposed as a non-harmful carrier for drug delivery. The larger CPE may remain bound to the nanoparticulate Laponite while the smaller OPE may be released at very low concentrations. Additionally by coupling the loading of a CPE or OPE onto nanoparticles with the binding of a recognition element such as a peptide or antibody can target the CPE or OPE to specific cell types or pathogens.

The most recent studies we have reported where the smaller OPE (end-only functionalized) have been found active against hard to inactivate (or destroy) biofilms and yeast cells (fungi) and spores suggest that these materials are sufficiently versatile for uses in the large space between peptides and synthetic antibiotics and harsh reagents such

as bleach and other materials generating reactive oxygen intermediates or chloride reagents.

### 8.3 References


1. Jones, E. M.; Dubey, M.; Camp, P. J.; Vernon, B. C.; Biernat, J.; Mandelkow, E.; Majewski, J.; Chi, E. Y., Interaction of Tau Protein with Model Lipid Membranes Induces Tau Structural Compaction and Membrane Disruption. *Biochemistry* **2012,** *51* (12), 2539-2550.

2. Wang, Y.; Jett, S. D.; Crum, J.; Schanze, K. S.; Chi, E. Y.; Whitten, D. G., Understanding the dark and light-enhanced bactericidal action of cationic conjugated polyelectrolytes and oligomers. *Langmuir* **2013,** *29* (2), 781-792.

3. Bozzola, J. J.; Russell, L. D., *Electron Microscopy: Principles and Techniques for Biologists* 1ed.; Jones & Bartlett Pub: London, **1992**.

4. Dufrêne, Y., *Life at the Nanoscale: Atomic Force Microscopy of Live Cells*. Pan Stanford Publishing Pte. Led.: Singapore, **2011**.

5. Wang, S.; Wu, Y.; Guo, R.; Huang, Y.; Wen, S.; Shen, M.; Wang, J.; Shi, X., Laponite Nanodisks as an Efficient Platform for Doxorubicin Delivery to Cancer Cells. *Langmuir* **2013**, *29* (16), 5030-5036.